Aus dem Institut für Prophylaxe und Epidemiologie der Kreislaufkrankheiten der

Ludwig-Maximilians-Universität München

Direktor: Prof. Dr. med. Christian Weber

WISP1 Regulation by MicroRNAs

in Pulmonary Fibrosis

Dissertation zum Erwerb des Doktorgrades der Naturwissenschaften
an der Medizinischen Fakultät der Ludwig-Maximilians-Universität München

vorgelegt von

Barbara Berschneider

aus Regensburg

2014

Meiner Familie

Gedruckt mit Genehmigung der Medizinischen Fakultät
der Ludwig-Maximilians-Universität München

Betreuer: PD Dr. rer. nat. Peter Neth

Zweitgutachter: Prof. Dr. rer.nat. Wolfgang Zimmermann

Dekan: Prof. Dr.med. Dr.h.c. Maximilian Reiser, FACR, FRCR

Tag der mündlichen Prüfung: 6. November 2014

TABLE OF CONTENTS

ABBREVIATIONS

A

A	adenosine
aa	amino acids
Ad	adenoviral
Ago	argonaute protein
APS	ammonium peroxodisulfate
α-SMA	alpha smooth muscle actin
ATII	alveolar type II
ATP	adenosine triphosphate

B

BALF	bronchoalveolar lavage fluid
BGN	biglycan
BLEO	bleomycin
BMSC	bone marrow stromal cells
BMP	bone morphogenic protein
bp	base pairs
BSA	bovine serum albumine

C

C	cytosine
CCN	CYR61, CTGF, NOV protein family
cDNA	complementary DNA
CDS	coding sequence
CLIP	cross-linking immunoprecipitation
CMV	cytomegalovirus
ctrl	control
CT-value	cycle of threshold value in quantitative PCR
°C	degrees Celsius

D

d	day(s)
Da	dalton
DGCR8	Di George Syndrome critical region gene 8
DMEM	Dulbecco´s modified Eagle´s medium
DMSO	dimethyl sulfoxide
DNA	deoxyribonucleic acid
dNTP	desoxynucleotide triphosphate
ds	double-stranded
DTT	dithiothreitol

E

E. coli	*Escherichia coli*
ECL	enhanced chemiluminescence
ECM	extracellular matrix
EDTA	ethylenediaminetetraacetic acid
EMT	epithelial-to-mesenchymal transition

F

FB	fibroblast(s)
FBS	foetal bovine serum
FC	fold change
fw	forward
FZD	Frizzled

G

G	guanosine
g	gram, standard acceleration
GFP	green fluorescent protein
GSK	glycogen synthase kinase
gDNA	genomic DNA

H

h	hour (s)
H-E	haematoxylin-eosin
hs(a)	*homo sapiens*
HEK	human embryonic kidney
HITS	high-throughput sequencing
HRCT	high resolution computer tomography
HRP	horse radish peroxidase

I

IgG	immunoglobulin protein G
IL	interleukin
i. p.	intraperitoneal
IPF	idiopathic pulmonary fibrosis
i. v.	intravenous

K

k	kilo
KCl	potassium chlorid

L

l	liter
LEF	lymphocyte enhancer factor

M

m	milli
M	molar
mA	milli Ampere
MCS	multiple cloning site
min	minutes
miR(NA)	microRNA
miRISC	miRNA induced silencing complex
MMP	matrix metalloprotease
mmu	*mus musculus*
mRNA	messenger RNA
μ	micro

N

n	nano
n. d.	not detectable
NaCl	sodium chloride
nt	nucleotide(s)

O

ON	over night

P

p	pico
p.a.	pro analysis
PAGE	polyacrylamide gel electrophoreses
PAR	photoactivatable-ribonucleoside-enhanced
PBS	phosphate buffered saline
PBST	phosphate buffered saline with Tween 20
PCR	polymerase chain reaction
PFA	paraformaldehyde
poly(A)	poly adenylation
rpm	revolutions per minute

Q

qRT-PCR	quantitative real time PCR

R

RNA	ribonucleic acid
RNAi	RNA interference
RNP	ribonucleoprotein particle
RT	room temperature
rv	reverse

S

s	seconds
SEM	standard error of the mean
SD	standard deviation
SDS	sodium dodecyl sulfate
siRNA	small interfering RNA
SP	surfactant protein
ss	single-stranded
SVM	support vector machine

T

T	thymidine
TAE	Tris-acetate-EDTA
TCF	T-cell factor
TE	Tris-EDTA
TGF	transforming growth factor
TEMED	N,N,N',N'-Tetramethylethylendiamin
TNF	tumor necrosis factor
Tris	tris(hydroxymethyl)-aminomethane

U

U	unit, uridine
UIP	usual interstitial pneumonia
UTR	untranslated region

V

| V | volt, volume |

W

| w | weight |
| WISP1 | WNT1-inducible signaling pathway protein 1 |

1 ZUSAMMENFASSUNG

Die idiopathische pulmonale Fibrose (IPF) ist die häufigste und schwerwiegendste Form der idiopathischen interstitiellen Pneumonien. Charakteristisch für IPF ist eine überhöhte Produktion an extrazellulärer Matrix, was zu massiven Veränderungen des Lungengewebes und verminderter Lungenfunktion führt. *WNT1-inducible signaling pathway protein 1* (WISP1) ist in IPF deutlich erhöht und wurde als profibrotischer Faktor mit therapeutischem Nutzen identifiziert. WISP1 trägt zum Krankheitsverlauf bei, indem es mesenchymale Veränderungen in Epithelzellen hervorruft und extrazelluläre Matrix produzierererende Fibroblasten aktiviert. Über die Regulation von WISP1 ist jedoch wenig bekannt. MicroRNAs (miRNAs) sind kurze, einzelsträngige RNAs, die die Proteinexpression auf post-transkriptionaler Ebene regulieren. Vor kurzem konnte gezeigt werden, dass miRNAs an der Entstehung von IPF beteiligt sind. Ob miRNAs auch zu erhöhter WISP1 Produktion und dadurch negativ zum Krankheistverlauf von IPF beitragen, wurde bisher nicht geklärt.

Die vorliegende Arbeit eruierte die miRNA-vermittelte Regulation von WISP1 in pulmonaler Fibrose. Hierfür wurden bioinformatische Methoden, molekular- und zellbiologische Verfahren, sowie Tiermodelle als auch humane Proben verwendet. *In silico* Analysen von humanen und murinen miRNA-Datensätzen von fibrotischem Lungengewebe ergaben 13 übereinstimmende miRNAs, die in Fibrose herunter reguliert sind, und dadurch zu einer WISP1-Erhöhung beitragen können. Bioinformatische Untersuchungen sagten Bindestellen im WISP1 3' untranslatiertem Bereich (3'UTR) für die in Lungenfibrose erniedrigten miRNAs, nämlich miR-30a/d, miR-92a und miR-203a vorher. In humanem und murinem fibrotischem Gewebe konnte gezeigt werden, dass diese Kandidaten-miRNAs erniedrigt sind, während WISP1 erhöht ist. Mittels Reportergenanalysen wurde der direkte Einfluss der Kandidaten-miRNAs auf die WISP1 3'UTR untersucht. Des Weiteren wurde die miRNA-vermittelte endogene WISP1-Regulation analysiert, wobei gezeigt werden konnte, dass dem zellulären Umfeld eine Rolle zukommt. MiR-92a regulierte WISP1 auf mRNA-Ebene in primären humanen Fibroblasten in Abhängigkeit des Zellspenders. Durch Einführung eines fibrotischen Umfeldes, hervorgerufen durch den fibrotischen Faktor *transforming growth factor* (TGF)-β1 erhöhte sich die WISP1-Expression *in vitro* und *in vivo*. Dieser WISP1-Anstieg konnte durch Überexpression von miR-30a und miR-92a signifikant reduziert werden. Außerdem wurde eine negative Korrelation von miR-92a und WISP1 sowohl in einem TGF-β1-induzierten Lungenfibrosemodell als auch in primären Lungenfibroblasten von IPF-Patienten gefunden. Diese Daten weisen daraufhin, dass es eine miRNA-abhängige Regulation von WISP1 gibt, die maßgeblich durch miR-92a vermittelt wird, die jedoch in Lungenfibrose gestört ist.

2 SUMMARY

Idiopathic pulmonary fibrosis (IPF) is the most common and fatal form of idiopathic interstitial pneumonia. It is characterized by excessive extracellular matrix production leading to distorted lung architecture and impaired lung function. WNT1-inducible signalling pathway protein 1 (WISP1) was previously identified as a highly expressed profibrotic mediator in IPF. WISP1 contributes to disease progression by mediating epithelial to mesenchymal transition (EMT) of alveolar epithelial type II (ATII) cells and by activating fibroblasts. Yet, only limited knowledge exists about WISP1 regulation in general and during IPF in particular. MicroRNAs (miRNAs), short, single-stranded (ss) RNAs that regulate protein expression in a post-transcriptional manner, have recently been demonstrated to contribute to IPF pathogenesis. If disturbed miRNA expression can influence WISP1 expression and therefore contributes to IPF pathogenesis, however, still remains elusive.

This study presents a functional analysis of WISP1 regulation by miRNAs in pulmonary fibrosis applying *in silico* analysis, reporter gene assays, *in vitro* and *in vivo* experimental fibrosis models as well as *ex vivo* human fibrosis tissue specimens and cells. *In silico* analysis of human and murine miRNA data sets revealed 13 overlapping miRNAs downregulated in pulmonary fibrosis. A novel supervised machine learning approach predicted miR-30a/d, miR-92a and miR-203a target sites in regions of the human WISP1 3' untranslated region (3'UTR) preferentially bound by the miRNA ribonucleoprotein (RNP) complex. Both miRNAs were decreased in IPF samples, whereas WISP1 protein was increased. Candidate miRNA binding to the WISP1 3'UTR was investigated with reporter gene assays. Furthermore, *in vitro* miRNA regulation of endogenous WISP1 was found to be regulated by the cellular microenvironment, as miR-92a mediated *WISP1* mRNA repression in a donor cell specific way. Implementing a profibrotic environment with transforming growth factor (TGF)-β1, WISP1 expression increased in primary lung fibroblasts *in vitro* and in rat lung homogenates *in vivo*. Notably, miR-30a and miR-92a reversed TGF-β1 induced WISP1 expression in lung fibroblasts. An inverse relationship for WISP1 and miR-92a was found in a TGF-β1 dependent lung fibrosis model *in vivo*. In addition, WISP1 was significantly increased in primary IPF fibroblasts, which negatively correlated with miR-92a level *ex vivo*. Taken together, these findings indicate a regulatory role of miR-92a for WISP1 expression in pulmonary fibrosis.

3 INTRODUCTION

3.1 Idiopathic pulmonary fibrosis

In general, idiopathic pulmonary fibrosis (IPF) is the most common form of idiopathic interstitial pneumonia and it is a chronic, progressive and irreversible disorder limited to the lungs, occurring primarily in elderly people. It is characterized by progressive worsening of dyspnoea and a decline in lung function, and it is associated with a poor prognosis (King et al, 2011; Raghu et al, 2011).

3.1.1 Clinical features of IPF

The clinical presentation summarized in the official American Thoracic Society / European Respiratory Society / Japanese Respiratory Society / Latin American Thoracic Association statement about IPF from 2011 by Raghu *et al.* is the following: Adult patients present with unexplained chronic exceptional dyspnoea, and commonly unproductive cough, bibasilar inspiratory crackles and finger clubbing. Typically, elderly people present in the sixth and seventh decade and patients aged less than 50 years are rare. More men than women have been reported to develop IPF (Raghu et al., 2011). From the time of diagnosis the median survival is 3 years (King et al, 2011).

According to the recent statement the diagnosis of IPF requires: *"1) Exclusion of other known causes of interstitial lung disease (like domestic and occupational environmental exposures, connective tissue disease, and drug toxicity); 2) the presence of an usual interstitial pneumonia (UIP) pattern on high-resolution computed tomography (HRCT) in patients not subjected to surgical lung biopsy; 3) specific combinations of high-resolution computed tomography and surgical lung biopsy patterns in patients subjected to surgical lung biopsy. These diagnostic criteria are quite different from previous recommendations. A surgical lung biopsy is not essential any more for making the diagnosis of IPF, as HRCT is specific for the recognition of a UIP pattern."* (Raghu et al, 2011)

In a study published in 2006, the incidence of IPF in the United States is estimated to be between 6.8 and 16.3 per 100 000 persons, and the prevalence of IPF is estimated to be between 14.0 and 42.7 per 100 000 persons depending on the case definition used (Raghu et al, 2006). Data from the UK published in 1999 estimate the incidence about five cases and the prevalence 15-18 cases per 100 000 persons per year (Gibson et al, 2013).

Potential risk factors are cigarette smoking, environmental factors such as metal and wood dust, microbial agents and gastroesophageal reflux (Raghu et al, 2011).

In general, treatment options for IPF are limited. The current guidelines recommend supplemental oxygen for resting hypoxaemia, pulmonary rehabilitation and lung transplantation for appropriate candidates. Furthermore, pharmacologic agents targeting co-morbidities and dampen fibrosis should be considered if appropriate (Loomis-King et al, 2013; Raghu et al, 2011).

3.1.2 Pathological features of IPF

The radiological and/or histopathological pattern of IPF is called UIP. As radiological technique HRCT is performed. According to the current guidelines, UIP is characterized on HRCT by the presence of reticular and ground glass opacities and honeycombing. As shown in Figure 3.1, on HRCT, honeycombing is manifested as clustered cystic airspaces appearing usually subpleural with well-defined walls (Raghu et al, 2011).
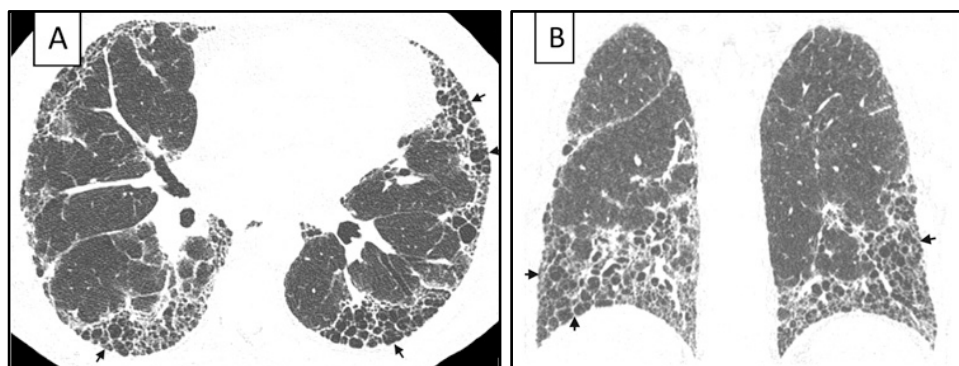
Figure 3.1: HRCT images with UIP patterns.
UIP pattern, with extensive honeycombing: (A) axial and (B) coronal HRCT images show basal predominant, peripheral predominant reticular abnormality with multiple layers of honeycombing (arrows) (adopted from Raghu *et al.* (Raghu et al, 2011), reprinted with permission of the American Thoracic Society. Copyright © 2014 American Thoracic Society).

Cavazza *et al.* describe the histological key features of IPF as the following: heterogeneous, patchy appearance of the lung tissue, distorted lung architecture and occurrence of fibroblast foci. Areas of normal, healthy lung tissue are in close proximity with honeycomb changes and fibrotic regions (spatial heterogeneity). Fibrotic scares arise predominantly in the subpleural and paraseptal parenchyma while in central lobular regions fibrosis occurs less or only at advanced disease cases. Honeycombs are cystic fibrotic airspaces filled with mucus or inflammatory cells and are frequently surrounded by bronchiolar epithelium. It is thought, that honeycombs represent regions where the injury already occurred, whereas so-called fibroblastic foci represent areas of ongoing fibrosis. These foci consist of proliferating fibroblasts and myofibroblasts (characterized mainly by α-smooth muscle actin (α-SMA) expression) producing mainly collagens and other components of the extracellular matrix in excess. Hyperplastic ATII cells frequently line fibroblast foci. In general, these different stages of disease: normal tissue, active disease areas and already injured regions, can usually be observed on one lung tissue specimen and are denoted as temporal heterogeneity. Furthermore, mild inflammation mainly characterized by neutrophils and macrophages can be seen (Cavazza et al, 2010).
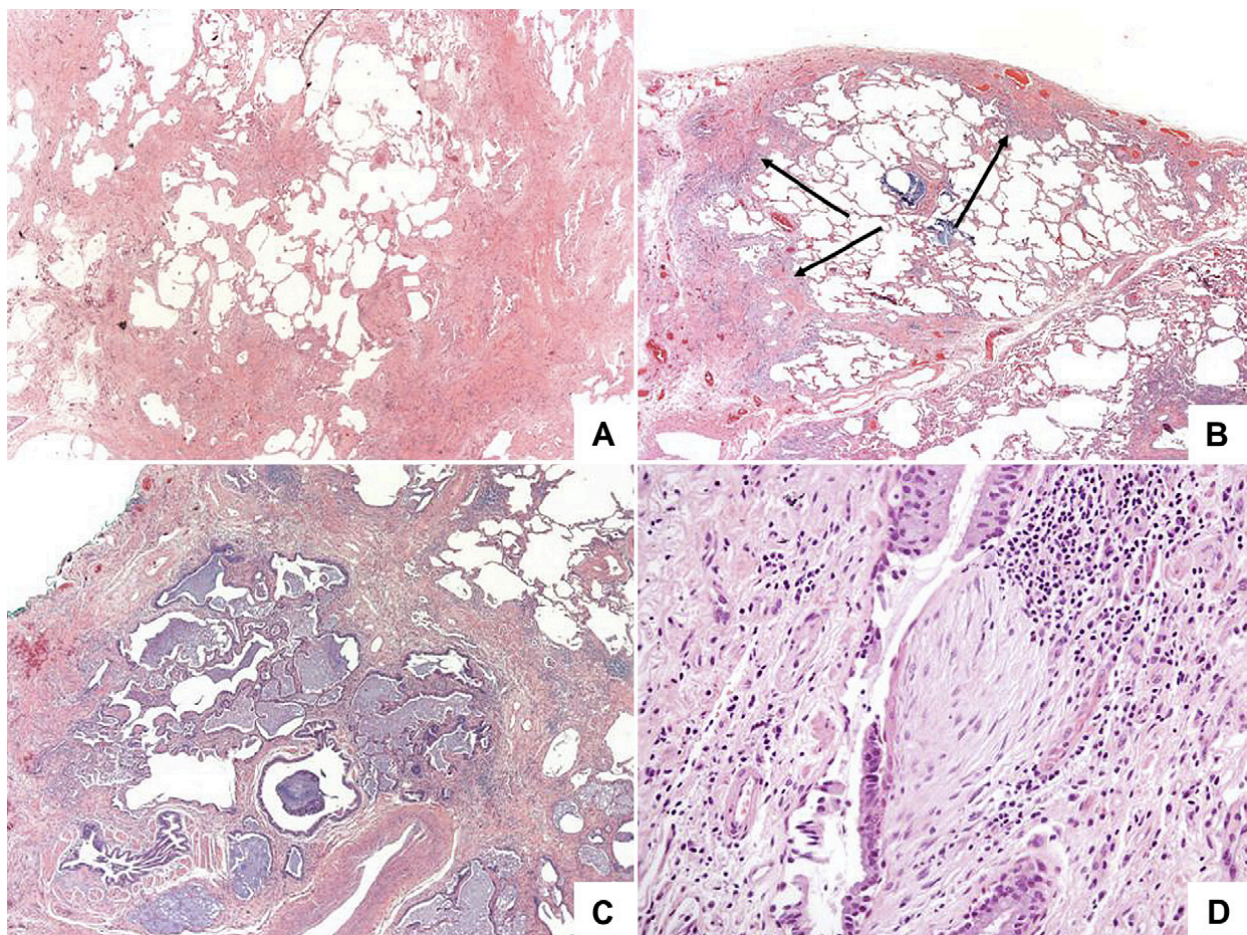
Figure 3.2: Histology of usual interstitial pneumonia.
A) Alternating areas of scarred and normal lung (haematoxylin-eosin (H-E), 20x magnification). B) Fibrotic regions in the periphery, subpleural and paraseptal (arrows), with relative sparing of the centrolobule (H-E, 20x magnification). C) Honeycomb of enlarged airspaces lined by bronchiolar epithelium, frequently filled by mucus and surrounded by dense scars (H-E, 20x magnification). D) A fibroblastic focus consisting of myofibroblasts lined either by hyperplastic epithelial cells or denuded (H-E, 100x) (adopted from (Cavazza et al, 2010)).

3.1.3 Pathomechanisms of IPF

Currently, it is believed that IPF is the result of an aberrant wound healing process. Around 15 years ago, a paradigm shift proceeded considering IPF as an epithelial injury-driven, rather than an inflammation-driven disease (Gross & Hunninghake, 2001; Selman et al, 2001). The IPF pathomechanism therefore thought to encompass the following steps. Repetitive microinjuries damage the alveolar epithelium leading to activation of alveolar epithelial cells and to alveolar-capillary basement disruption. This permits fibrogenic cell infiltrates of the alveolar interstitium and activation of fibroblasts and myofibroblast foci formation with subsequent exaggerated deposition of extracellular matrix. In addition, impaired reepithelialisation and tissue remodelling results in distorted lung architecture (King et al, 2011; Selman et al, 2001).

3.1.3.1 *Genetic predispositions of pulmonary fibrosis*

Although IPF occurs with unknown cause, genetic predispositions have been described in families with interstitial lung diseases. Mutations in surfactant protein (SP) C, a hydrophobic protein specifically secreted by ATII cells, are described to be associated with pulmonary fibrosis (Nogee et al, 2001; Thomas et al, 2002). These mutations affect the BRICHOS domain, which prevents SPC from aggregating while it is inserted into membranes (Wolters et al, 2014). In addition, single nucleotide polymorphisms in SPA lead to protein instability and retention in the endoplasmatic reticulum (ER) (Wang et al, 2009b). Both SPC and SPA mutations appear with 1% frequency in patients developing sporadic IPF (Wolters et al, 2014).

Moreover, mutations in TERT and TERC, factors responsible for telomere length, are found with 3% frequency in pulmonary fibrosis patients and even more IPF patients possess short telomeres (Alder et al, 2008; Armanios et al, 2007). This is not surprising as telomere length is an indicator for ageing, and as IPF occurs predominantly in elderly patients. However, how this affects the development of IPF still needs to be explored, as a recent animal study by Liu *et al.* suggested that the pathogenesis of pulmonary fibrosis was independent of telomere length (Liu et al, 2013c).

The predominant mutation (35%) in IPF affects the *MUC5B* promoter leading to an increase in MUC5B expression, a mucin glycoprotein and major component of airway mucus (Seibold et al, 2011). Collectively, analysis of genetic mutations in pulmonary fibrosis substantiates the hypothesis that IPF is an epithelial driven disorder, as all mutations identified thus far affect epithelial cells (Wolters et al, 2014).

3.1.3.2 *Key cell types in pulmonary fibrosis*

Alveolar epithelial cell injury is believed to be the key driver of pulmonary fibrosis. Katzenstein *et al.* and others reported hyperplasia of ATII cells and denudation of the alveolar epithelium within fibroblastic foci in tissue of IPF patients (Kasper & Haroske, 1996; Katzenstein & Myers, 1998). Moreover, ATII cell apoptosis was described in IPF patients by showing a positive staining for the apoptosis marker caspase 3 for 70-80% of the ATII cells (Korfei et al, 2008). The same study reported about ER stress in ATII cells of IPF patients, and ER stress and unfolded protein response has been discussed as a central pathway promoting IPF (Korfei et al, 2008). In addition to human IPF data revealing the alveolar epithelium as site of injury, targeted ATII depletion in a mouse model of pulmonary fibrosis connected injury with the development of pulmonary fibrosis (Sisson et al, 2010). Altogether these data point to and as classically described, that injuries to the lung epithelium result in ineffective reconstitution and repair of the lung epithelium and mediate pulmonary fibrosis by inducing the accumulation of myofibroblasts. Myofibroblasts are the key effector cells characterized by α-SMA expression and they secret an excessive amount of extracellular matrix related proteins, including collagen alpha-1 (type I) (COL1A1) and fibronectin 1 (FN1) (Klingberg et al, 2013). Additionally, these cells are resistant to apoptosis and exhibit an invasive phenotype leading to disease progression (Li et al, 2011; Maher et al, 2010). Under on-going debate is the origin of the

myofibroblast, and currently resident fibroblasts, fibrocytes, endothelial cells, pericytes and epithelial cells have been suggested to give rise to a myofibroblast (Fernandez & Eickelberg, 2012b). The mechanism, by which epithelial cells but also endothelial cells acquire fibroblast like properties while losing cell polarity and cell-cell contacts, is termed epithelial-to-mesenchymal transition (EMT) or EndoMT. This process is characterized by losing epithelial cell specific proteins like E-cadherin and tight junction protein 1 while acquiring mesenchymal marker like vimentin (VIM), FN1 and α-SMA. However, if EMT-derived fibroblasts contribute to IPF progression is discussed controversially (Wolters et al, 2014). In conclusion, lung remodelling in fibrosis may result from an abnormal epithelium unable to repair and its dysfunctional interaction with the mesenchyme.

3.1.3.3 *Growth factor signalling in pulmonary fibrosis*

Several factors and signalling pathways have been described thus far to be involved in the pathogenesis of IPF. Among others, soluble mediators, such as components of the coagulation cascade, matrix metalloproteinases (MMPs) as well as their inhibitors, and pro-inflammatory cytokines, like tumour necrosis factor (TNF)-α and interleukin (IL)-1β, are described to contribute to disease progression (Chambers & Scotton, 2012; Wynn & Ramalingam, 2012). Besides other cytokines, TGF-β1 plays a key role in fibrogenesis (Fernandez & Eickelberg, 2012a). TGF-β1 belongs to the TGF superfamily, and is a pleotropic cytokine that is as well as its receptor ubiquitously expressed by all cells and tissues in the body. Its expression is increased in tissue samples both from experimental (Coker et al, 1997) and human fibrosis (Coker et al, 2001). Overexpression of active TGF-β1 *in vivo* leads to persistent lung fibrosis (Sime et al, 1997), while blocking TGF-β1 signalling ameliorates pulmonary fibrosis in rodent models (Bonniaud et al, 2005; Coker et al, 2001). TGF-β1 is secreted and stored in the ECM in an inactive form. Activation can occur by physical processes like acidification and oxidation or due to a number of proteases, such as plasmin, thrombin and matrix metalloproteinases (Jenkins, 2008). Furthermore, local TGF-β1 activation can result from interactions with thrombospondin and integrins (Goodwin & Jenkins, 2009).

TGF-β1 is a multifunctional cytokine involved in embryogenesis, immunity, wound healing, cancerogenesis and fibrogenesis (Wynn & Ramalingam, 2012). Canonical TGF-β1 signalling involves binding of TGF-β1 to a heteromeric receptor complex of TGF-β receptor I and II. After receptor activation, the intracellular signalling transducers, mainly Smad2 and 3, get phosphorylated and activated, and bind to the co-regulator Smad4. Smad heterodimers shuffle to the nucleus and regulate target gene expression. Furthermore, inhibitory Smads like Smad7, control activated receptor turnover, and thus block TGF-β1 signalling (Feng & Derynck, 2005).

In epithelial cells, TGF-β1 signalling can lead to epithelial cell apoptosis (Hagimoto et al, 2002), inhibition of proliferation (Ryan et al, 1994), and induction of EMT (Kim et al, 2006), as well as cell migration (Yu et al, 2008). In mesenchymal cells, TGF-β1 stimulates cell proliferation via fibroblast growth factor 2 and platelet-derived growth factor as well as α-SMA expression (Fernandez & Eickelberg, 2012a; Tatler & Jenkins, 2012).

TGF-β1, and other members of the TGF superfamily play a major role in embryogenesis. Subsequently, microarray and pathohistological analysis of IPF and experimental fibrosis tissue revealed aberrant activation of other developmental pathways like Sonic Hedgehog, Notch and Wnt (Selman et al, 2008). The Wnt pathway is subgrouped in canonical Wnt/β-catenin and in non-canonical Wnt/planar cell polarity and Wnt/Ca^{2+} signalling pathways. Wnt signalling plays a major role in embryogenesis in general and in lung development in particular. In humans, 19 Wnt ligands, 10 frizzled receptors (FZD) and LRP5/6 co-receptors are known. The central player of the canonical Wnt signalling cascade is β-catenin. In the absence of Wnt ligands, cytosolic β-catenin gets phosphorylated by the destruction complex consisting of glycogen synthase kinase (GSK)-3β and casein kinase 1α on the axin/adenomatous polyposis coli scaffold, ubiquitinated and degraded by the proteasome. Wnt ligand binding leads to deactivation of the destruction complex, non-phosphorylated β-catenin accumulates in the cytosol and shuffles to the nucleus where it interacts with transcription factors such as T cell-factor/lymphoid-enhancer-factor (TCF/LEF) and different co-activators like p300 and CBP. In adults, deregulation of the Wnt/β-catenin pathway provokes abnormalities and leads to diseases, including cancer and fibrosis (Clevers, 2006).

Increased β-catenin levels in the nucleus were reported in histological sections of IPF patients (Chilosi et al, 2003). Gene array analysis showed overexpression of WNT2, WNT5a, FZD5 and 10, Wnt regulators like SFRP1 and 2 as well as downstream mediator WNT1-inducible pathway protein 1 (WISP1) (Selman et al, 2006; Selman et al, 2008). Furthermore, our group reported abnormal levels of Wnt components in IPF, especially in primary ATII cells and evidence for functional Wnt activation by demonstrating increased phosphorylation of LRP6 and GSK-3β (Königshoff et al, 2008). The relevance of Wnt/β-catenin signalling activation in IPF is substantiated through reports showing that experimental fibrosis can be attenuated by blocking Wnt/β-catenin signalling (Henderson et al, 2010; Kim et al, 2011). However, a recent report by Tanjore *et al.* reported that ATII cell-specific β-catenin knockout animals suffer from enhanced fibrosis in an experimental fibrosis model (Tanjore et al, 2013). Hence, further studies are needed to shed light on the specific role of β-catenin levels in lung fibrogenesis. In addition, it was confirmed that WISP1 was upregulated in IPF and in experimental lung fibrosis. WISP1 was mainly expressed in hyperplastic ATII cells, and induced EMT-like changes in these cells, whereas it stimulated collagen expression in lung fibroblasts. Interestingly, administration of WISP1 neutralizing antibodies abrogated experimental fibrosis (Königshoff et al, 2009).

In summary, current evidence suggests that Wnt signalling mediates fibrogenesis due to canonical but also non-canonical mechanisms by mediating fibroblast matrix deposition either direct (Königshoff et al, 2009) or indirect through fibroblast protection from apoptosis (Chang et al, 2010; Vuga et al, 2009) and through the induction of EMT (Königshoff et al, 2009).

3.1.4 Animal models of lung fibrosis

There exist several animal models of pulmonary fibrosis (Degryse & Lawson, 2011). Outlined below are the two ones applied in this study.

3.1.4.1 *Bleomycin model of pulmonary fibrosis*

Bleomycin is a peptide antibiotic, mainly used as anticancer drug. One serious side effect of bleomycin in humans is the development of pulmonary fibrosis (Moeller et al, 2006). However, this led to its use in experimental fibrosis models. Among currently applied models, bleomycin application is most frequently used, and results in direct cell injury through the induction of DNA strand breaks. Subsequently, cell necrosis and apoptosis occur, followed by inflammatory cell infiltrates and elevated proinflammatory cytokine levels, for instance IL-1, TNF-α, IL-6 and interferon-γ, and fibrosis development is characterized by increased expression of profibrotic markers, such as TGF-β1, FN1, and COL1A1 (B et al, 2013). Different delivery routes are applied, among which intratracheal administration is the most common one (Degryse & Lawson, 2011). The timeline of developing fibrosis depends on the administration route and utilized mouse strain. For intratracheal administration of a single bleomycin dose in mice, fibrosis develops in a short time frame of two to four weeks. This fibrotic process peaks around *day 14*, and remains elevated until *day 21* post injury. Inflammation arises within the first week, and therefore the therapeutic agent should be applied at least seven days after bleomycin application for intervention studies (B et al, 2013). The advantages of bleomycin are that it is well characterized, clinically relevant and fibrosis develops fast. However, the disadvantages are that fibrosis is reversible, the effect is inflammation-driven and many UIP features, such as temporal heterogeneity and fibroblast foci are lacking (Degryse & Lawson, 2011; Moeller et al, 2006; Moore & Hogaboam, 2008)

3.1.4.2 *Overexpression of TGF-β1*

Transgene and gene delivery approaches for the overexpression of profibrotic cytokines, such as TNF-α, IL-1β and TGF-β1, are used as lung fibrosis models (B et al, 2013), and especially overexpression of a specific cytokine may provide relevant insights into the molecular mechanisms of disease progression in multiple cell types. TGF-β1 overexpression was achieved by inducible transgenic epithelial cell expression or by adenoviral delivery (Lee et al, 2004; Sime et al, 1997). In the rat, adenoviral TGF-β1 overexpression leads to mononuclear cell infiltration on *day 3 - 7* and a two-fold lung collagen content increase by *day 14*. Furthermore, epithelial cell apoptosis and changes in soluble mediators occurred, terminating in persistent lung scarring (Sime et al, 1997).

3.2 WISP1

WISP1 is a cysteine-rich, secreted matricellular protein. Matricellular proteins modulate primarily cellular responses, such as cell growth, differentiation and survival than rather exhibit structural properties within the ECM (Chen & Lau, 2009). The murine WISP1 homologue was first discovered in 1996 by mRNA expression level comparison between low and high metastatic cells and therefore named "expressed in low metastatic cells" (Elm1) (Hashimoto et al, 1998). In 1998, human WISP1 was identified as a WNT1-induced gene in the WNT1 overexpressing mammary epithelial cell line C57MG (Pennica et al, 1998).

WISP1 was grouped into the CCN protein family, due to its structural characteristics. The CCN acronym is termed after the first three discovered family members: cysteine-rich 61 (CYR61/CCN1), connective tissue growth factor (CTGF/CCN2), and nephroblastoma over-expressed (NOV/CCN3). The three WISP proteins (WISP1-WISP3), all identified by Pennica *et al.* in the screen mentioned above (Pennica et al, 1998), were allocated to the CCN family in 2003 and renamed CCN4/WISP1, CCN5/ WISP2 and CCN6/WISP3 (Brigstock et al, 2003). In this work, the proteins are named by their original name.

3.2.1 WISP1 gene and protein structure

The human *WISP1* gene is located on chromosome 8q24.1 - q24.3 and the sequence is 40 652 bp long (NCBI Gene ID 8840). The gene is composed of five exons and four introns, the human mRNA is 5 194 nt (NCBI Reference Sequence: NM_003882.3) and codes for a protein with 376 aa with a predicted molecular mass of 40 kDa. The murine protein homologue exhibits the same length and the aa sequence is to 84% identical. Murine and human WISP1 proteins comprise 38 conserved cysteine residues and four potential N-linked glycosylation sites (Pennica et al, 1998).

As depicted in Figure 3.3, all CCN family members possess one N-terminal localization sequence and four conserved structural modules, except WISP2, which lacks the last structural domain. Each structural unit, as well as the localization sequence, arises from a separate exon.

The first module (module I) of WISP1 is structurally related to the insulin-like growth factor binding domain (IGFBP) (Desnoyers, 2004). The second module (module II) comprises the von Willebrand factor type C domain (vWC) that contains a cysteine rich consensus motif found in chordin-like molecules, collagen, or thrombospondins. It exhibits a putative binding site for bone morphogenic proteins (BMP) and TGF, however, it may also function as an oligomerisation domain (Abreu et al, 2002). The third module (module III) is homologous to the thrombospondin type I repeat (TSP) and involved in cell surface and polysaccharide interaction. The fourth module (module IV) is structurally related to the carboxyl-terminal (CT) domain, which contains a cysteine knot motif that is able to participate in oligomerisation, as well as receptor and glycoprotein binding (Desnoyers, 2004).

Figure 3.3 Schematic presentation of CCN proteins.
All CCN family members share structural homology. They consist of four protein modules (IGFBD, vWC, TSP1 and CT) and possess one N-terminal secretory peptide signal (light blue). The hinge region between vWC and and TSP1 is depicted with a downward tip. WISP2 uniquely lacks the CT domain and WISP1v the vWC domain.

Besides the full length *WISP1* mRNA, several groups have described shorter WISP1 transcripts. Tanaka *et al.* identified an alternatively spliced *WISP1* mRNA variant (WISP1v) lacking exon 3 in scirrhous gastric carcinoma cells, and suggested that WISP1v is involved in cancer progression (Tanaka et al, 2001). Different groups confirmed WISP1v expression in different cells and tissues, such as osteoblasts, chondrocytes and various carcinomas (Cervello et al, 2004; Inkson et al, 2008; Tanaka et al, 2003; Yanagita et al, 2007), however the molecular function of this variants still needs to be determined in detail.

3.2.2 WISP1 expression

WISP1 expression has been observed during development, in particular in bone and lung. During murine embryonic skeletogenesis, WISP1 is expressed in the condensing mesenchyme from embryonic day 10.5 on, and later in osteoplastic cell lineages next to bone formation sites (French et al, 2004). Similar results have been reported during murine limb development (Witte et al, 2009). In the lung, Sharma and colleagues reported that WISP1 expression was altered during lung development. In particular, high WISP1 expression was observed during organogenesis and respiratory tree formation (pseudoglandular stage), while WISP1 expression was lower during epithelial differentiation (canalicular stage) (Sharma et al, 2010). Further, WISP1v expression has been observed in human bone marrow stromal cells (BMSC) (Inkson et al, 2008) and in increasing amounts during terminal chondrocyte differentiation *in vitro* (Yanagita et al, 2007).

Under tissue homeostasis, *WISP1* mRNA was detected in several organs, such as heart, kidney, lung, pancreas, placenta, ovary, small intestine and spleen. Only low or no expression was reported in brain, liver, skeletal muscle, colon, peripheral blood leukocytes, prostate, testis, breast, and thymus (Pennica et al, 1998).

Elevated WISP1 expression has recently been described in several diseases, mainly in cancer. Initially, *WISP1* mRNA was discovered in a WNT1 over expressing cell line and in colon tumours (Pennica et al, 1998). Furthermore, its expression was confirmed to be elevated in colon tumours by various reports (Davies et al, 2007; Khor et al, 2006) and it was increased in hepatocellular carcinoma (Calvisi et al, 2005), lung carcinoma (Chen et al, 2007), in breast cancer (Bauer et al, 2010; Xie et al, 2001), and prostate cancer (Ono et al, 2013). As mentioned above, WISP1v expression is strongly associated with cancer tissues, for instance scirrhous gastric carcinoma (Tanaka et al, 2001), cholangiocarcinoma (Tanaka

et al, 2003), and hepatocellular carcinoma cells (Cervello et al, 2004). However the functional role and relative importance of WISP1 in cancer need further investigation.

Besides WISP1 expression in cancer, further diseases of the skeleton, heart and lung were associated with elevated WISP1. Increased WISP1 levels were found in the synovium and cartilage in experimental and human osteoarthritis (Blom et al, 2009). Moreover, WISP1 was elevated in cardiomyocytes and cardiac fibroblasts in the border zone and non-infarcted region after experimental myocardial infarction (Colston et al, 2007; Venkatachalam et al, 2009).

In lung fibrosis, WISP1 was reported to be upregulated (Königshoff et al, 2009; Selman et al, 2006), as well as in lung injury models (Heise et al, 2011; Li et al, 2012a; Zemans et al, 2013). Furthermore, a WISP1 nucleotide polymorphism was associated with impaired lung function in asthmatic patients (Sharma et al, 2010) and elevated WISP1 was connected with airway remodelling in a rat asthma model (Yang et al, 2013).

Altogether, WISP1 expression profiles suggest an important role during development and cancerogenesis, and associates WISP1 closely with tissue remodelling processes.

3.2.3 WISP1 function

The knowledge about WISP1 function is still limited, however, the main effects described thus far have been repression of apoptosis and enhancement of cytoprotection, proliferation, migration and invasion. Moreover, WISP1 mediates osteogenesis as well as wound healing and fibrotic remodelling (reviewed in (Berschneider & Königshoff, 2011)).

As a primary feature WISP1 was reported to be cytoprotective. Cytoprotective WISP1 functions are mainly mediated by activation of Akt signalling. Su *et al.* demonstrated that WISP1 protected lung carcinoma cells from intrinsic p53-dependent, but not extrinsic Fas ligand-activated, cell death by signalling via Akt and upregulation of anti-apoptotic Bcl-xL expression and inhibition of cytochrome c release (Su et al, 2002). Similar results were obtained from cardiomyocytes after myocardial infarction. Here, WISP1 mediated Akt activation, enhanced survivin expression, and inhibition of pro-apoptotic Bax, accompanied by blocked cytochrome c release (Venkatesan et al, 2010). In addition, WISP1 attenuated TNF-α induced cardiomyocyte death (Venkatachalam et al, 2009). The Akt signalling cascade was also induced by WISP1, minimizing pro-apoptotic signalling in primary neurons to prevent them from oxidative stress induced death (Wang et al, 2012b). Furthermore, WISP1 inhibition of apoptosis, independent of Akt signalling, by inhibiting c-Myc induced apoptosis was described in rat fibroblast and epithelial cell lines (You et al., 2002), suggesting that WISP1 signalling is involved in several anti-apoptotic pathways.

Additionally, WISP1 induced primary human saphenous vein smooth muscle cell (Reddy et al, 2011) and cardiac fibroblast proliferation (Colston et al, 2007), and mediated TNF-α induced cardiac fibroblast proliferation (Venkatachalam et al, 2009). Moreover, WISP1-mediated positive effects on cell proliferation were reported for chondrocytes (French et al, 2004), osteoblasts (Kawaki et al, 2011) and BMSC (Inkson et al, 2009; Inkson et al, 2008). The proliferative effect of WISP1 on BMSC was mediated by WISP1 interaction with

biglycan (BGN), and WISP1 binding to the extracellular matrix protein BGN was already reported before (Desnoyers et al, 2001). However, Notch mediated anti-proliferative WISP1 effects on dermal fibroblasts were shown as well (Liu et al, 2012; Shao et al, 2011).

In addition to proliferation, WISP1 increased cell migration and motility in chondrosarcoma cells through induction of MMP2 (Hou et al, 2011) and oral squamous cell carcinoma cell invasion through integrins and JNK/p38 and increasing ICAM expression (Chuang et al, 2013). WISP1v led to increased invasion of cholangiocarcinoma cells *in vitro* (Tanaka et al, 2003). In contrast, WISP1 overexpression in lung cancer cells inhibited cell invasion *in vitro* and lung metastases in mouse models *in vivo* (Soon et al, 2003). Early reports on WISP1 proposed a negative correlation between expression and proliferation as well as invasion (Hashimoto et al, 1998).

Several groups demonstrated WISP1 influences on osteogenesis and chondrogenesis (French et al, 2004; Inkson et al, 2008; Yanagita et al, 2007). Lately, WISP1 effects in osteoblast maturation were described to be Smad-dependent. Here, WISP1 dependent Smad1/5/8 phosphorylation, increase in nuclear β-catenin, and ERK1/2 and p38/MAPK phosphorylation appeared to increase several mediators of bone formation in murine osteoblasts (Kawaki et al, 2011). Furthermore, WISP1 contributed to osteogenesis by enhancing BMP2 activity, a cytokine belonging to the TGF superfamily, which signals mainly via Smad1, 5 and 8 (Ono et al, 2011). These reports suggest Smad-dependent WISP1 influences on bone formation. Besides Smad-mediated WISP1 effects, integrin-dependent WISP1 effects were demonstrated for osteogenesis in BMSC but also in other tissues and cells. WISP1 signalling was mediated by integrin $\alpha_5\beta_1$ in BMCS and in chondrosarcoma cells (Hou et al, 2011; Ono et al, 2011), integrin $\alpha_v\beta_5$ and $\alpha_6\beta_1$ in synovial fibroblasts (Hou et al, 2013; Liu et al, 2013b), integrin $\alpha_v\beta_3$ in oral squamous cell carcinoma cells (Chuang et al, 2013) and integrin $\alpha_v\beta_5$ in lung cancer cells (Soon et al, 2003).

Besides changing cell behaviour, WISP1 changed cell gene expression and induced the expression of several MMPs (Blom et al, 2009; Hou et al, 2011; Reddy et al, 2011) and collagens (Colston et al, 2007; Kawaki et al, 2011; Venkatachalam et al, 2009; Wang et al, 2009a).

In lung fibrosis, WISP1 mediates remodelling processes by promoting EMT and activation of fibroblasts (Königshoff et al, 2009). Additionally, Yang *et al.* showed induction of COL1A1 and FN1 by WISP1 in lung fibroblast (Yang et al, 2013). Recently, WISP1 was associated with further lung injuries. WISP1 was increased in macrophages and alveolar epithelium in a sensitive mouse model of ventilator induced lung injury. Here, upregulation of WISP1 led to an increase in alveolar capillary permeability, which was abrogated by WISP1 neutralization and elevated by WISP1 recombinant protein (Li et al, 2012a). Moreover, lung epithelial cell injury is a central event in various lung diseases, and mechanical stress can contribute to it. WISP1 was increased in ATII cells undergoing mechanical stress *in vitro* and contributed to upregulation of mesenchymal markers in these cells (Heise et al, 2011). In acute lung injury, inflammatory processes lead to epithelial injury. Zemans and colleagues reported β-catenin dependent repair mechanisms of lung epithelium after neutrophil transmigration (Zemans et al, 2011). Neutrophil transmigration induced WISP1

expression in the alveolar epithelium in a β-catenin/p300 dependent manner. Notably, recombinant WISP1 accelerated epithelial repair mechanisms (Zemans et al, 2013).

In summary, these data with previous reports of our group show that WISP1 is upregulated after lung injury and suggest a predominant role in lung tissue remodelling.

3.2.4 WISP1 regulation

Human WISP1 was initially discovered in Wnt1-overexpressing cells (Pennica et al, 1998). It has been demonstrated that WNT1, WNT3a, but not WNT4, induce WISP1 protein expression, which suggests that WISP1 is a target of the "canonical" Wnt/β-catenin pathway (Königshoff et al, 2009; Longo et al, 2002; Pennica et al, 1998; You et al, 2002). However, these regulatory mechanisms may also be cell type dependent as WNT11, a non-canonical ligand, mediated WISP1 expression in skin fibroblasts (Liu et al, 2012).

Several lines of evidence exist, showing that WISP1 is a β-catenin responsive gene (Calvisi et al, 2005; Wang et al, 2009a; Wang et al, 2012a; Xu et al, 2000). Xu *et al.* conducted WISP1 promoter analysis and revealed that the WISP1 promoter possesses one putative cyclic-AMP response element (CRE) and five putative TCF/LEF binding sites. In their study WISP1 expression was mainly mediated by CRE binding protein (CREB), and not by TCF/LEF (Xu et al, 2000). Wang *et al.* showed in colon epithelial cell lines, that WISP1 induction was mediated by β-catenin, TCF/LEF as well as by CREB (Wang et al, 2009a). A β-catenin dependent WISP1 induction has been further underlined in another study using cardiomyocytes, demonstrating that WISP1 was able to induce its own expression via Akt, GSK-3β and β-catenin (Venkatesan et al, 2010). A β-catenin dependent WISP1 auto regulation was also reported in neurons (Wang et al, 2012a).

The same signalling mediators involved in WISP1 induction were reported upon angiotensin II treatment in cardiomyocytes, but here, in addition p38 MAPK-mediated CREB signalling can induce WISP1 as well (Shanmugam et al, 2011). In myocytes, WISP1 was identified as a target of the p38 isoform gamma (Wang et al, 2008), and for cardiac fibroblasts an ERK1/2 and CREB mediated WISP1 induction was further reported (Venkatachalam et al, 2009).

Besides WISP1 regulation by Wnt ligands and self-regulation, cytokines like interleukins (IL-18, IL-1β), TNF-α and TGF-β1 were shown to induce WISP1 expression (Colston et al, 2007; Parisi et al, 2006; Reddy et al, 2011; Venkatachalam et al, 2009). In vascular smooth muscle cells, WISP1 is upregulated by IL-18 (Shanmugam et al, 2011). In cardiomyocytes, IL-1β and TNF-α stimulation induced WISP1 expression *in vitro* (Colston et al, 2007). TNF-α mediated WISP1 increase was further reported for cardiac fibroblasts (Venkatachalam et al, 2009) and lung smooth muscle cells (Knobloch et al, 2013).

In murine osteoblasts, it has been demonstrated that TGF-β1 and BMP-2 induce, whereas cortisol represses, WISP1 expression (Parisi et al, 2006). However, in a chicken model of embryonic limb development, TGF-β1 did not induce WISP1 expression *in vivo* (Lorda-Diez et al, 2011). As TGF-β1 represents a main mediator of tissue fibrosis and remodelling in multiple organ systems, further studies are needed to fully appreciate the interaction of TGF-β1 and WISP1 in this context.

On protein interaction level, other extracellular matrix proteins affect WISP1. In the extracellular space, the leucine rich repeat proteoglycans, BGN and decorin, have been reported to regulate WISP1 protein activity and availability (Desnoyers et al, 2001). Inkson *et al.* suggested that WISP1 and BGN functionally interact and control each other's activity in the regulation of osteoblast differentiation and proliferation (Inkson et al, 2009). Furthermore, BGN deficiency led to decrease of WISP1 expression *in vitro* in BMSC and *in vivo* in BGN deficient mice at *day 14* post fracture (Berendsen et al, 2011). BGN may act as a Wnt reservoir in the intracellular space and therefore also plays a role in WISP1 induction. Moreover, in other organ systems, it has been suggested that WISP1 and BGN act synergistically. In a myocardial infarction model, both proteins were upregulated and led to amplified WISP1 signalling with increased tissue remodelling (Colston et al, 2007). Importantly, BGN has also been involved in fibrotic processes in the lung (Kolb et al, 2001). Similarly, altered WISP1 expression has been observed in lung disease (Heise et al, 2011; Königshoff et al, 2009; Li et al, 2012a; Zemans et al, 2013).

In summary, WISP1 is mainly regulated by its own and the β-catenin pathway, by cytokines and by ECM proteins. These data point in general to a close interaction between WISP1, TGF-β1, and ECM proteins, like BGN, altogether modulating tissue remodelling. However, nothing is known thus far about WISP1 regulation by non-coding RNAs like microRNAs in general and especially in pulmonary fibrosis.

3.3 MicroRNAs

MicroRNAs (miRNAs) are small, 22 nt long, ssRNAs involved in post-transcriptional gene regulation by pairing to the mRNAs of protein coding genes (Bartel, 2009). In humans, more than 1 000 miRNAs have been identified thus far (miRBASE, January 2014) (Kozomara & Griffiths-Jones, 2014). They were discovered around 20 years ago and revolutionized the existing picture of gene regulation. Until now, they were reported to play a role in development and tissue homeostasis, but differential miRNA expression occurs also in cancer and many other diseases like fibrosis (Mendell & Olson, 2012).

3.3.1 MiRNA biogenesis

In the nucleus, miRNAs are commonly transcribed by RNA polymerase II from independent miRNA genes or from introns of protein-coding genes as part of longer primary transcripts, so-called pri-miRNAs. They possess like other RNA polymerase II transcripts a 5'-cap and a 3'-poly(A) tail (Figure 3.4). The pri-miRNA transcripts form stem loop structures, and the mature miRNAs is part of the imperfectly paired double-stranded hairpin stem connected by a short, terminal loop and two ss flanking regions up- and downstream of the hairpin. In addition, miRNAs can occur in clusters, meaning one pri-miRNA bears several mature miRNAs.

In the canonical pathway, miRNA biogenesis is a two-step procedure, catalysed by two members of the RNAse III family enzymes, Drosha and Dicer. First, pri-miRNAs structures

are processed in the nucleus by the microprocessor complex consisting of the two core components Drosha and DGCR8 (Di George Syndrome critical region gene 8). The dsRNA-binding protein DGCR8 interacts with the base of the stem loop structure guiding the positioning of Drosha. Drosha endonucleolytically cleaves the dsRNA stem generating a 60 – 100 nt long, hairpin-shaped RNA molecule called miRNA precursor (pre-miRNA). After nuclear processing, the pre-miRNA is recognized by exportin 5, a nuclear export receptor, and actively transported in a Ran-GTP dependent manner into the cytosol.
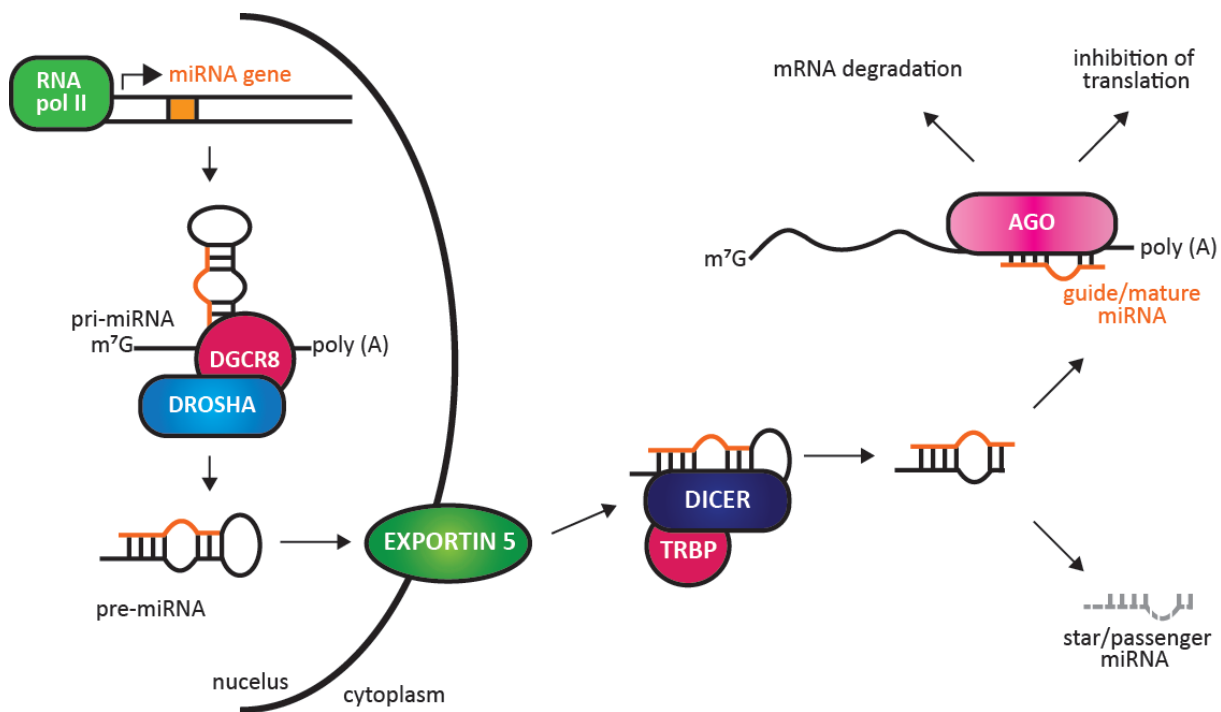
Figure 3.4: MiRNA biogenesis
The primary miRNA (pri-miRNA) transcript is typically produced by RNA polymerase II (pol II). The Drosha and DGCR containing microprocessor cleavage results in precursor miRNA (pre-miRNA). The pre-miRNA is exported out of the nucleus by Exportin 5 to be further processed by the Dicer complex. The mature miRNA strand is loaded onto Argonaute to form the miRNA-Induced Silencing Complex (miRISC); the other strand, called the star or passenger, is degraded. miRISC is then capable of down-regulating gene expression through mRNA decay or translation inhibition (adopted from (Finnegan & Pasquinelli, 2013)).

In the cytosol, the miRNA duplex develops by Dicer, assisted by TRPB and further proteins. The PAZ domain of Dicer interacts with the 3' overhang of the pre-miRNA and positions it correctly for the cleavage by the two catalytic domains 22 nt upstream within the ds stem. The cleavage product is the miRNA duplex, consisting of 22 nt with 2 nt long, 3' overhangs on both ends.

The mature miRNA strand, the guide strand, is incorporated together with Argonaute protein (Ago) in the miRNA induced silencing complex, miRISC, while the passenger strand, also called the star (*)-strand is degraded. The functional miRNA strand is chosen due to its thermodynamic properties. The strand with the less stable base pairing at the 5' end is chosen as mature miRNA strand and guides miRISC to silence target mRNAs through mRNA cleavage, translational repression and deadenylation (all reviewed in (Krol et al, 2010; Treiber et al, 2012)).

MiRNA biogenesis is tightly regulated at all different processing steps, for instance at miRNA transcriptional level and at Drosha and Dicer processing as well as at RISC stability, as miRNAs control various cellular processes and have tremendous effects on gene regulation (Finnegan & Pasquinelli, 2013).

3.3.2   MiRNA target recognition and function

MiRNAs are predicted to regulate about 50% of all protein coding genes (Lewis et al, 2005), however, the degree of regulation is quite modest, as even for overexpressed miRNA the downregulation of endogenous targets is less than 50% (Baek et al, 2008; Selbach et al, 2008). Furthermore, one miRNA can target several genes as well as one target can be regulated by multiple miRNAs. So, uncovering the function of specific miRNAs is labour intensive and challenging.

Several criteria were reported to be important for miRNA target recognition. Bartel summarised the main features of miRNA target recognition as the following: Perfect continuous Watson-Crick pairing between the mRNA and "seed" region of the miRNA (nucleotide 2-7 at the 5' end) is the primary determinant for target recognition. Beyond seed pairing supplementary and compensatory pairing of the miRNA 3' part can influence target recognition modestly. Furthermore, the site accessibility on the mRNA, which is mainly characterized by its local AU content, has an impact on target recognition (all reviewed in (Bartel, 2009)).

Based on these binding mechanisms, thermodynamic properties like site accessibility and target site conservation, several target prediction attempts have been proposed and developed (Huang et al, 2010). However, target prediction is still challenging, as the seed pairing is quite short and non-seed regions are difficult to predict. Furthermore, exceptions for miRNA targeting without seeds (Lal et al, 2009) and seed containing bulges (Chi et al, 2012) have been reported, building up to the complexity of miRNA target recognitions and its prediction.

In order to explore miRNA function, among other things, global effects of miRNA action on mRNA and protein levels were investigated using genome-wide approaches (Baek et al, 2008; Selbach et al, 2008). In these studies miRNA overexpression in mammalian cells was performed and subsequently mRNA and protein levels were analysed by microarray and mass spectrometry. Significant correlations between mRNA and protein of miRNA targets were found. This implements, that miRNAs not only change protein levels but also mRNA levels.

In animals, miRNAs modify gene expression by translation inhibition or mRNA degradation (reviewed in (Fabian et al, 2010; Huntzinger & Izaurralde, 2011)) (Figure 3.4). MiRNA mediated protein regulation can interfere at several steps with mRNA translation, in particular with translation initiation, elongation and even at the post-initiation level. The mRNA degradation process is initiated by miRISC recruitment of a deadenylase complex, which promotes deadenylation of miRNA-targeted mRNAs. The deadenylated mRNAs are less stable and subsequently degraded. These steps can occur in discrete cytoplasmic foci so-called processing (P) bodies as well as stress granules.

In summary, miRNAs act mainly through inhibiting translation and promoting deadenylation.

3.3.3 MiRNAs in pulmonary fibrosis

Since the discovery of the first miRNA lin-14, numerous miRNAs have been described to be involved in various physiological processes and disturbed miRNA expression is associated with pathologies, such as cancer and fibrosis (Mendell & Olson, 2012). In lung fibrosis, several miRNAs, among them miR-155, miR-21, miR-29 and let-7d, are reported to play a role in its pathophysiology (Pandit et al, 2011).

MiR-155 was the first miRNA reported to be associated with experimental lung fibrosis (Pottier et al, 2009). Bleomycin induced lung fibrosis in two different mouse strains revealed increased miR-155 levels during fibrosis progression. MiR-155 levels could be modulated by the cytokines TNF-α, IL-1β and TGF-β1 in human lung fibroblasts. Functional studies revealed that overexpression of miR-155 leads to downregulation of fibroblast growth factor 7 and to an increase of fibroblast migration. In IPF patients, miR-155 was increased as well, however increased serums levels could not be observed (Li et al, 2013).

Another upregulated miRNA in lung fibrosis is miR-21. Liu and colleagues found miR-21 increased in lungs from bleomycin-treated mice as well as in lungs of IPF tissue specimens. They demonstrated that miR-21 is a TGF-β1 target gene and that miR-21 is involved in TGF-β1-induced fibroblast activation via interference with Smad signalling. Importantly, miR-21 inhibition diminished the severity of experimental lung fibrosis *in vivo* (Liu et al, 2010). Furthermore, miR-21 was increased not only in lung fibrosis but also in cardiac fibrosis (Roy et al, 2009; Thum et al, 2008).

Besides these upregulated miRNAs, the miR-29 family is one of the downregulated miRNAs in fibrosis in general and in lung fibrosis specifically (Vettori et al, 2012). Cushing *et al.* showed decreased miR-29 levels in experimental fibrosis and revealed that miR-29 inhibition in human lung fibroblats led to upregulation of collagens and other fibrosis-related genes like integrins and laminins (Cushing et al, 2011). MiR-29 gene transfer showed the therapeutic potential of this miRNA in established experimental fibrosis (Xiao et al, 2012). MiR-29 is also regulated by TGF-β1 and is not only associated with lung fibrosis, but also with fibrotic disorders of the skin, heart, liver and kidney (Vettori et al, 2012). To this end, miR-29 regulates expression of extracellular matrix components in several organs.

Pandit and colleagues reported a functional role for miRNAs in experimental lung fibrosis and human IPF (Pandit et al, 2010). In particular, miRNA let-7d was found to be decreased in IPF. Let-7d was downregulated by TGF-β1 and inhibition of let-7d resulted in differential expression of mesenchymal and epithelial cell markers in ATII cells *in vitro* and *in vivo* (Pandit et al, 2010).

Altogether, in IPF altered miRNA levels lead to diseases progression and disturbed miRNA expression is closely related with profibrotic cytokine expression, especially to that of TGF-β1.

3.4 Aims of this study

It was previously shown that the matricellular WISP1 is highly increased in pulmonary fibrosis, and that interfering with WISP1 expression during disease development can have a major impact on disease progression and abrogates the fibrotic outcome. However, there is only limited knowledge about WISP1 regulation during fibrotic disease progression and nothing is known about miRNA-mediated regulation of WISP1 in lung fibrosis.

Therefore, the aims of this study were defined as the following:

1) Identification of miRNAs, which are both downregulated in IPF and predicted to bind to WISP1.
2) Anlysis of candidate miRNAs and WISP1 expression in IPF and experimental fibrosis tissue specimens as well as in single cells thereof.
3) Investigation of WISP1 regulation by candidate miRNAs *in vitro* and *ex vivo*.

To this end, miRNA data sets of IPF and experimental fibrosis were analysed and downregulated miRNAs were explored for their binding capacity with novel and established miRNA binding prediction tools. Expression analysis was conducted with qRT-PCR, Western Blot and ELISA. Binding analysis of candidate miRNAs to the WISP1 3'UTR were investigated with several luciferase reporter constructs. WISP1 mRNA and protein expression upon ectopic candidate miRNA overexpression and inhibition was determined. To shed light on miRNA-mediated WISP1 regulation during disease progression a profibrotic microenvironment was implemented *in vitro* and *ex vivo.* In order to do so, TGF-β1-treated cells were used for *in vitro* studies, and a TGF-β1-dependent experimental fibrosis model was investigated for the *ex vivo* studies.

Altogether, these analyses should provide insights if WISP1 was regulated by miRNAs in pulmonary fibrosis and how this contributed to disease development.

4 MATERIALS AND METHODS

4.1 Materials

4.1.1 Laboratory equipment and software

Table 4.1: Laboratory equipment

Product	Manufacturer
-80 °C freezer U570 HEF	New Brunswick; Hamburg, Germany
-20 °C freezer MediLine LGex 410	Liebherr; Biberach, Germany
Agarose gel running chamber	Biorad; Hercules, USA
Analytical scale XS20S Dual Range	Mettler Toledo; Gießen, Germany
Autoclave DX-45	Systec; Wettenberg, Germany
Autoclave VX-120	Systec; Wettenberg, Germany
Bacterial shaker Innova 42	New Brunswick; Hamburg, Germany
Cell counter Casy Modell TT	Roche Diagnostics; Mannheim, Germany
Cell culture work bench Herasafe KS180	Thermo Fisher Scientific; Schwerte, Germany
Centrifuge MiniSpin plus	Eppendorf; Hamburg, Germany
Centrifuge Rotina 420R	Hettich; Tuttlingen, Germany
Centrifuge with cooling, Micro200R	Hettich; Tuttlingen, Germany
CO_2 cell Incubator BBD6620	Thermo Fisher Scientific; Schwerte, Germany
Demineralized water	Thermo Fisher Scientific; Schwerte, Germany
Dispenser, Ceramus 2-1 ml	Hirschmann Laborgeräte; Eberstadt, Germany
Dry ice container Forma 8600 Series, 8701	Thermo Fisher Scientific; Schwerte, Germany
Electronic pipet filler	Eppendorf; Hamburg, Germany
Electrophoretic Transfer Cell, Mini Protean Tetra Cell	Biorad; Hercules, USA
Film developer Curix 60	AGFA; Morsel, Belgium
Fluorescence Mikroscope AxioImager M2	Zeiss; Jena, Germany
Fridge MediLine LKv 3912	Liebherr; Biberach, Germany
Gel electrophoresis chamber MINIeasy	Carl Roth; Karlsruhe, Germany
Gel imaging system ChemiDoc XRS+	Biorad; Hercules, USA
Ice machine ZBE 110-35	Ziegra; Hannover, Germany
Intelli-Mixer RM-2	Schubert & Weiss Omnilab; Munich, Germany
Light Cycler LC480II	Roche Diagnostics; Mannheim, Germany
Liquid nitrogen cell tank BioSafe 420SC	Cryotherm; Kirchen/Sieg, Germany
Liquid nitrogen tank Apollo 200	Cryotherm; Kirchen/Sieg, Germany
Magnetic stirrer KMO 2 basic	IKA; Staufen, Germany

Product	Manufacturer
Mastercycler gradient	Eppendorf; Hamburg, Germany
Mastercycler Nexus	Eppendorf; Hamburg, Germany
Microbiological Incubator HERATherm IGS60	Thermo Fisher Scientific; Schwerte, Germany
Sartorius Micro-Dismembrator S	Thermo Fisher Scientific; Schwerte, Germany
Microscope Axio Imager M2 (flourescence)	Zeiss; Jena, Germany
Microscope Axiovert 40	Zeiss; Jena, Germany
Microscope LSM 710 (confocal)	Zeiss; Jena, Germany
Multipette stream	Eppendorf; Hamburg, Germany
NanoDrop 1000	PeqLab; Erlangen, Germany
pH meter InoLab pH 720	WTW; Weilheim, Germany
Pipettes Research Plus	Eppendorf; Hamburg, Germany
Plate centrifuge 5430	Eppendorf; Hamburg, Germany
Plate reader TriStar LB941	Berthold Technologies; Bad Wildbach, Germany
Plate reader Sunrise	Tecan; Crailsheim, Germany
Roll mixer	VWR International; Darmstadt, Germany
Power supply Power Pac HC	Biorad; Hercules, USA
Scale XS400 2S	Mettler Toledo; Gießen, Germany
Shaker Duomax 1030	Heidolph; Schwabach, Germany
Thermomixer compact	Eppendorf; Hamburg, Germany
Ultra pure water supply MilliQ Advantage A10	Merck Millipore; Darmstadt, Germany
LSM top table centrifuge MCF-2360	Schubert & Weiss Omnilab; Munich, Germany
Vortex Mixer	IKA; Staufen, Germany
Vacuum pump NO22AN.18 with switch 2410	KNF; Freiburg, Germany
Water bath Aqua Line AL 12	Lauda; Lauda-Königshofen, Germany

Table 4.2: Software

Software	Producer
Axio Imager Software	Zeiss; Jena, Germany
Endnote X6	Thomson Reuters; San Francisco, USA
GATC Viewer	GATC; Konstanz, Germany
GraphPad Prism 5	GraphPad Software; La Jolla, USA
Imaris Software, Version	Bitplane; Zurich, Switzerland
Image Lab Version	Biorad; Hercules, USA
LightCycler® 480 SW 1.5	Roche Diagnostics; Mannheim, Germany
Vector NTI Advanced 9	Invitrogen, Life Technologies; Carlsbad, USA
Magelan Software	Tecan; Crailsheim, Germany
Tristar MicroWin 2000	Berthold Technologies; Bad Wildbach, Germany

4.1.2 Chemicals and consumables

Table 4.3: Chemicals and reagents

Product	Manufacturer
0.25% Trypsin - EDTA solution	Sigma-Aldrich; Taufkirchen, Germany
87% Glycerol	AppliChem; Darmstadt, Germany
Agar bacteriology grade	AppliChem; Darmstadt, Germany
Agarose Biozym	Biozym Scientific GmbH; Oldendorf, Germany
Ampicillin sodium salt	Carl Roth; Darmstadt, Germany
Ammonium peroxodisulfate (APS)	AppliChem; Darmstadt, Germany
Bovine serum albumin (BSA)	Sigma-Aldrich; Taufkirchen, Germany
Bromophenol blue	AppliChem Darmstadt, Germany
Casyton	Roche Diagnostics; Mannheim, Germany
Chloroform	AppliChem; Darmstadt, Germany
Complete® Mini without EDTA (Protease-inhibitor)	Roche Diagnostics; Mannheim, Germany
Coomassie Brilliant Blue R-250 staining solution	BioRad; Hercules, USA
DAPI (4', 6-diamidino-2-phenylindole)	Sigma-Aldrich; Taufkirchen, Germany
Desoxyribonucleotides mix (dNTPs)	Fermentas, Thermo Fisher Scientific; Schwerte Germany
Dimethyl sulfoxide (DMSO)	Carl Roth; Karlsruhe, Germany
Dithiothreitol (DTT)	AppliChem; Darmstadt, Germany
Ethanol, p.a.	AppliChem; Darmstadt, Germany
Foetal bovine serum (FBS) "GOLD", heat inactivated	PAA, GE Healthcare; Freiburg, Germany
Fluorescence mounting medium	Dako; Hamburg, Deutschland
Glucose	AppliChem; Darmstadt, Germany
Glycine, molecular biology grade	AppliChem; Darmstadt, Germany
Isopropanol, p.a.	AppliChem; Darmstadt, Germany
Light Cycler 480 SybrGreen l Master Mix	Roche Diagnostics; Mannheim, Germany
Lipofectamine2000	Invitrogen, Life Technologies; Carlsbad, USA
Lipofectamine LTX with PLUS reagent	Invitrogen, Life Technologies; Carlsbad, USA
Lipofectamine RNAiMAX	Invitrogen, Life Technologies; Carlsbad, USA
Methanol, p.a.	AppliChem; Darmstadt, Germany
Non-fat dried milk powder	AppliChem; Darmstadt, Germany
Nonidet P-40	AppliChem; Darmstadt, Germany
Paraformaldehyde (PFA)	AppliChem; Darmstadt, Germany
Penicillin-Streptomycin (10 000 U/ml)	Gibco, Life Technologies; Carlsbad, USA
Peptone from Casein	AppliChem; Darmstadt, Germany

Product	Manufacturer
Ponceau S solution	Sigma-Aldrich; Taufkirchen, Germany
Poly-L-lysine (0.01% solution)	Sigma-Aldrich; Taufkirchen Germany
Random hexamers	Applied Biosystemes, Life Technologies; Carlsbad, USA
Recombinant human TGF-β1 protein	R&D Systems; Minneapolis, USA
Recombinant human WISP1 protein	R&D Systems; Minneapolis, USA
Rotiphorese Gel 30 (37,5:1) 500ml	Carl Roth; Darmstadt, Germany,
Sodium dodecyl sulphate (SDS) pellets	Carl Roth; Darmstadt, Germany
Sodium chloride	AppliChem; Darmstadt, Germany
SuperSignal West Dura Extended Duration Substrate	Pierce, Thermo Fisher Scientific; Schwerte, Germany
SuperSignal West Femto Substrate	Pierce, Thermo Fisher Scientific; Schwerte Germany
SybrSafe (10 000x in DMSO)	Invitrogen Life Technologies; Carlsbad, USA
TEMED	AppliChem; Darmstadt, Germany
Tris base, buffer grade	AppliChem; Darmstadt, Germany
Triton X-100	AppliChem; Darmstadt, Germany
Tween 20	AppliChem; Darmstadt, Germany
UltraPure DNase/RNase-Free Distilled Water	Invitrogen, Life Technologies; Carlsbad, USA
Yeast extract	AppliChem; Darmstadt, Germany

Table 4.4: Consumables

Product	Manufacturer
96 well MaxiSorp ELISA plate	Nunc; Wiesbaden, Germany
96 well plates, white, for luciferase assay	Berthold Technologies; Bad Wildbad, Germany
Amicon Ultra 3K-0.5 mL centrifugal filters	Merck Millipore; Billerica, USA
Cell culture dishes	Corning, Thermo Fisher Scientific; Schwerte; Germany
Cell culture flasks	Nunc; Wiesbaden, Germany
Cell culture multi well plates	TPP Techno Plastic Products; Trasadingen, Switzerland
Cell scraper/lifter	Corning, Thermo Fisher Scientific; Schwerte, Germany
Chamber slides	BD Bioscience; Heidelberg, Germany
Cryovials 1.5 ml	Greiner Bio-One; Frickenhausen, Germany
Cryovials for microdismembrator 1.2 ml	Nalgene, Thermo Fisher Scientific; Schwerte, Germany
Falcon tubes (5 ml, 50 ml)	BD Bioscience; Heidelberg, Germany
Filter tips	Biozym Scientific; Hessisch Oldendorf, Germany

Product	Manufacturer
Glas Pasteur pipettes	VWR International; Darmstadt, Germany
Hyperfilm ECL Film	Amersham, GE Healthcare; Freiburg, Germany
Measuring pipettes sterile, single use (2, 5, 10, 25 and 50 ml)	VWR International; Darmstadt, Germany
Nylon filters, pore size 70 µm	BD Bioscience; Heidelberg, Germany
PCR plates	Kisker Biotech; Steinfurt, Germany
Reaction tubes (0.5, 1.5 and 2 ml)	Eppendorf; Hamburg, Germany Greiner Bio-One; Frickenhausen, Germany
Stainless steel grinding balls (9 mm)	Neolab; Heidelberg, Germany
Sealing foil for PCR plates	Kisker Biotech; Steinfurt, Germany
Tips	Eppendorf; Hamburg, Germany Kisker Biotech; Steinfurt, Germany
Whatman blotting paper 3 mm	GE Healthcare; Freiburg, Germany

4.1.3 Buffers and solutions

Buffer / Solution	Concentration	Substance
DNA loading buffer (6x) (Fermentas, Thermo Fisher Scientific; Schwerte, Germany)	10 mM 0.03% 0.03% 60% 60 mM	Tris/HCl, pH 7.6 Bromophenol blue Xylene cyanol FF Glycerol EDTA
Fast Digest buffer (10x) (Fermentas, Thermo Fisher Scientific; Schwerte, Germany)	-	-
HEPES (N-2-hydroxyethylpiperazine-N-2- ethane sulfonic acid) (Gibco, Life Technologies; Carlsbad, USA)	1 M	HEPES
High Fidelity (HF) buffer (5x) (Finnzymes, Thermo Fisher Scientific; Schwerte, Germany)	-	-
Laemmli loading buffer (4x)	8% (w/v) 40% (v/v) traces 250 mM 400 mM	SDS Glycerol Bromophenol blue Tris/HCl, pH 6.8 DTT freshly added
PBS pH 7.4 (10x)	1.37 M 27 mM 100 mM 20 mM	NaCl KCl Na_2HPO_4 KH_2PO_4

Buffer / Solution	Concentration	Substance
Restore Plus Western Blot stripping buffer (Pierce, Thermo Fisher Scientific; Schwerte Germany)	-	-
RIPA protein lysis buffer	150 mM 10 mM 0.1% (w/v) 1% (v/v) 1% (w/v) 5 mM	NaCl Tris/HCl, pH 7.2 SDS Triton X-100 Sodium deoxycholate EDTA
SDS-PAGE running buffer	250 mM 1.92 M 1% (w/v)	Tris/HCl, pH 7.4 Glycine SDS
T4 Ligation buffer (Fermentas, Thermo Fisher Scientific; Schwerte, Germany)	400 mM 100 mM 100 mM 5 mM	Tris/HCl, pH 7.8 MgCl$_2$ DTT ATP
TAE (50x)	2 M 5.71% (v/v) 50 mM	Tris/HCl Glacial acetic acid EDTA, pH 8
TBS, pH 7.4 (10x)	10 mM 150 mM	Tris/HCl pH 7.4 NaCl
TBST		TBS supplemented with 0.05% Tween-20
TE buffer pH 8.0 (Ambion, Life Technologies; Carlsbad, USA)	10 mM 1 mM	Tris pH 8.0 EDTA
Transfer buffer (10x)	50 mM 400 mM	Tris/HCl Glycine
Transfer buffer (1x)	10% 200 ml	10x Transfer Buffer Methanol

4.1.4 Standards and kits

Table 4.5: Standards

Product	Manufacturer
1 kb DNA ladder	Peqlab; Erlangen, Germany
100 bp DNA ladder	Peqlab; Erlangen, Germany
Ultra low range DNA ladder I	Peqlab; Erlangen, Germany
Protein marker V	Peqlab; Erlangen, Germany

Table 4.6: Kits

Product	Manufacturer
BCA Protein Assay Kit	Pierce, Thermo Fisher Scientific; Schwerte, Germany
RNase-Free DNase Set	Qiagen; Hilden, Germany
Dual-Luciferase Reporter Assay System	Promega; Mannheim, Germany
hWISP1 DuoSet ELISA (DY1627)	R&D Systems; Minneapolis, USA
mWISP1 ELISA	Uscn Life Science; Hubei, China
miRNeasy Mini Kit	Qiagen; Hilden, Germany
miScript II Reverse Transcription Kit	Qiagen; Hilden, Germany
miScript SYBR Green PCR Kit	Qiagen; Hilden, Germany
RNeasy Mini Kit	Qiagen; Hilden, Germany
peqGOLD Cycle-Pure Kit	Peqlab; Erlangen, Germany
peqGOLD Gel Extraction Kit	Peqlab; Erlangen, Germany
peqGOLD Tissue DNA Mini Kit	Peqlab; Erlangen, Germany
Qiagen HiSpeed Plasmid Midi Kit	Qiagen; Hilden, Germany
Qiagen Plasmid Mini Kit	Qiagen; Hilden, Germany
TaqMan Un Master Mix II, no UNG	Applied Biosystems, Life Technologies; Carlsbad, USA
TaqMan MicroRNA Reverse Transcription Kit	Applied Biosystems, Life Technologies; Carlsbad, USA

4.1.5 Enzymes

Product	Manufacturer
Collagenase I	Biochrom; Berlin, Germany
Dispase	BD Bioscience; Heidelberg, Germany
DNase I	AppliChem; Darmstadt, Germany
FastAP Thermosensitive Alkaline Phosphatase	Fermentas, Thermo Fisher Scientific; Schwerte, Germany
FastDigest EcoRV	Fermentas, Thermo Fisher Scientific; Schwerte, Germany
FastDigest NotI	Fermentas, Thermo Fisher Scientific; Schwerte, Germany
FastDigest SacI	Fermentas, Thermo Fisher Scientific; Schwerte, Germany
FastDigest XhoI	Fermentas, Thermo Fisher Scientific; Schwerte, Germany
Phusion Hot Start II High Fidelity Polymerase	Fermentas, Thermo Fisher Scientific; Schwerte, Germany
RNase inhibitor 20U/μl	Invitrogen, Life Technologies; Carlsbad, USA

Product	Manufacturer
T4 DNA Ligase	Fermentas, Thermo Fisher Scientific; Schwerte, Germany
MuLV Reverse Transcriptase 5 000 U	Invitrogen, Life Technologies; Carlsbad, USA

4.1.6 Plasmids

Identification	Description	Origin
pCMV6-A-GFP	Precision shuttle mammalian vector with independent turboGFP expression	OriGene; Rockville, USA
pCMV6-XL6	Negative control vector to WISP1 expression vector	OriGene; Rockville, USA
pCMV6-XL6 hWISP1	WISP1 expression under a CMV promoter	OriGene; Rockville, USA
pMi30a	pmirGLO vector containing 3x WISP1 3'UTR hsa-miR 30a binding site	generated within this study
pMi30d	pmirGLO vector containing 3x WISP1 3'UTR hsa-miR 30d binding site	generated within this study
pMi92a	pmirGLO vector containing 3x WISP1 3'UTR hsa-miR 92a binding site	generated within this study
pMi203a	pmirGLO vector containing 3x WISP1 3'UTR hsa-miR 203 binding site	generated within this study
pmirGLO	quantitative measurement to study miRNA activity with luciferase assays	Promega; Darmstadt, Germany
pmirGLOW	pmirGLO vector containing the full length hWISP1 3'UTR at the MCS	generated within this study
pmirGLOW1	pmirGLO vector containing the hWISP1 3'UTR from nt 1 – nt 1145 at the MCS	generated within this study
pmirGLOW2	pmirGLO vector containing the hWISP1 3'UTR from nt 1160 – nt 2041 at the MCS	generated within this study
pmirGLOW3	pmirGLO vector containing the hWISP1 3'UTR from nt 1971 – nt 3979 at the MCS	generated within this study
pSi30a	pmirGLO vector containing 2x the reverse complement sequence of hsa-miR-30a	generated within this study
pSi30d	pmirGLO vector containing 2x the reverse complement sequence of hsa-miR-30d	generated within this study
pSi92a	pmirGLO vector containing 2x the reverse complement sequence of hsa-miR-92a	generated within this study
pSi203	pmirGLO vector containing 2x the reverse complement sequence of hsa-miR-203a	generated within this study

In general, lyophilised, desalted oligonucleotides were purchased form Eurofins MWG Operon; Ebersberg, Germany and dissolved in DNase/RNAse–free water to obtain a 100 µM concentration. Oligonucleotids for plasmid generation of pSi and pMi plasmids were purchased from Metabion International AG; Martinsried, Germany. These oligonucleotides were HPLC purified and analysed by mass spectrometry.

4.1.6.1 *Molecular cloning*

Table 4.7: Oligonucleotides for plasmid generation

Generated plasmid	Oligonucleotides	Sequence 5' - 3'
pMi30a	Mi30a_1fw	CGATATCGAACCAGCTCTCATCACACATTTAAAAGATGATTCTGTTTACCGAACCAGCTCTCATCACACATTTAAAAGATGATTCTGTTTACCGAACCAGCTCTCATCACACATTTAAAAGATGATTCTGTTTACCC
	Mi30a_1rv	TCGAGGGTAAACAGAATCATCTTTTAAATGTGTGATGAGAGCTGGTTCGGTAAACAGAATCATCTTTTAAATGTGTGATGAGAGCTGGTTCGGTAAACAGAATCATCTTTTAAATGTGTGATGAGAGCTGGTTCGATATCGAGCT
pMi30d	Mi30a_2fw	CGATATCTCTCCACTGATTGAGTGTTTACTTCTCCACTGATTGAGTGTTTACTTCTCCACTGATTGAGTGTTTACTC
	Mi30a_2rv	TCGAGAGTAAACACTCAATCAGTGGAGAAGTAAACACTCAATCAGTGGAGAAGTAAACACTCAATCAGTGGAGAGATATCGAGCT
pMi92a	Mi92a_fw	CGATATCATAGGAAAACATTGCAATAATAGGAAAACATTGCAATAATAGGAAAACATTGCAATAC
	Mi92a_rv	TCGAGTATTGCAATGTTTTCCTATTATTGCAATGTTTTCCTATTATTGCAATGTTTTCCTATGATATCGAGCT
pMi203a	Mi203_fw	CGATATCCCCGTGTTCAGGACACATCTATTGCAGAGACTCATTTCACCCCGTGTTCAGGACACATCTATTGCAGAGACTCATTTCACCCCGTGTTCAGGACACATCTATTGCAGAGACTCATTTCACC
	Mi203_rv	TCGAGGTGAAATGAGTCTCTGCAATAGATGTGTCCTGAACACGGGGTGAAATGAGTCTCTGCAATAGATGTGTCCTGAACACGGGGTGAAATGAGTCTCTGCAATAGATGTGTCCTGAACACGGGGATATCGAGCT
pmirGLOW	3'UTR XhoI_WISP1 fw1	CACTATCTCGAGGTAGCAGGCACAAATCTTGGGTCTTG
	3'UTR NotI_WISP1 rv1	GTACTAGCGGCCGCTGATTCCACCATCTGCACATTTATTGAAC
pmirGLOW1	3'UTR XhoI_WISP1 fw1	CACTATCTCGAGGTAGCAGGCACAAATCTTGGGTCTTG
	3'UTR NotI 1kb_rv	GTACTAGCGGCCGCTGAGGTCAGCAGAACGAAAGGCTGTG
pmirGLOW2	3'UTR XhoI_sec_fw	CACTATCTCGAGGTACTGGTAGGAAGATGGAGGTTTACCG

Generated plasmid	Oligonucleotides	Sequence 5' - 3'
	3'UTR NotI_sec_rv	GTACTAGCGGCCGCTGACATGTAGCTTTGGAAGAAGAGAGCTTCG
pmirGLOW3	3'UTR XhoI_thr_fw	CACTATCTCGAGGTACTTGATGAATACAGGAAGCTGTGCATG
	3'UTR NotI_WISP1 rv1	GTACTAGCGGCCGCTGATTCCACCATCTGCACATTTATTGAAC
pSi30a	Si30a_fw	CGATATCCTTCCAGTCGAGGATGTTTACACTTCCAGTCGAGGATGTTTACAC
	Si30a_rv	TCGAGTGTAAACATCCTCGACTGGAAGTGTAAACATCCTCGACTGGAAGGATATCGAGCT
pSi30d	Si30d_fw	CGATATCCTTCCAGTCGGGGATGTTTACACTTCCAGTCGGGGATGTTTACAC
	Si30d_rv	TCGAGTGTAAACATCCCCGACTGGAAGTGTAAACATCCCCGACTGGAAGGATATCGAGCT
pSi92a	Si92a_fw	CGATATCACAGGCCGGGACAAGTGCAATAACAGGCCGGGACAAGTGCAATAC
	Si92a_rv	TCGAGTATTGCACTTGTCCCGGCCTGTTATTGCACTTGTCCCGGCCTGTGATATCGAGCT
pSi203	Si203_fw	CGATATCCTAGTGGTCCTAAACATTTCACCTAGTGGTCCTAAACATTTCACC
	Si203_rv	TCGAGGTGAAATGTTTAGGACCACTAGGTGAAATGTTTAGGACCACTAGGATATCGAGCT

4.1.6.2 *SiRNA*

WISP1 siRNAs and control siRNAs were purchased from Dharmacon, Thermo Fisher Scientific; Schwerte, Germany. The lyophilised products were dissolved in sterile, DNase/RNase-free water in order to obtain 100 µM stock solutions, and stored at -80 °C. The stock solutions were diluted with water 1:10 in order to obtain 10 µM working solution.

siRNA	Target sequence 5' - 3'
ON-TARGETplus human WISP1 siRNA #6	AACCUGAGCUGUAGGAAUC
ON-TARGETplus human WISP1 siRNA #7	CCAACUAGGCAGGCACAAA
ON-TARGETplus human WISP1 siRNA #8	ACUCGGAUCUCCAAUGUUA
ON-TARGETplus Non-targeting pool (pool of 4 siRNAs)	UGGUUUACAUGUCGACUAA UGGUUUACAUGUUGUGUGA UGGUUUACAUGUUUUCUGA UGGUUUACAUGUUUUCCUA

4.1.6.3 *Sequencing primers*

Primer name	Sequence 5' - 3'
pmirGLOW 3'UTR fw	GGTGTTGTGTTCGTGGACGAGG
pmiRGLOW_fw2	AGGGCTTTGGGCAGTTGGC
pmirGLOW_fw3	CATCGGAACCAGCTCTCATCAC
pmirGLOW_fw4	CAGAATTTCCCTGCAATGGTGTG
pmirGLOW_fw5	GCCTTGTACTGTGTGTGCATAGC
pmirGLOW_fw6	GCATCTGTGCGGTATTTCACACC
pmirGLOW_fw7	CTCCTGGATCACTACAAGTACCTCACC
pmirGLOW_fw8	GACCTGTCCGGTGCCCTG
pmirGLOW_fw9	TTGTCCAGATAGCCCAGTAGCTGAC
pmirGLOW_fw10	TAGACTGGATGGAGGCGGATAAAG
pmirGLOW_fw11	GGTAGCTCTTGATCCGGCAAAC
pmirGLOW_fw12	CGCTGAGCAATGGAAGCGG
pmirGLOW_fw13	AGCAAGACCGACTACCAGGGCTTC
pmirGLOW_fw14	CGAGGCTACAAACGCTCTCATCG

4.1.6.4 *MiRNA – mimics and inhibitors*

MiRIDIAN miRNA mimics and hairpin inhibitors were purchased from Dharmacon, Thermo Fisher Scientific; Schwerte, Germany. 5 nmol of lyophilised product was dissolved in 500 µl sterile, DNase/RNase–free water to obtain 10 µM stock solutions. The stock solutions were aliquoted and stored at -80 °C. A Cy3-labelled pre-miR negative control #1 was purchased from Applied Biosystems, Life Technologies; Carlsbad, USA.

MiRNA inhibitor/mimic	Mature miRNA sequence 5' - 3'
hsa-miR-30a	UGUAAACAUCCUCGACUGGAAG
hsa-miR-30d	UGUAAACAUCCCCGACUGGAAG
hsa-miR-92a	UAUUGCACUUGUCCCGGCCUGU
hsa-miR-203	GUGAAAUGUUUAGGACCACUAG
cel-miR-67 "negative control I"	UCACAACCUCCUAGAAAGAGUAGA
cel-miR-239b "negative control II"	UUGUAUACACAAAAGUACUG
miRNA mimic housekeeping positive control #2 GAPDH	-

4.1.6.5 *MiScript primer assays*

All miScript primer assays were purchased from Qiagen; Hilden, Germany. The lyophilised product was reconstituted in 550 µl TE buffer pH 8.0, mixed by vortexing and stored at -20 °C.

Assay name	Assay ID
hs_RNU6-2_1	MS00033740
hs_miR-92_1	MS00006594
hs_miR-30d_2	MS00009387
hs_miR-30a-5p_1	MS00007350
hs_miR-203_1	MS00003766

4.1.6.6 *TaqMan assays*

TaqMan microRNA assays were purchased from Applied Biosystems, Life Technologies; Carlsbad, USA.

Assay name	Assay ID
hsa-miR-30a	000417
hsa-miR-30d	000431
hsa-miR-92a	000431
hsa-miR-203	000507
hsa-miR-338	000548
snoRNA202 mouse control miRNA assay	001232
RNU43 human control miRNA assay	001095

4.1.6.7 *Quantitative PCR*

In general, primers for quantitative PCR were designed with PrimerBLAST from NCBI (http://www.ncbi.nlm.nih.gov/tools/primer-blast/) and give an amplicon with 80-150 bp length, maximal with 200 bp length.

Table 4.8: Human quantitative PCR primers

Gene	Direction	Sequence 5' - 3'
ACTA2	fw	CGAGATCTCACTGACTACCTCATGA
	rv	AGAGCTACATAACACAGTTTCTCCTTGA
COL1A1	fw	CAAGAGGAAGGCCAAGTCGAG
	rv	TTGTCGCAGACGCAGATCC
CTGF	fw	CCTGCAGGCTAGAGAAGCAGA
	rv	TTTGGGAGTACGGATGCACTT

Gene	Direction	Sequence 5' - 3'
CYR61	fw	AAAGGCAGCTCACTGAAGCG
	rv	GCACTGGGACCATGAAGTTGT
FN1	fw	CCGACCAGAAGTTTGGGTTCT
	rv	CAATGCGGTACATGACCCCT
GAPDH	fw	TGACCTCAACTACATGGTTTACATG
	rv	TTGATTTTGGAGGGATCTCG
HPRT1	fw	AAGGACCCCACGAAGTGTTG
	rv	GGCTTTGTATTTTGCTTTTCCA
NOV	fw	CCGTCAATGTGAGATGCTGAA
	rv	TTGGTGCGGAGACACTTTTTT
SERPINE1	fw	GACATCCTGGAACTGCCCTA
	rv	GGTCATGTTGCCTTTCCAGT
WISP1	fw	GGCATGAGGTGGTTCCTG
	rv	GGAGCTGGGGTAAAGTCCAT
WISP2	fw	TACAGGTGCCAGGAAGGTGC
	rv	CAGATGCAGGAGTGACAAGGG
WISP3	fw	GGCGTGTGCGCATATCTTG
	rv	AGGCAGCTGAACAGTGGGTG

Table 4.9: Murine quantitative PCR primers

Gene	Direction	Sequence 5' - 3'
Hprt1	fw	CCTAAGATGAGCGCAAGTTGAA
	rv	CCACAGGACTAGAACACCTGCTAA
Wisp1	fw	GTCCTGAGGGTGGGCAACAT
	rv	GGGCGTGTAGTCGTTTCCTCT

Table 4.10: Rat quantitative PCR primers

Gene	Direction	Sequence 5' - 3'
Col1a1	fw	ACTGCCCTCCTGACGCATGG
	rv	CACAGCCGTGCCATTGTGGC
Gapdh	fw	GTGATGGGTGTGAACCACGAG
	rv	CCACGATGCCAAAGTTGTCA
Fn1	fw	GCAACGGCAGAGGGGAGTGG
	rv	CACAGTGGCCGTACGGTGCG
Wisp1	fw	AACCTGCGGCCATGTGA
	rv	TGGTACACAGCCAGGCATTTC

4.1.7 Antibodies

Table 4.11: Primary antibodies for WB

Antigen	Source	Dilution	Solution	Manufacturer
WISP1 AF1627	Goat	1:1 000	2.5% milk in TBST	R&D Systems; Minneapolis, USA
α-SMA ab5694	Rabbit	1:2 000	5% BSA in TBST	Abcam; Cambridge, UK
COL1A1 600-401-103	Rabbit	1:5 000	5% BSA in TBST	Rockland Immunochemicals; Gilbertsville, USA
BSA sc-57504	Mouse	1:100	5% milk inTBST	Santa Cruz Biotechnology; Dallas, USA

Table 4.12: Primary antibodies for immunofluorescence

Antigen	Source	Dilution	Solution	Manufacturer
COL1A1 600-401-103	Rabbit	1:100	0.1% BSA in PBS	Rockland Immunochemicals; Gilbertsville, USA
α-SMA A5228	Mouse	1:500	0.1% BSA in PBS	Sigma; Taufkirchen, Germany
hWISP1 sc-25441	Rabbit	1:50	0.1% BSA in PBS	Santa Cruz Biotechnology; Dallas, USA
FN1 ab6328	Mouse	1:200	0.1% BSA in PBS	Abcam; Cambridge, UK

Table 4.13: Secondary antibodies for immunofluorescence

Antigen	Source	Dilution	Solution	Manufacturer
Rabbit-IgG (H-L), Alexa Fluor 555 conjugated A21429	Goat	1:1 000	0.1% BSA in PBS	Molecular Probes, Invitrogen; Carlsbad, USA
Mouse-IgG, FITC conjugated F0479	Goat	1:500	0.1% BSA in PBS	Dako; Hamburg, Germany
Mouse-IgG- Alexa Fluor 548 conjugated A11030	Rabbit	1:1000	0.1% BSA in PBS	Molecular Probes, Invitrogen; Carlsbad, USA

Table 4.14: Secondary antibodies for WB, HRP-linked

Antigen	Source	Dilution	Solution	Manufacturer
Goat IgG 611620	Rabbit	1: 20 000	5% milk TBST	Invitrogen, Life Technologies; Carlsbad, USA
Mouse IgG NA931V	Sheep	1:20 000	5% milk in TBST	GE Healthcare; Freiburg, Germany
Rabbit IgG NA934V	Donkey	1:30 000	5% milk in TBST	GE Healthcare; Freiburg, Germany

Table 4.15: Directly HRP-conjugated antibodies for WB

Antigen	Source	Dilution	Solution	Manufacturer
β-actin A3854	Mouse	1:50 000	5% milk in TBST	Sigma Aldrich; Taufkirchen, Germany
GAPDH 3683	Rabbit	1:2 000	5% BSA in TBST	Cell Signaling Technology; Boston, USA

4.1.8 Bacteria

One Shot TOP10 chemical competent *E. coli* were purchased from Invitrogen, Life Technologies; Carlsbad, USA, and cultured in LB medium or in SOC medium following transformation. LB medium was sterilized by autoclaving and 50 µg/ml ampicillin were added.

Medium	Concentration	Substance
LB medium, pH 7.2	1% (w/v)	NaCl
	0.5% (w/v)	Yeast extract
	1% (w/v)	Peptone
SOC medium, pH 7 (Invitrogen, Life Technologies; Carlsbad, USA)	0.5% (w/v)	Yeast extract
	2% (w/v)	Peptone
	10 mM	NaCl
	2.5 mM	KCl
	10 mM	$MgCl_2$
	10 mM	$MgSO_4$
	20 mM	Glucose

For the manufacturing of agar plates, 15 g bacto-agar were added to 1 l of LB medium, autoclaved, cooled down to 60 °C, 50 µg/ml ampicillin added and poured into petri dishes.

4.1.9 Cell lines and primary cells

Table 4.16: Commercially available cell lines and primary cells

Cell line name	Description	Supplier
16HBE14o-	Human bronchial epithelial cells	Kind gift of S. Krauss-Etschmann; Helmholtz Zentrum Munich (originally established by Dr. Grünert)
A549	Human lung carcinoma cells	ATCC; LGC Standards; Wesel, Germany
HEK 293T	Human embryonic kidney epithelial cells	Kind gift of V. Heismeier; Helmholtz Zentrum Munich
HFL1	Human foetal lung fibroblasts	ATCC, LGC Standards; Wesel, Germany
Mlg	Murine newborn lung fibroblasts	ATCC, LGC Standards; Wesel, Germany
MLE12	Murine lung epithelial cells, SV40 transformed	ATCC, LGC Standards; Wesel, Germany
MRC5	Human foetal lung fibroblasts	ATCC, LGC Standards; Wesel, Germany
Human bronchial epithelial primary cells (phBEC)	-	PromoCell; Heidelberg, Germany

Table 4.17: Primary murine cells

Cell type	Source
Primary murine alveolar type II (pmATII) cells	C57BL/6N mice, Charles River; Sulzfeld, Germany
Primary murine lung fibroblasts (pmFB)	C57BL/6N mice, Charles River; Sulzfeld, Germany

Table 4.18: Primary human fibroblasts cell sources, all categorized as "non-fibrotic"

Identification	Tissue information
ASK006	Non-carcinogenic lung tissue resection from patient with adenocarcinoma and COPD
ASK013	Non-carcinogenic lung tissue resection from patient with lung metastasis of leiomyosarcoma of the uterus
MLT003	Lung explant/donor lung
MLT005	Lung explant of α1-antitrypsin deficiency/emphysema
MLT013.01	Lung explant/donor lung
MLT014	Lung explant/donor lung

Table 4.19: Primary human fibroblasts, a kind gift of E. S. White

Identification	Fibroblast information
L0028	Fibrotic origin
L0026	Fibrotic origin
S101B	Fibrotic origin
S099B	Fibrotic origin
S086A	Fibrotic origin
L0032	Fibrotic origin
L0029	Non-fibrotic origin
L0031	Non-fibrotic origin
L0024	Non-fibrotic origin
L0025	Non-fibrotic origin

Table 4.20: Cell culture media

Identification	Manufacturer
D-MEM/F12	Gibco, Life Technologies; Carlsbad, USA
DMEM (low glucose)	Sigma Aldrich; Taufkirchen, Germany
Hams-F12	Lonza; Basel, Switzerland
MEM	Gibco, Life Technologies; Carlsbad, USA
RPMI 1640	Gibco, Life Technologies; Carlsbad, USA
OptiMEM – I Reduced Serum Medium	Gibco, Life Technologies; Carlsbad, USA
Airway Epithelial Cell Growth Medium	PromoCell; Heidelberg, Germany

4.1.10 Animals

Six to eight weeks old female C57BL/6N mice were purchased from Charles River Laboratories; Sulzfeld, Germany, and could settle down for at least one week. All mice were housed under standard conditions and had access to water and standard rodent chow *ad libidum*.

4.1.11 Human Tissue

Human tissue specimens from IPF patients and donors were obtained as described in (Zuo et al, 2010). The study protocol was approved by the Ethics Committee at the Justus-Liebig-University School of Medicine; Gießen, Germany. Informed consent was received in written form from each subject for the study protocol. Total RNA from human tissue specimens was used for miRNA expression analysis. Human tissue for primary human fibroblasts (phFB) isolations was obtained from lung tissue biopsies, resections and explanted lungs from the University Hospital Großhadern of the LMU (Ludwig-Maximilians-University, Munich). Participants provided written informed consent to participate in this study, in accordance with approval by the local ethics committee of the Ludwig-Maximilians-University of Munich, Germany (Project 333-10).

4.2 Methods

All microbiology and molecular biology methods were performed according to common laboratory practice described in "Molecular Cloning" (Sambrook & Russell, 2001)

4.2.1 Animal models of pulmonary fibrosis

4.2.1.1 *Bleomycin model of pulmonary fibrosis*

Mice experiments were performed in accordance with the guidelines of the Ethics committee of the Helmholtz Zentrum Munich and were approved by the Regierungspräsidum Oberbayern, Germany. The animal experiments were performed in our group by Dr. Barkha Srivastava and Dr. Verena Aumiller with assistance from Andrea Wegener and Constanze Heise.

Eight to ten weeks old mice were used for bleomycin application. Mice were narcotized with *i. p.* administration of 0.2 mg/ml medetomidin (Orion Pharma, Hamburg), 2.0 mg/ml midazolam (Roche Pharma, Mannheim) and 0.02 mg/ml fentanyl (Janssen-Cliag, Neuss) per kg body weight. 5 U bleomycin sulphate (Sigma Aldrich, Taufkirchen) per kg body weight were dissolved in 200 μl sterile saline solution (B. Braun, Melsungen) and intratracheally applied through a 20 G INTROCAN cannula by Micro Sprayer application (Penn Century, Wyndmoor, USA), constituted of the two parts, the high pressure syringe (model FMJ-250) and the intratracheal aerosolizer (IA-1C). After the instillation procedure, the narcosis was antagonised subcutaneously with 0.29 mg/ml atipamezole (Orion Pharma, Hamburg), 0.059 mg/ml flumazenil (Hexal, Holzkirchen) and 0.14 mg/ml Naloxon (Actavis, Munich) per kg body weight. Narcosis and antagonist were obtained through the Tierärztliche Hausapotheke of the Helmholtz Zentrum Munich. After 14 days mice were narcotised with 100 mg/ml ketamine (bela pharm; Vechta, Germany) and 0.7 mg/ml Rompun (bela pharm; Vechta, Germany) per kg body weight i. p., followed by opening up the abdomen and cutting the *Vena cava*. After lung and trachea exposure, the mice were intubated intratracheally via a small incision. The lungs were lavaged twice with 300 μl sterile PBS and the combined bronchoalveolar lavage fluid (BALF) was cleared by centrifugation for 5 min at 500 x g and snap frozen. After removal of the thymus the lung was rinsed via the right ventricle of the heart with 0.9% NaCl solution, excised and either used for cell isolations or snap frozen in liquid nitrogen for RNA analysis. Different gauche size cannulas were purchased from B. Braun (Melsungen, Germany) and all surgical instruments were purchased from Fine Science Tools (Heidelberg, Germany).

4.2.1.2 *Adenoviral TGF-β1-induced fibrosis*

Rat lung tissue samples were obtained from M. Kolb and C. Sambori; Hamilton, Canada. The construction of adenoviral vectors, administration of adenoviruses and characterization of the animal model has been well described in (Sime et al, 1997). Briefly, female Sprague-Dawley rats (body weight: 225–250 g) were intratracheally instilled with 1×10^8 plaque forming units AdTGF-β1 or AdDL70 (empty virus serving as control) each under isoflurane anesthesia. At the indicated days after adenovirus administration, rats were sacrificed by

abdominal bleeding and lungs were excised. Lungs were snap frozen in liquid nitrogen and grinded into powder. RNA was isolated as described below. The animals were treated in accordance with the guidelines of the Canadian Council of Animal Care and approval was received from the university animal research ethics board.

4.2.2 Cell biology

4.2.2.1 *Primary cell isolations*

4.2.2.1.1 Isolation of primary alveolar type II cells

PmATII cells were isolated as described before (Königshoff et al, 2009), with modifications established in our group by Dr. Kathrin Mutze. Julia Kipp and Anastasia van den Berg performed the cell isolations according to the following protocol. Per one cell isolation four mice were used.

Mice were narcotised with 100 mg/ml ketamine (bela pharm; Vechta, Germany) and 0.7 mg/ml Rompun (bela pharm; Vechta, Germany) per kg body weight i. p., followed by opening up the abdomen and cutting the *Vena cava*. After lung and trachea exposure, the mice were intubated intratracheally via a small incision. The thymus was removed and the lungs rinsed via the right ventricle of the heart with 0.9% NaCl solution. Each lung was filled with 1.5 ml dispase followed by 0.3 ml low melting agarose (Sigma Aldrich, Taufkirchen) solution for sealing, removed from the thorax and incubated for 45 min in 1 ml dispase at room temperature. The lungs were transferred into a cell culture dish containing 5 ml (+)-medium (DMEM supplemented with 3.6 mg/ml glucose, 2% glutamine, 10 mM HEPES, 0.04 mg/ml DNase I and 1% penicillin/streptomycin), the lobes were separated and the cells were removed from the lung matrix by sweeping out with curved forceps. Cells were collected and sequentially filtered through 100, 20, and 10 µm nylon meshes and centrifuged for 10 min at 250 x g. Over night with CD16/32- and CD45-antibody (BD Bioscience; Heidelberg, Germany) coated cell culture dishes were washed with 5 ml (-)-medium (corresponds to (+)-medium without DNase I). The supernatant of the cells was discarded after centrifugation, the cells were resuspended in (-)-medium and the cell suspension was distributed on the coated cell culture dishes, and were incubated for 30 min at 37 °C for negative selection. Cell suspension of unattached cells were removed from the dishes and distributed onto new dishes without antibody coating and incubated at 37 °C for 25 min. Cell suspension was collected and cells harvested by centrifugation for 10 min at 200 x g, washed with PBS and snap-frozen in liquid nitrogen for RNA analysis.

4.2.2.1.2 Isolation of primary fibroblasts

Katharina Lippl and Daniela Dietel performed isolations of primary fibroblasts either from mouse tissue or from human lung tissue specimens according to the following protocol.

Mice lungs were excised as described in section 4.2.2.1.1 but without any enzymatic treatment. For human fibroblasts, specimens from lung lobes or segmental lung resections, and for murine fibroblasts, one mouse lung, were dissected into 1-2 mm^3 pieces and

digested with 1 mg/ml of collagenase I at 37 °C for 2 h. Subsequently, digested samples were filtered through nylon filters with a pore size of 70 μm. Filtrates, containing phFB, were centrifuged at 400 x g at 4 °C for 5 min. Cell pellets were resuspended in DMEM/F-12 medium supplemented with 20% FBS and 1% penicillin/streptomycin and plated on 10 cm cell culture dishes.

PhFB from IPF patients were obtained from E. S. White, Michigan, USA and were isolated as published (White et al, 2003) according to the following protocol. IPF lung fibroblasts were obtained from de-identified patients undergoing surgical lung biopsy for their interstitial lung disease or from explants of patients with known IPF undergoing lung transplantation. Lung biopsy specimens were only used from patients with confirmed UIP histopathology. Because samples cannot be traced back to individuals directly or indirectly, the University of Michigan Institutional Review Board has determined this project to be not regulated. Lungs were received through Gift of Life donations ("normal") or explanted during transplantation (UIP or IPF). Sample tissue was taken from parenchymal regions, avoiding major airways.

Tissue pieces were placed in a 150 mm tissue culture dish with DMEM media containing 10 % FBS pre-warmed to 37 °C. Tissue was minced with a sterile scalpel blade until the remaining pieces did not exceed a size of 2 mm in diameter and incubated at 37 °C with 5% CO_2, changing media every two to three days. As soon as outgrowing fibroblasts had reached approximately 50-60% confluence (one to two weeks), remaining tissue pieces were removed.

4.2.2.2 *Cryopreservation of mammalian cells*

For cell preservation, cells were stored in liquid nitrogen in freezing medium containing cell specific medium supplemented with 20% FBS and 10% DMSO. For this, cells were washed with PBS and detached with pre-warmed trypsin/EDTA solution for 5 min at 37 °C. Medium containing FBS was added and cells were counted with the Casy cell counter. Cells were harvested by centrifugation and resuspended in freezing medium in a concentration of 1-2 x 10^6 cells/ml, transferred into cryovials and frozen in a Mister Frosty (Omnilab) at -80 °C over night (ON) and kept for long-term storage in liquid nitrogen.

4.2.2.3 *Culturing and sub-culturing of mammalian cells*

The different cell lines and primary cells used were cultured in the appropriate media containing 1% penicillin/streptomycin as indicated in Table 4.21 at 37 °C in a humidified cell incubator with 5% CO_2. Medium was changed two to three times a week after washing with PBS. Cells were sub-cultured when cell density reached 80-90%. For this purpose, cells were washed with PBS, pre-warmed trypsin/EDTA solution was added and the cells were incubated for 5 min at 37 °C. Cells were completely detached from the surface by tapping against the cell culture dish/flasks and re-suspended in cell culture medium and sub-cultured as indicated in Table 4.21. All cell lines were passaged up to 25 times. Primary human cells were sub-cultured up to 12 passages. Primary murine alveolar type II cells were used freshly isolated and primary murine lung fibroblasts were used till passage 4.

Table 4.21: Cell specific culturing information

Cell name	Culture medium	Split ratio
16HBE14o⁻	MEM + 10% FBS	1:5 – 1:10
A549	DMEM/F-12 + 10% FBS	1:10 – 1:15
HEK 293T	DMEM/F-12 + 10% FBS	1:10 – 1:15
HFL1	DMEM/F-12 + 10% FBS	1:3 – 1:5
phFB	DMEM/F-12 + 20% FBS	1:3 – 1:5
pmATII		-
MRC5	Ham's F12 + 10% FBS + 5% GlutaMax	1:3 – 1:5
Human bronchial epithelial primary cells (phBEC)	Airway Epithelial Cell Growth Medium	1:3

4.2.2.4 *Cell treatments*

200 000 – 300 000 phFB were seeded per six-well cavity in complete medium. After synchronizing for 24 h in starvation medium (0.1% FBS containing medium), cells were treated with 2 ng/ml TGF-β1 in starvation medium for the indicated times, washed 3 times with PBS and stored at -80 °C for later protein or mRNA analysis. For immunofluorescence analysis, 50 000 cells were seeded in a 24-well cavity containing a cover slip and processed as described before.

4.2.2.5 *Lipotransfection of cells*

In order to transfect cells with various plasmids and for miRNA overexpression and inhibition transient transfections were applied. Forward transfections, meaning cells were transfected the day after seeding, were used for transfection efficiency analysis, luciferase reporter assays, miRNA inhibition and overexpression as well as for WISP1 overexpression. Reverse transfections were used for WISP1 knock down with siRNA technology. In general, the liposomes were prepared in OptiMEM for 1 h at room temperature (RT) and transfections were performed modified as outlined below according to the manufacturer's protocol.

<u>Transfection efficiency analysis</u>

A549 cells were transfected for transfection efficiency analysis either with GFP reporter plasmid or with Cy3-labeled miRNA mimic. For plasmid transfection analysis, 70 000 cells were seeded into a 24-well cavity, transfected the next day with 0.5 µg GFP reporter plasmid, Lipofectamine LTX in different ratios (DNA:LTX varied from 1:1 up to 1:2.5 in 0.5 steps) and PLUS reagent in a ratio 1:1, corresponds to 0.5 µl. GFP expression was analysed after 24 h with a confocal microscope and the Imaris Software. For miRNA transfection analysis, 26 000 cells were seeded in a cavity of a 8-well chamber slide, transfected the next day with 0.2 µg mimic, 0.4 µl Lipofectamine LTX (ratio DNA:LTX 1:2) and 0.2 µl PLUS reagent. Cy3-labeled cells were analysed after 24 h with a confocal microscope.

<u>Transfection for luciferase reporter assays</u>

Co-transfections of reporter plasmids with miRNA mimics or inhibitors were performed in duplicates and quadruplicates. Per 48-well cavity, 250 ng total plasmid DNA was used consisting of 200 ng carrier plasmid, pCMV6-XL6 and 50 ng of reporter plasmid. Liposomes were generated with 50 µl OptiMEM and 200 µl of the appropriate cell culture medium. The detailed setup is listed in Table 4.22.

Table 4.22: Transfection setup of luciferase reporter assays.

Cell type	Cells per 48-well cavity	Transfection reagent (TR)	Amount of TR	miRNA mimic or inhibitor	PLUS reagent
A549	60 000	Lipofectamine LTX	1 µl	5-50 pmol (20-200 nM)	0.5 µl
phFB	40 000	Lipofectamine 2000	1.25 µl	-	-
HEK	100 000	Lipofectamine LTX	1 µl	100 nM	-

<u>Transfection for miRNA inhibition and overexpression</u>

200 000 - 300 000 phFB were seeded per 6-well cavity, and transfected the next day with liposomes prepared in 300 µl OptiMEM. The liposomes were prepared with varying concentration of miRNA inhibitors and mimics (5 nM – 100 nM in total) with Lipofectamine2000 in a ratio from DNA:Lipofectamine of 1:2.5 according to the manufacturer's protocol. Cells were washed once with PBS and transfected in 1.2 ml fresh medium with 300 µl of liposome mixture in OptiMEM.

<u>Transfection for simultaneous cell treatment and miRNA overexpression</u>

300 000 phFB cells were seeded per 6-well cavity. After 24 h, cells were washed with PBS and synchronized for 24 h with medium containing 0.1% FBS. Cells were transfected as described above, whereas the 1.2 ml fresh medium consisted of 0.1% FBS-DMEM/F-12 and 3 ng TGF-β1.

<u>Transfection for WISP1 overexpression</u>

1.8×10^6 A549 cells were seeded into a 10 cm dish. The next day, cells were transfected for 6 h and then the medium was changed to starvation medium containing 0.1 % FBS. Cells were transfected with 12.5 µg pCMV6-XL6 WISP1, 25 µl Lipofectamine LTX and 12.5 µl PLUS reagent in 2 ml OptiMEM added to 8 ml of cell culture medium. Cells and supernatants were collected after 24 h for further analysis and as WISP1 positive controls.

Transfection for WISP1 knock down with siRNA technology

The liposomes were prepared in 500 µl OptiMEM containing either 10 nM or 30 nM siRNAs against WISP1 or control siRNAs and 5 µl RNAiMax directly in a 6-well cavity. After 30 min incubation 300 000 phFBs were added and analysed after the indicated time points for WISP1 expression by mRNA and protein analysis.

4.2.3 Microbiology

4.2.3.1 *Transformation of chemically competent E. coli*

Transformation of TOP10 chemically competent *E. coli* was performed with ligation products or plasmids. Bacteria were thawed on ice and quickly centrifuged. For each transformation approach 25 µl of *E. coli* were transferred into a sterile 1.5 ml tube. 1.5 µl of 10 ng/µl plasmid or 2.5 µl ligation product were added to the bacteria and mixed by tapping against the tube. The mixture was incubated on ice for 30 min and then the heat shock transformation was performed for 30 s at 42 °C in a thermomixer. The mixture was put on ice and chilled for 2 min. 200 ml of pre-warmed SOC medium was added to each bacteria-containing tube and incubated at 37 °C for 1 h at 300 rpm. Everything was plated on antibiotics-containing pre-warmed agar plates and incubated at 37 °C ON. The next day single colonies were picked.

4.2.3.2 *Storage of E. coli*

Glycerol stocks were prepared in order to maintain *E. coli* cultures containing a plasmid of interest. To 0.4 ml ON grown bacteria culture 0.6 ml 87 % sterile glycerol was added and thoroughly mixed by vortexing. The mixture was shaken at 37 °C for 30 min and stored at -80 °C for long-term storage. For recovery, parts of the stocks were scratched with a fresh pipette tip and cultured in LB medium containing 50 µg/ml ampicillin.

4.2.3.3 *Cultivation of E. coli*

For plasmid isolations either a single colony was picked from the agar plate or a pipette tip was inoculated with bacteria from a glycerol stock. According to the plasmid purification scale (mini/midi) the growth medium volume was chosen, and 50 µg/ml ampicillin were added and inoculated with bacteria. The solution was incubated ON at 37 °C shaking at 250 rpm.

4.2.4 Molecular biology

4.2.4.1 *Isolation of genomic DNA (gDNA)*

Cellular gDNA was isolated using peqGOLD Tissue DNA Mini Kit, a silica-based column method, according to the manufacture's protocol. After trypsinization, 2×10^6 cells were sedimented by centrifugation at 5 000 x g at RT for 5 min. The supernatant was discarded and the cell pellet resuspended in 400 µl DNA lysis buffer T enriched with 20 µl proteinase K and 15 µl RNase A and mixed thoroughly by vortexing for 10 s. Cell lysis was

achieved by incubating the mixture in a thermomixer for 30 min at 50 °C. 200 µl DNA binding buffer were added and mixed by pipetting. The prepared mixture was loaded on a PerfectBind DNA column and centrifuged in a top table centrifuge for 1 min at 10 000 x g. The flow-through was discarded. The gDNA was bound to the column was washed by adding 650 µl of the prepared DNA wash buffer on the column with subsequent centrifugation for 1 min at 10 000 x g. The flow-through was discarded and the washing step repeated. The column was dried by centrifugation for 2 min at 10 000 x g. The gDNA was eluted by adding 100 µl elution buffer directly onto the column membrane, incubating for 3 min at RT and centrifuging for 1 min at 6 000 x g.

4.2.4.2 *Polymerase chain reaction (PCR)*

DNA fragments were amplified by PCR reactions. Input material was gDNA, plasmid DNA or cDNA. The pmirGLOW vector was cloned using A549 gDNA as template. The plasmids pmirGLOW1-3 were cloned using the pmirGLOW vector as input. PCR reactions from various cDNAs confirmed the expression of WISP1 3'UTR. The standard PCR reaction mixture is described in Table 4.23 and the PCR protocol in table Table 4.24. Phusion Hot Start II high-fidelity DNA polymerase was used. The following amounts were used for the different templates: 300 ng gDNA per 150 µl reaction volume, 30 ng plasmid DNA per 150 µl reaction volume and 30 ng cDNA per 150 µl reaction volume. Cycle steps (2) – (4) were repeated 25 – 30 times.

Table 4.23: 150µl PCR reaction mixture

Reagent	Concentration	Volume	Final concentration
H_2O		up to 150 µl	
high fidelity buffer	5x	30 µl	1x
dNTPs	2 mM per dNTP	15 µl	200 µM per dNTP
forward primer	100 µM	0.9 µl	600 nM
reverse primer	100 mM	0.9 µl	600 nM
template	variable	variable	variable
DMSO	100%	4.5 µl	3%
Phusion DNA polymerase	2 U/µl	1.5 µl	0.02 U/µl

Table 4.24: General PCR reaction conditions

Cycle step	Temperature	Time
(1) Initial denaturation	98 °C	30 s
(2) Denaturation	98 °C	10 s
(3) Annealing	60 °C	30 s
(4) Elongation	72 °C	30 s per 1 kb
(5) Final elongation	72 °C	7 min
(6) Cooling	4 °C	on hold

4.2.4.3 *Separation of DNA fragments by gel electrophoresis*

PCR amplified or digested DNA fragments were separated by electrophoresis on an agarose gel for size inspection or separation for further plasmid cloning. 0.8 - 2% agarose content was used according to the fragment size. The amount of agarose was dissolved in 1x TAE buffer by heating in a microwave. After cooling down, SybrSafe was added to a 1x final concentration and the gel was poured into the chamber. The DNA samples were mixed with 6x loading buffer and water to a final concentration of 1x loading buffer, added into the gel pockets in addition to an appropriate molecular weight marker and electrophoretic separated in 1% TAE buffer by applying 5 - 7 V/cm. The DNA bands were visualized with illumination at 470 nm using the XcitaBlue Conversion Screen from the ChemicDoc.

4.2.4.4 *DNA purification from agarose gels*

For subsequent cloning, DNA needed to be purified from agarose gels after size separation. The DNA containing agarose was cut out of the gel and DNA was purified using peqGOLD Gel Extraction Kit. Equal volume of binding buffer was added to the DNA containing gel fragment and the gel was dissolved by heating it at 60 °C for around 7 min in a thermomixer with modest shaking. If the colour of the solution was red to orange, the pH was adjusted with approximately 5 µl of 3 M sodium acetate pH 5.2 until the solution colour was yellow. The DNA/agarose mixture was added on a PerfectBind DNA column, centrifuged for 1 min at 10 000 x g and the flow-through discarded. The column was washed by adding 300 µl binding buffer to the column and centrifuging for 1 min at 10 000 x g. The washing was repeated twice with 750 µl GC buffer and the column was dried by centrifuging for 1 min at 10 000 x g. The DNA was eluted with 30 µl elution buffer and centrifugation for 1 min at 5 000 x g.

4.2.4.5 *Annealing of ssDNA*

DsDNA oligonucleotides were generated from customized, ssDNA oligonucleotides for cloning of pSi and pMi constructs. The ssDNA oligonucleotides were dissolved in TE buffer according to the synthesis report in order to get a final concentration of 100 µM. For annealing, 10 µl of 100 µM corresponding reverse and 10 µl of 100 µM corresponding forward strand were combined and 1 µl 1 M NaCl solution was added. The reaction was

incubated at 95 °C for 5 min and the annealing performed at RT for 1 h. The dsDNA oligonucleotides were stored at -20 °C until further use.

4.2.4.6 DNA digest with restriction enzymes

DNA digest with restriction enzymes were performed either for analytical analysis of DNA plasmids isolated from *E. coli* or for preparative purpose of cloning PCR fragments into vectors. FastDigest restriction enzymes were used in 1x FastDigest Green Buffer. For analytical plasmid analysis, 1 µg DNA was digested in 20 µl final volume up to 15 min at 37 °C according to the manufacture's recommendations. For preparative purpose, 5 µg of plasmid vector or the highest possible amount of gel purified PCR product were digested.

4.2.4.7 Dephosphorylation of plasmid DNA

In order to minimize the risk for re-ligation of vector backbone, a dephosphorylation step was included to the restriction digest or subsequently added. 1 µl FastAP Thermosensitive Alkaline Phosphatase was used in 20 µl final reaction volume with 1x reaction buffer or FastDigest buffer for 10 min at 37 °C. The reaction was stopped by heat inactivation of the enzyme at 75 °C for 5 min.

4.2.4.8 Ligation of DNA

For new plasmid generation vector backbone and insert were ligated 1:1 up to 1:5 in molar ratios using T4 DNA ligase. In addition, one 1:0 setup was included for estimation of relegation of backbone. Between 100 ng and 300 ng total DNA were used in 20 µl final volume, containing DNA fragments, 5% PEG 4 000 solution, 1x T4 DNA ligation buffer and 1 U T4 DNA ligase. The reaction was incubated at 22 °C for 10 min and the enzyme was heat inactivated at 65 °C for 10 min. 10 % ligation reaction of bacteria suspension were used for bacteria transformation.

4.2.4.9 Molecular cloning

Molecular cloning was carried out according to the detailed steps described in 4.2.4.1 - 4.2.4.8 and the oligonucleotides listed in 4.1.6.1.

The human WISP1 3'UTR was PCR amplified from A549 gDNA and cloned NotI/XhoI into the backbone of pmirGLO resulting in the pmirGLOW vector. For this, the PCR product was agarose gel purified, excised and gel purified followed by double XhoI, NotI restriction digest resulting in the insert fragment. The pmirGLO backbone vector was double digested with XhoI, NotI and dephosphorylated followed by column purification and ligation with the insert.

The human WISP1 3'UTR fragments 1-3 were PCR amplified from the pmirGLOW vector and cloned NotI/XhoI into the pmirGLO backbone as described above for pmirGLOW resulting in pmirGLOW1-3.

The pSi and pMi constructs were generated by annealing of the complementary ssDNA strands and SacI/XhoI cloned into the double digested and purified pmirGLO backbone vector.

The correctness of the sequences of the obtained plasmids was verified by appropriate restriction digests and by sequencing (see 4.2.4.12). For sequence analysis Vector NTI was used.

4.2.4.10 *Plasmid purification*

Plasmid purifications were performed either with the Qiagen Plasmid Mini Kit for screening of cloned plasmids or for plasmid PCR template generation or with the Qiagen HiSpeed Plasmid Midi Kit for plasmid purification used in cell culture experiments.

4.2.4.11 *Nucleic acid concentrations measurements*

For RNA and DNA concentration determination, the absorbance at 260 nm was measured using the NanoDrop 1000 spectrophotometer. As blank, H_2O or elution buffer was measured.

4.2.4.12 *DNA sequencing*

In order to confirm newly generated plasmid sequences, the plasmids were sent for sequencing to GATC Biotech AG, Konstanz, Germany. The plasmid sequences were analysed by Sanger sequencing using an ABI3730 instrument. Specific sequencing primers are listed in 4.1.6.3.

4.2.4.13 *RNA isolation of mRNA and miRNA*

Total RNA was isolated from cells or lung tissue using miRNeasy Mini Kit from Qiagen.

Tissue homogenization was performed as following: 40 – 100 mg frozen lung tissue were grinded with a stainless steel grinding ball in a cryotube applying 3 000 rpm for 30 s in the microdismembrator. In order to avoid thawing of the tissue, the homogenized material was snap frozen in liquid nitrogen before shaking another 30 s with 3 000 rpm in the microdismembrator. The frozen powder was dissolved in 700 µl QIAzol and incubated for 15 min at RT. The mixture was shaken for 10 s with 3 000 rpm in the microdismembrator. After this lysis procedure, the RNA isolation was performed just as for RNA isolation from cells and according to the manufacture's protocol.

For cell lysis, 600 µl QIAzol were added per well of a six-well plate. The mixture was incubated for 2 min at RT, scratched with a cell lifter and transferred into a 1.5 ml tube. The cells were homogenized by vortexing for 30 s and then incubated at RT for 5 min. 140 µl chloroform per 700 µl QIAzol were added and the mixture was shaken vigorously for 15 s by vortexing. After incubation at RT for 3 min, phases were separated by centrifuging for 15 min at 12 000 x g at 4 °C. The upper aqueous phase was transferred into a new tube, 1.5 volumes of 100 % ethanol were added and mixed thoroughly by pipetting. The sample mixture was pipetted into an RNeasy Mini column and centrifuged for 15 s at RT at 10 000 x g. The column was washed with 350 µl RWT buffer and on-column DNAse digest was performed applying 80 µl of DNase mixture per column for 15 min at RT. The column was washed with another 350 µl RWT buffer. Then, 500 ml RPE Buffer were added into the column and centrifugation was performed for 15 s at 10 000 x g, a second washing was performed with 500 µl RPE Buffer and also a centrifuging for 2 min at 10 000 x g. The

column was dried by centrifugation at full speed for 1 min and the RNA was eluted with 35 µl RNase/DNase-free water pipetted directly onto the column and centrifugation for 1 min at 8 000 x g.

4.2.4.14 *cDNA synthesis*

In this work, three different methods for cDNA synthesis were used. For analysis of only mRNA expression, cDNA synthesis reagents from ABI were used. This is the case for siRNA treated cell experiments and WISP1 analysis in pmATII cells. For analysis of only miRNA expression, TaqMan MicroRNA Assays were applied. This was the case for miRNA analysis from total human and murine lung homogenate. Further, combined mRNA and miRNA cDNA synthesis was performed using miScript II reverse transcription kit. This was the case for all cell culture experiments and rat whole lung tissue samples.

Life Technologies reagents for mRNA derived cDNA:

1 µg of total RNA was reverse transcribed using MuLV reverse transcriptase and random hexamers as primers. In Table 4.25 the reaction mixture content is listed. First, RNA was filled up to a total volume of 20 µl and denatured at 90 °C for 10 min. The samples were put on ice and remaining reagents were added in order to get 40 µl total volume. Annealing was performed at 20 °C for 10 min followed by reverse transcription at 43 °C for 75 min. Finally, the enzyme was heat inactivated at 99 °C for 5 min.

Table 4.25: mRNA – cDNA synthesis

Reagent	Stock Concentration	Final concentration in 40 µl	Volume
10x Buffer II	100 mM	10 mM, 1x	4 µl
$MgCl_2$	25 mM	5 nM	8 µl
dNTPs	10 mM	0.5 nM	2 µl
Random hexamers	50 µM	2.5 µM	2 µl
RNase inhibitor	5 U/µl	0.25 U/µl	1 µl
MuLV reverse transcriptase	50 U/µl	2.5 U/µl	2 µl
H_2O			1 µl
total volume			20 µl

TaqMan microRNA assay technology for miRNA analysis:

Using the TaqMan technology, for each miRNA a specific cDNA sample was generated. The cDNA synthesis was performed in 15 µl total volume, which contained 7 µl of Master Mix, 3 µl of the 5x miRNA specific reverse transcription primer and 5 µl of 2 ng/µl total RNA (10 ng). The Master Mix was prepared on ice according to Table 4.26, subsequently RNA and reverse transcription primers were added. The reverse transcription reaction conditions were: 16 °C for 30 min; 42 °C for 30 min; 85 °C for 5 min; and then maintained at 4 °C until used or stored for long term at -20 °C.

Table 4.26: TaqMan miRNA master mix

Reagent	Stock concentration	Final concentration	Volume
dNTP	100 mM	1 mM	0.15 µl
reverse transcriptase	50 U/µl	0.5 U/µl	1.00 µl
reverse transcription buffer	10x	1x	1.50 µl
RNase inhibitor	20 U/µl	0.26 U/µl	0.19 µl
H$_2$O		-	4.16 µl
total volume			7.00 µl

<u>miScript technology for combined mRNA and miRNA analysis:</u>

The miScript technology was applied in order to generate cDNA of mRNA and miRNA within one reaction. 1 µg of total RNA was diluted with RNase -ree water on ice to a final volume of 12 µl, 8 µl master mix (containing 4 µl 5x miScript reverse transcription buffer, 2 µl miScript reverse transcriptase mix and 2 µl nucleic acid mix) were added and then the RNA was reverse transcribed in a total volume of 20 µl. The reverse transcription reaction conditions were: 37 °C for 60 min; 95 °C for 5 min and then maintained at 4 °C until used or stored for long term at -20 °C.

4.2.4.15 *Quantitative PCR (qPCR)*

The different qPCR reactions are as the following. In general, for mRNA analysis, 12.5 ng cDNA were applied, for miRNA analysis (ABI and Qiagen technology) 2 ng.

For mRNA analysis, the master mix composition is listed in Table 4.27 and the qPCR conditions in Table 4.28. Cycle steps (2) – (4) were repeated 45 times. All mRNA primers were tested for their efficiency and only primers with an efficiency higher than 1.8 were applied.

Table 4.27: mRNA - qPCR master mix

Reagent	Stock concentration	Final concentration	Volume
Light Cycler 480 SybrGreen l Master Mix	2x	1x	5 µl
Primer Mix	10 µM each	0.5 µM	0.5 µl
H$_2$0			2 µl
cDNA	5 ng/µl	12.5 ng/µl	2.5 µl
total			10 µl

Table 4.28: mRNA - qPCR reaction conditions

Cycle step	Temperature	Time
(1) Initial denaturation	95 °C	5 min
(2) Denaturation	95 °C	5 s
(3) Annealing	59 °C	5 s
(4) Elongation	72 °C with single acquisition	10 s
(5) Melting curve	95 °C	5 s
	60 °C	1 min
	60 °C -95 °C with continuous acquisition	
(6) Cooling	4 °C	on hold

For miRNA analysis applying Applied Biosystems technology, the cDNA was diluted 1:3 and 3 µl of the diluted cDNA were utilized with 0.75 µl 20x TaqMan primers in 15 µl PCR reaction with 7.5 µl 2x TaqMan Un Master Mix II, no UNG. The conditions for the PCR were: 95 °C for 10 min followed by 45 cycles of 95 °C for 15 s and 60 °C for 1 min.

For miRNA analysis applying Qiagen technology, the cDNA was diluted 1:5 and 2 µl of the diluted cDNA (1 ng/µl) were utilized with 1 µl 10x miScript Universal Primer, 1 µl specific 10x miScript Primer Assay, and 5 µl 2x QuantiTect Sybr Green PCR Master Mix in 10 µl PCR reaction. The conditions for the PCR were: 95 °C for 15 min followed by 45 cycles of 95 °C for 15 s, 55 °C for 30 s and 70 °C for 30 s. The commercially available primer assays were not tested for their efficiency. The manufacturer guarantees a high efficiency. It was assumed that these primers perform with similar efficiency with cDNA from different human cells. Therefore a comparision of the relative miRNA levels comparison between the different cells was possible.

All qPCR assays were performed in duplicates. For standardization of relative mRNA expression, human and mouse hypoxanthine-guanine phosphoribosyltransferase (*HPRT*) or rat glyceraldehyde-3-phosphate dehydrogenase (*GAPDH*) primers were used. For standardization of relative miRNA expression, RNU43, snoRNU202 or RNU6 were used. Relative transcript abundance of a gene is expressed in ΔC_t values ($\Delta Ct = C_t^{reference} - C_t^{target}$). Relative changes of mRNA/miRNA levels are presented as $\Delta\Delta C_t$ values ($\Delta\Delta C_t = \Delta C_t^{treated} - \Delta C_t^{control}$).

4.2.5 Protein biochemistry

4.2.5.1 *Protein isolation and concentration determination*
Cells frozen for analysis at -80 °C were scratched with a cell lifter in RIPA lysis buffer on ice (per one 6-well cavity 50-60 µl RIPA buffer were used). Cell lysates were transferred to a microcentrifuge tube, frozen in liquid nitrogen and thawed on ice. Protein extracts were clarified by centrifugation at 12 000 x g at 4 °C. Protein concentrations were determined using the BCA assay from 1:5 diluted samples according to the manufacture's protocol.

4.2.5.2 *Protein concentration from supernatants*
Amicon Ultra centrifugal filter units were applied to concentrate cell supernatants according to the manufacturer's guidelines. Briefly, cell culture supernatants were thawed at 4 °C while shaking and 500 µl per sample were transferred into a 3K Amicon Ultra centrifugal filter unit. Samples were centrifuged at 4 °C for 30 min at 14 000 x g, flow throughs were discarded and concentrated samples were recovered by centrifugation at 4 °C for 2 min at 1 000 x g. In doing so, the samples were 10 times concentrated and such concentrated samples were used for instance in ELISA measurements. For Western blot analysis of cell supernatants, concentrated protein samples were acetone-precipitated according to the technical resource note, TR0049.1, from Pierce. Shortly, four times the samples' volume of -20 °C cold acetone was added to the samples and thoroughly mixed by vortexing. After 1 h incubation at -20 °C, proteins were precipitated by centrifugation at 4 °C for 10 min at 15 000 x g. Liquid was carefully removed by pipetting, the pellet was air dried for 30 min at RT and then suspended in RIPA buffer. Protein concentrations were determined using the BCA assay from 1:5 diluted samples.

4.2.5.3 *Protein analysis with Western Blotting*
Protein samples were mixed with protein loading buffer and RIPA buffer for equal volumes. 20 µg total protein were loaded for lung homogenates and 40 µg for cell lysates and supernatants.

Proteins were separated on 10% SDS-polyacrylamide gels. Proteins were transferred to nitrocellulose membrane. Membranes were blocked with 5% non-fat dry milk in TBST at RT for 1 h. Primary antibody incubation was done at 4 °C ON while shaking. After three times washing with TBST, membranes were incubated with appropriate horseradish peroxidase (HRP)-coupled secondary antibody. Proteins were visualized by enhanced chemiluminescence. Signals were measured either using the ChemiDoc or an x-ray film, which was automatically developed with the film developer Curix 60.

As a positive control for WISP1 protein 2 ng recombinant human WISP1 protein was loaded on the gel. Note that the size difference from endogenous WISP1 obtained from cell supernatants to the recombinant protein derives from 10-His tag on the C terminal site of the recombinant protein. Furthermore, A549 cells transfected with the WISP1 overexpression plasmid were used as WISP1 positive control. 250 ng of cell lysate or 5 µg protein from cell supernatants were loaded on the gel.

4.2.5.4 *Enzyme-linked immunosorbant assay (ELISA)*

Human WISP1 protein concentrations in cell supernatants were analysed with the WISP1 DuoSet (DY1627) ELISA from R&D Systems according to the manufacture's protocol using Nunc MaxiSorp flat-bottom 96 well plate. Cell supernatants were either used without further processing or ten times concentrated using the Amicon Ultra centrifugal filter units as described under 4.2.5.2. Mouse WISP1 protein concentrations in BAL fluids were analysed using the murine WISP1 ELISA Kit (E96895M) from Uscn Life Science. BALF was used without further processing. Data analysis was performed generating a nonlinear curve fit for the standard with the GraphPad Prism Software V5.

4.2.5.5 *Protein analysis with immunofluorescence (IF)*

Cells were seeded either for transfection or treatment and subsequent IF staining into 12-well cavity plates containing coverslips. After the indicated time points cells were washed once with PBS and fixed with ice cold aceton:methanol solution (ratio 1:1) for 5-10 min at RT. After washing three times with PBS, cells were incubated with blocking solution (5% BSA in PBS) for 30 min at room temperature. After washing three times with PBS containing 0.1% BSA (0.1% BSA-PBS), cells were incubated with the primary antibody in 0.1% BSA-PBS for 1 h at RT. After washing three times with 0.1% BSA-PBS, cells were incubated with the secondary antibody-conjugated with the fluorophore in 0.1% BSA-PBS for 1 h at RT in the dark, followed by three washing steps with 0.1% BSA-PBS. The used primary and secondary antibodies and the applied dilutions can be found in Table 4.12 and Table 4.13. DNA was stained with DAPI (final concentration 0.5 µg/ml) for 5 min at RT. After washing three to five times with 0.1% BSA-PBS, cells were fixed again with 4% PFA for 10 min at RT, mounted on microscopy slides with fluorescence mounting medium and examined with an Axio Imager fluorescence microscope.

4.2.5.6 *Luciferase assays*

Cells transfected with luciferase reporter vector were analysed after 48 h with the dual-luciferase reporter assay system from Promega according to the manufacture's protocol. Measurements were performed either in duplicates or in quadruplicates. The at -80 °C stored cell culture plates were brought to room temperature and per 48-well cavity 65 µl 1x PLB were added. For cell lysis, the plates were agitated on an orbital shaker at RT for 20 min. 20 µl of each lysate were transferred into a white 96 well plate. The luciferase activities were measured using a plate reading luminometer from Berthold with an automatic injection system. First, the firefly luciferase activity was measured by adding 100 µl of luciferase assay reagent per well and the emitted light was measured for 10 s. Second, the firefly activity was quenched and simultaneously the *Renilla* luciferase activity was measured by injecting 100 µL of stop and glow reagent into the well. The emitted light was measured for 10 s. The firefly luciferase activity was normalized to the *Renilla* luciferase activity by dividing the relative light units. As a control measurement non-transfected cells were used.

4.2.6 Bioinformatics Analysis

Daniel Ellwanger from the Department of Genome-oriented Bioinformatics, Technische Universität München, Center of Life and Food Science; Freising Weihenstephan, Germany conducted all bioinformatics analyses.

4.2.6.1 *Preparation of expression data*

Two human miRNA expression profiles were obtained from the NCBI Gene Expression Omnibus (GEO, http://www.ncbi.nlm.nih.gov/geo/) under series *GSE13316* (10 IPF, 10 control samples) and *GSE21394* (9 IPF/UIP, 6 control samples) (Cho et al, 2011; Pandit et al, 2010). The raw data was normexp background corrected (Ritchie et al, 2007) quantile normalized (Bolstad et al, 2003) and log2 transformed. Processed miRNA expression data of a murine bleomycin-induced lung fibrosis model was obtained from Liu *et al.* (Liu et al, 2010) (ArrayExpress accession *E-MEXP-2749*, www.ebi.ac.uk/arrayexpress/; 9 samples, pooled reference). Values for within-array replicate spots were replaced with their average, at which only probes with an intensity of greater than 95% of the negative controls were considered. For the human IPF studies, the fold changes were computated by $g_A(i)$ / $g_B(i)$, where $g_A(i)$ and $g_B(i)$ are the concentrations of the *i*-th miRNA in IPF and control samples, respectively. For the murine data the miRNA expression after 7 and 14 days of bleomycin instillation was compared to *day 0*. Statistical significance was determined by the Wilcoxon rank-sum test.

4.2.6.2 *Identification of target sites*

To determine potential binding sites of candidate miRNAs, first, the WISP1 3'UTR was filtered by regions likely bound by the miRNA-containing ribonucleoprotein complexes (miRNPs). Recent studies using cross-linking and immunoprecipitation (CLIP) provide a properly mapping of transcriptome-wide binding sites of RNA-binding proteins. In particular, CLIP of AGO provides specific regions of likely AGO binding and miRNA target sites (Chi et al, 2009; Hafner et al, 2010). The photoactivatable-ribonucleoside-enhanced CLIP (PAR-CLIP) data from Kishore *et al.* (Kishore et al, 2011) was prepared and 1 000 positive (AGO^+) and 1 000 negative instances (AGO^-) were extracted. AGO^+ corresponds to a nucleotide (nt) located at the centre of a crosslink-centred region of 41 nt length, whereas AGO^- is a nucleotide located in the centre of a 41 nt region not bound by AGO. Several features have been proposed that should increase the probability for the detection of a true miRNA target site (Wen et al, 2011). These characteristics were used and adapted, which are independent of any specific miRNA to enable an unbiased detection of potential AGO binding sites. In the end, a support vector machine (SVM) was trained using the following features: conservation, local AU, GU and U content, AU and GC asymmetry bias, compositional entropy, relative position, structural accessibility, and aggregation of mature miRNA patterns. The performance was evaluated by a 5-fold cross-validation (accuracy of 75.30%) and tested for any experimental bias against a set composed of 2 000 instances from a high-throughput sequencing of RNA isolated by CLIP setup (HITS-CLIP) (accuracy of 68.85%) (Kishore et al, 2011). All potential AGO^+ sites were predicted for the WISP1 3'UTR (Ensembl transcript ENST00000250160) (www.ensembl.org (Flicek et al, 2012)).

Segments composed of 20 nt up- and 20 nt downstream of an AGO[+] site were classified as region with increased affinity for the miRNP. It has been shown that complementarity to the miRNA seed region is most predictive to changes in mRNA levels in response to changes in miRNA concentration (Lewis et al, 2005). According to the set of miRNA seed types it was searched for all potential sites, which are complementary to the first 6 to 8 nt of the miRNA 5' end: 6merα (1 - 6), 6merβ (2 - 7), 6merγ (3 - 8), 7merα (1 - 7), 7merβ (2 - 8), 8merα (1 - 8) for the WISP1 3'UTR (http://genome.ucsc.edu/ (Kent et al, 2002)) (Ellwanger et al, 2011). The stability defined by the hybridization energy ΔG_{hybrid} of the miRNA:mRNA heteroduplex was predicted by the tool IntaRNA requiring the given seed pairing (Busch et al, 2008).

4.2.6.3 *Statistical Analysis*

Statistical analyses were performed using the GraphPad Prism Software V5 and the R software environment (http://www.r-project.org/). Results are presented as mean with standard error of the mean (SEM) or standard deviation (SD), as indicated in the figure legends. Differences in samples were denoted statistical significant if $p < 0.05$ using one of the following tests: Wilcoxon rank-sum test, Student t-test or one-way ANOVA followed by Dunnett's post-test.

5 RESULTS

5.1 Identification of target miRNAs binding to WISP1 3'UTR

Gene expression is a highly regulated process (Chen & Rajewsky, 2007). In post-transcriptional gene regulation miRNAs play a pivotal role. MiRNAs were reported to be altered in pulmonary fibrosis (Pandit et al, 2011). In order to investigate WISP1 regulation by miRNAs crucial for IPF pathogenesis, one aim of the project was to investigate if downregulated miRNAs in IPF were able to bind to the *WISP1* mRNA. Therefore, as a first step three miRNA datasets from human and experimental pulmonary fibrosis were compared for overlapping downregulated miRNAs (GEO: *GSE13316*, (Pandit et al, 2010), *GSE21394* (Cho et al, 2011), and *E-MEX-P2749* (Liu et al., 2010) identifying four promising candidate miRNAs. In a second step, the candidate miRNA binding capacities to WISP1 were investigated.

5.1.1 Analysis of miRNA datasets from pulmonary fibrosis tissue specimens

In a miRNA microarray data set analysing ten IPF and ten control lung tissue specimens a total of 30 miRNAs were downregulated in IPF (GEO: *GSE13316*), Figure 5.1).
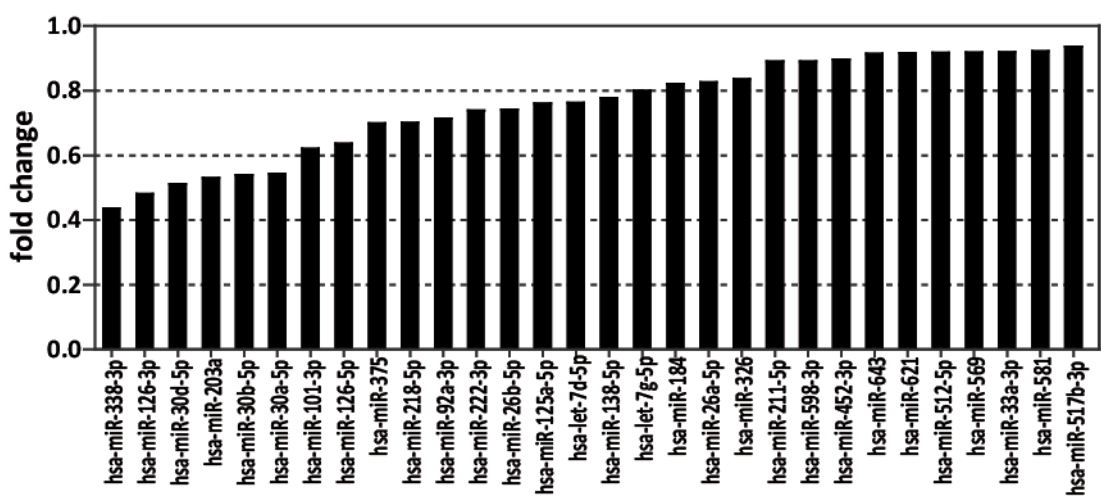
Figure 5.1: MiRNAs downregulated in IPF whole lung tissue.
30 miRNAs are significantly downregulated in a miRNA data set comparing ten IPF and ten donor whole lung tissue specimens (GEO: *GSE13316*, Wilcoxon rank-sum test p< 0.05). MiRNA designations are according to miRBase, Release 20.

A second human data set comparing nine IPF/UIP samples against six control samples (GEO: *GSE21394*) was investigated for decreased miRNAs according to the performed analysis, three miRNAs were downregulated in both human miRNA datasets (miRNA fold change (FC) in data set one and two: miR-30a FC 0.543 and 0.395, miR-30d FC 0.511 and 0.297, and miR-92a 0.714 and 0.449, respectively, Figure 5.2).
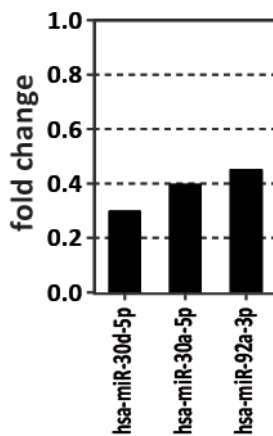
Figure 5.2: MiR-30d-5p, miR-30a-5p and miR-92a-3p were downregulated in a second human miRNA data set.
Analysis of a second miRNA data set (GEO: *GSE21394*) for overlapping downregulated miRNAs was performed. Nine IPF/UIP *versus* six control samples were compared.

Important biological mechanisms are conserved among species. Therefore, a murine miRNA data set from experimental fibrosis was analysed in addition for overlapping downregulated miRNAs. Three animal samples each for *day 0*, *day 7* and *day 14* were compared in the published data set *E-MEX-P2749* (Liu et al, 2010). The murine expression levels for all 30 miRNAs downregulated in IPF (data from the first human data set) were investigated. Figure 5.3 shows that 13 miRNAs were downregulated under experimental fibrotic conditions on *day 7* and *day 14* after bleomycin instillation compared with *day 0*.

A

Day 7 versus Day 0
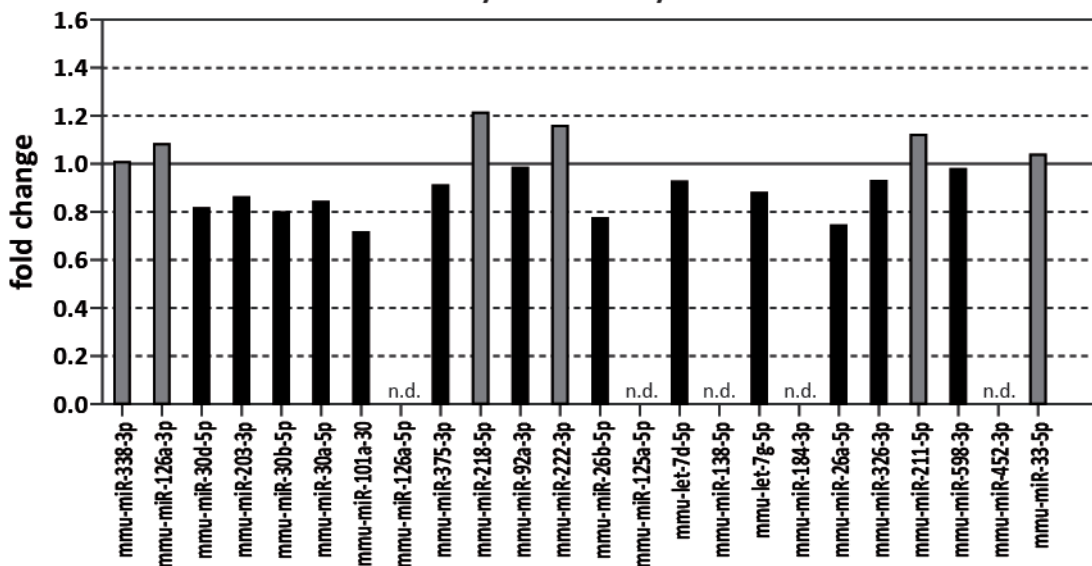
B

Day 14 versus Day 0
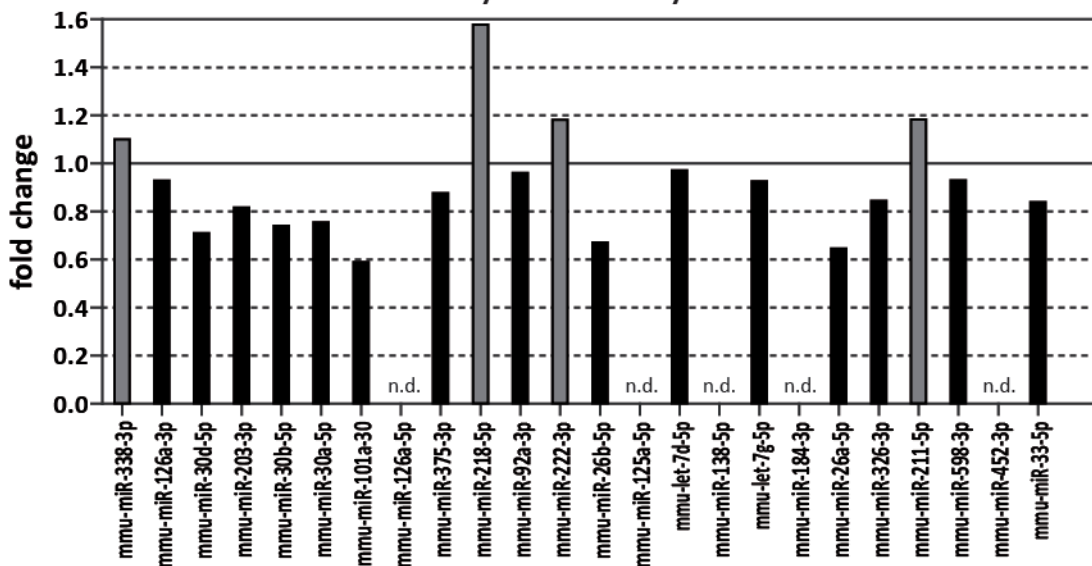
Figure 5.3: 13 miRNAs, downregulated in human IPF samples, were also identified to be downregulated in experimental lung fibrosis.

A) and B) *Day 7* and *14* miRNA data sets from lungs of bleomycin-instilled mice were investigated for expression levels of the same miRNAs, as reported in Figure 5.1. MiRNA designations are according to miRBase, release 20, but here the murine designations are displayed. Black bars represent FCs<1 and grey bars FCs>1, n.d. = not detectable.

5.1.2 Target miRNA identification

It is known that miRNAs target mRNAs mostly at the 3'UTR (Baek et al, 2008; Grimson et al, 2007).

In order to examine possible miRNA binding sites on the WISP1 3'UTR, a SVM based algorithm was applied to the miRNA expression data. For all 13 miRNAs downregulated in human and murine experimental fibrosis the predicted miRNA binding sites on the WISP1 3'UTR are listed in Table 5.1.

Table 5.1: **Number and type of binding sites for the combined downregulated miRNAs.)** (Candidate miRNAs are marked bold in first column)

miRNA	Seed anchor quantity and type on human WISP1 3'UTR						total
	6merα	6merβ	6merγ	7merα	7merβ	8mer	
hsa-miR-30d-5p	**2**	**1**	**1**		**2**		**6**
hsa-miR-203a	**3**	**1**	**1**			**1**	**6**
hsa-miR-30b-5p	2	1	1		2		6
hsa-miR-30a-5p	**2**	**1**	**1**		**2**		**6**
hsa-miR-101-3p		2			1	1	4
hsa-miR-375		1					1
hsa-miR-92a-3p		**2**	**2**	**1**			**5**
hsa-miR-26b-5p	1		1		1		3
hsa-let 7d-5p	2						2
hsa-let 7g-5p	1						1
hsa-miR-26a-5p	1		1		1		3
hsa-miR-326		1	1				2
hsa-miR-598-3p		1	1				2

MiRNA seed anchor types were classified according to the nomenclature introduced by (Ellwanger et al, 2011). Schematic representations of miRNA seed types are depicted in Figure 5.4.
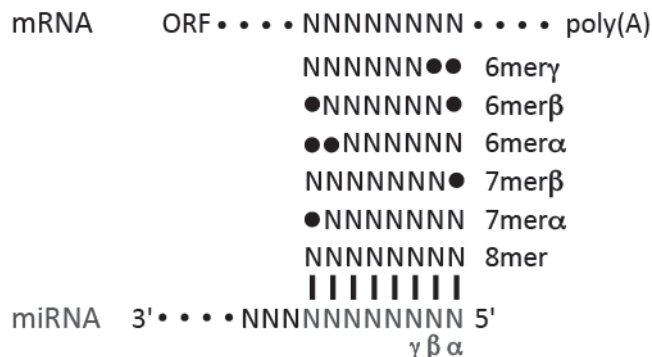
Figure 5.4: Definition of seed types.
The seed types were named by the start position relative to the 5′-end of the miRNA and the length of the consecutive seed match according to (Ellwanger et al, 2011).

Between one and six binding sites were found on the WISP1 3'UTR for all identified miRNAs. For further analysis the candidate miRNA group was narrowed down according to the following criteria: seed length, total number of binding sites and downregulated in human and murine pulmonary fibrosis. It is reported that the length of the miRNA seed has a major influence on the dynamics of the miRNA (Baek et al, 2008; Nielsen et al, 2007). Therefore, miRNAs with 7mer and 8mer seeds were chosen. Additionally, miRNAs may work in concert in order to regulate a single target transcript, and it was shown that more

binding sites repress a reporter gene to a higher extend (Lee et al, 2011) and that one 8mer has the repression capacity of two 7mers (Nielsen et al, 2007). So, miRNAs with in total five or six binding sites were evaluated as candidate miRNA. For these reasons, miR-30a-5p/d-5p (as representatives for miR-30 family, miR-30a/d), miR-92a-3p (miR-92a) and miR-203a were chosen as candidate miRNAs, which should be followed up on (Table 5.1, candidate miRNAs are marked bold). In addition to the binding prediction with the novel SVM tool, the binding of these candidate miRNAs to the WISP1 3'UTR were confirmed using the TargetScan prediction tool (TargetScan Human V6.2 (Lewis et al, 2005)). Figure 5.5 depicts the binding site positions of these candidate miRNAs on the WISP1 3'UTR. The 7mer and 8mer binding sites are underlined.
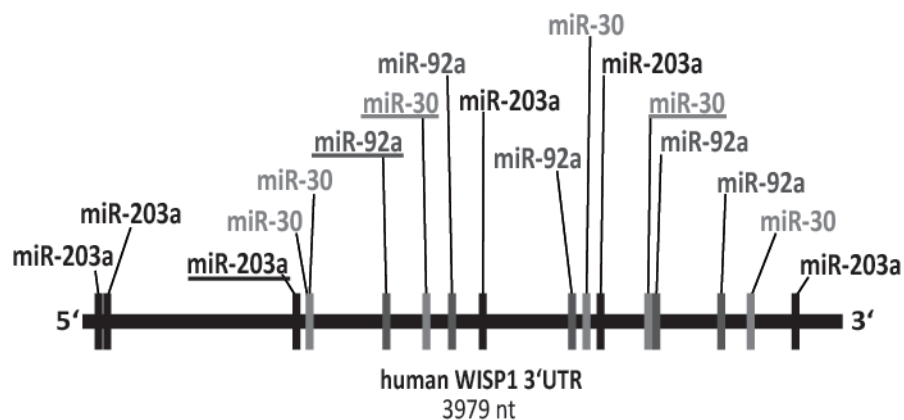
Figure 5.5: Schematic presentation of candidate miRNAs binding sites on the human WISP1 3'UTR.
According to USCS genome browser (GRCh 37/hg 19) the human WISP1 3'UTRs consists of 3979 nt and is depicted as a black line from its 5' to its 3' end. The different binding sites of the candidate miRNAs are depicted with vertical lines: miR-203a in black, miR-30 in light grey and miR-92a in dark grey. Underlined miRNAs represent the 7mer and 8mer positions of these miRNAs.

In Table 5.2 the exact start positions of the miRNA binding sites are listed. The binding sites seem to be randomly distributed over the whole 3'UTR.

Table 5.2: Exact start position of the candidate miRNAs binding site on the human WISP1 3'UTR.

miRNA	Start of binding site on human WISP1 3'UTR					
	6merα	6merβ	6merγ	7merα	7merβ	8mer
hsa-miR-30	2982, 3525	1183	1194		1811, 2657	
hsa-miR-203a	78, 2732, 3761	2109	125			1125
hsa-miR-92a-3p		2583, 3369	1947, 3027	1600		

In summary, 13 miRNAs downregulated in both experimental and human lung fibrosis were identified. Four miRNAs, miR-30a, miR-30d, miR-92a and miR-203a were chosen for evaluation as putative candidate miRNAs.

5.2 Analysis of miRNAs and WISP1 expression *in vivo* and *in vitro*

5.2.1 Expression analysis of candidate miRNAs and WISP1 in human samples

5.2.1.1 *Analysis of IPF tissue*

The different candidate miRNA expression levels of the published data sets described above were confirmed in IPF tissue. Therefore, whole lung tissue specimens were analysed for candidate miRNA expression. Significantly lower miRNA levels were detected for all candidate miRNAs in IPF compared to donor samples (mean +/- SEM of relative miRNA expression from donor *versus* IPF samples: miR-30a 5.17 +/- 0.10 *versus* 3.53 +/- 0.39, miR-30d 3.95 +/- 0.12 *versus* 2.07 +/- 0.42, miR-92a 2.92 +/- 0.13 *versus* 1.63 +/- 0.42, miR-203a: 0.63 +/- 0.17 *versus* -0.76 +/- 0.28, n=8 for donor and 7 for IPF tissue specimens, Figure 5.6). In addition, miR-338 was analysed, since it was the most downregulated miRNA in the first data set (miR-338: -2.86 +/- 0.27 SEM (donor) *versus* -5.78+/- 0.59 (IPF), Figure 5.6).
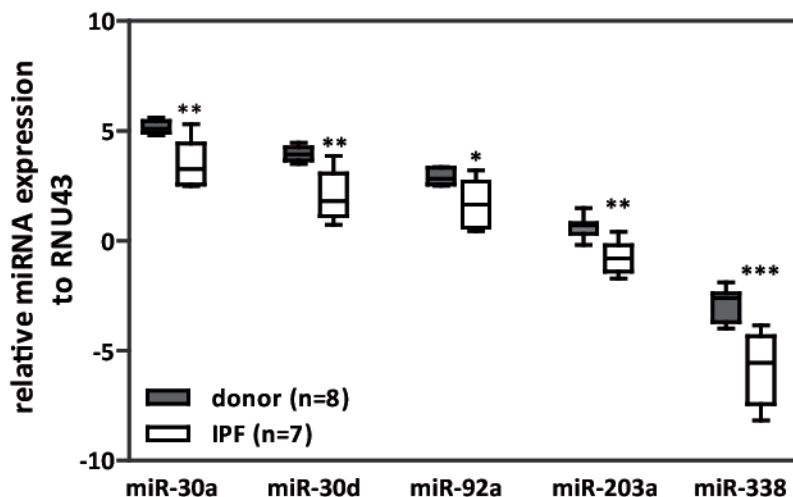
Figure 5.6: Candidate miRNA downregulation was confirmed in IPF tissue samples.
QRT-PCR analyses were conducted for candidate miRNAs and miR-338 as a positive control for downregulated miRNAs in IPF with eight donor (dark grey boxes) and seven IPF (open boxes) whole lung tissue samples. The expression levels of the miRNAs are shown relative to the housekeeping gene RNU43 and the expression values with Whisker Box Blots ranging from 10th-90th percentile (Mann Whitney test, * p<0.05, ** p<0.01, *** p<0.001).

Importantly, WISP1 was upregulated on protein level comparing six IPF whole lung tissue homogenate samples to six donor samples by Western Blotting as shown in Figure 5.7. COL1A1 and α-SMA levels were analysed as profibrotic markers, and both were upregulated in the IPF tissue samples.
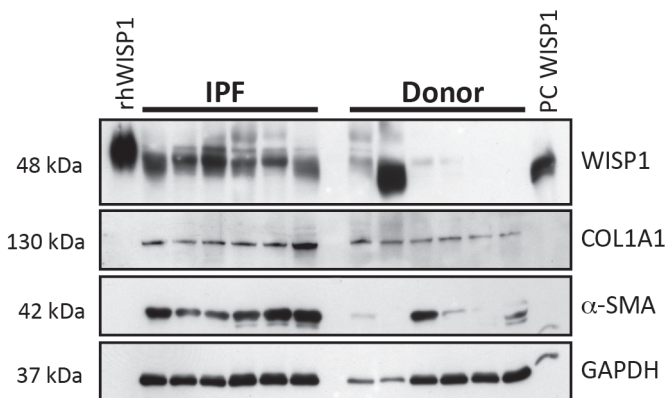
Figure 5.7: Human WISP1 protein was increased in IPF tissue.
Western Blot analysis was performed from six IPF and donor whole lung tissue specimens for WISP1, COL1A1 and α–SMA. GAPDH served as loading control. WISP1 loading controls are rhWISP1 protein (rhWISP1) and positive control WISP1 (PC WISP1: cell lysate from WISP1 overexpressing A549 cells).

Altogether, the downregulation of candidate miRNAs was accompanied by WISP1 protein upregulation in IPF tissue specimens.

5.2.1.2 *Analysis of human fibroblasts*

IPF is characterized among others by fibroblastic foci containing α-SMA positive myofibroblasts, and excessive ECM production mainly collagens and fibronectin (Klingberg et al, 2013). It was shown that WISP1 exhibited profibrotic effects on fibroblasts resulting in increased collagen production after WISP1 stimulation (Königshoff et al, 2009). In addition, WISP1 was associated with new collagen synthesis in experimental fibrosis in mice (Blaauboer et al, 2013). Therefore, *WISP1* mRNA expression was analysed in primary human fibroblasts (phFB) derived from IPF patients. *WISP1* is significantly increased in fibrotic phFB compared to non-fibrotic phFB on mRNA levels (mean +/- SD, relative mRNA expression: -0.74 +/- 2.13 (non-fibrotic phFB) *versus* 3.932 +/- 1.29 (fibrotic phFB), n=3, t-test p=0.046, Figure 5.8 A). For *CTGF*, another CCN family member and profibrotic cytokine, no significant difference was detected (mean +/- SD, relative mRNA expression: 8.600 +/- 2.213 (non-fibrotic phFB) *versus* 10.05 +/- 0.678 (fibrotic phFB)). In addition, *ACTA2*, the gene encoding for α-SMA, and extracellular matrix components *COL1A1* and *FN1* were investigated from the same samples (Figure 5.8 B). *COL1A1* was significantly higher expressed in these fibrotic fibroblasts (mean +/- SD, relative mRNA expression non-fibrotic phFB *versus* fibrotic phFB: *ACTA2* -3.664 +/- 0.895 *versus* -2.952 +/- 0.840; *COL1A1* 0.110 +/- 0.579 *versus* 1.600 +/- 0.381, t-test p = 0.0204; *FN1* 1.964 +/- 0.852 *versus* 1.125 +/- 0.351).
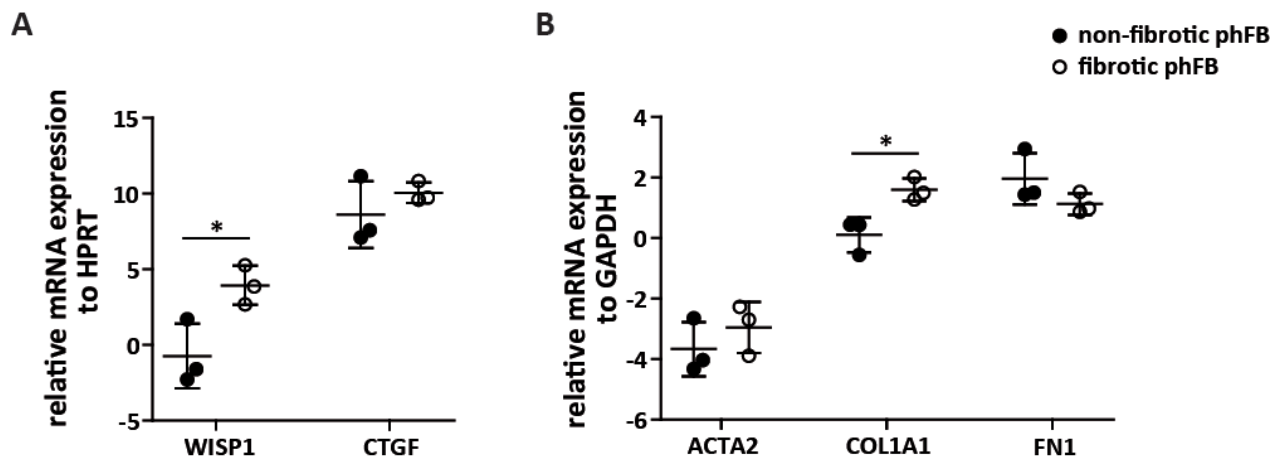
Figure 5.8: *WISP1* mRNA was higher expressed in phFB derived from IPF patients.
A) QRT-PCR of phFB derived from non-fibrotic and fibrotic lungs were investigated for *WISP1* and *CTGF* expression. Relative mRNA expression compared to the housekeeping gene *HPRT* is displayed. B) QRT-PCR of the same phFB was performed for the fibrotic markers *ACTA2*, *COL1A1* and *FN1*. Relative mRNA expression compared to the housekeeping gene *GAPDH* is displayed. Filled and open circles represent non-fibrotic and fibrotic phFB, respectively (n=3 +/- SD, unpaired t-test, * p<0.05).

As *WISP1* was significantly higher in profibrotic fibroblasts on mRNA level, in addition protein levels were addressed. WISP1 Western Blot analysis of five samples per group revealed that WISP1 expression was highly sample dependent (Figure 5.9 A). Tissue specimens, from which mRNA expression analysis was obtained before, were loaded in lane (3-8), and these protein results reflect *WISP1* mRNA data from Figure 5.8 A. As WISP1 is a secreted protein, WISP1 content in cell supernatant was measured. WISP1 ELISA analysis from cells' supernatants was in accordance with the Western Blot analysis as it is also indicated by Pearson correlation analysis (Figure 5.9 B-C) (WISP1 protein in pg/ml mean +/- SEM: non fibrotic 0.088 +/- 0.0216, n=5 *versus* fibrotic 0.118 +/-0.011 n=4; Correlation analysis: Pearson correlation coefficient r=0.7385, p=0.0231, R^2=0.5453).
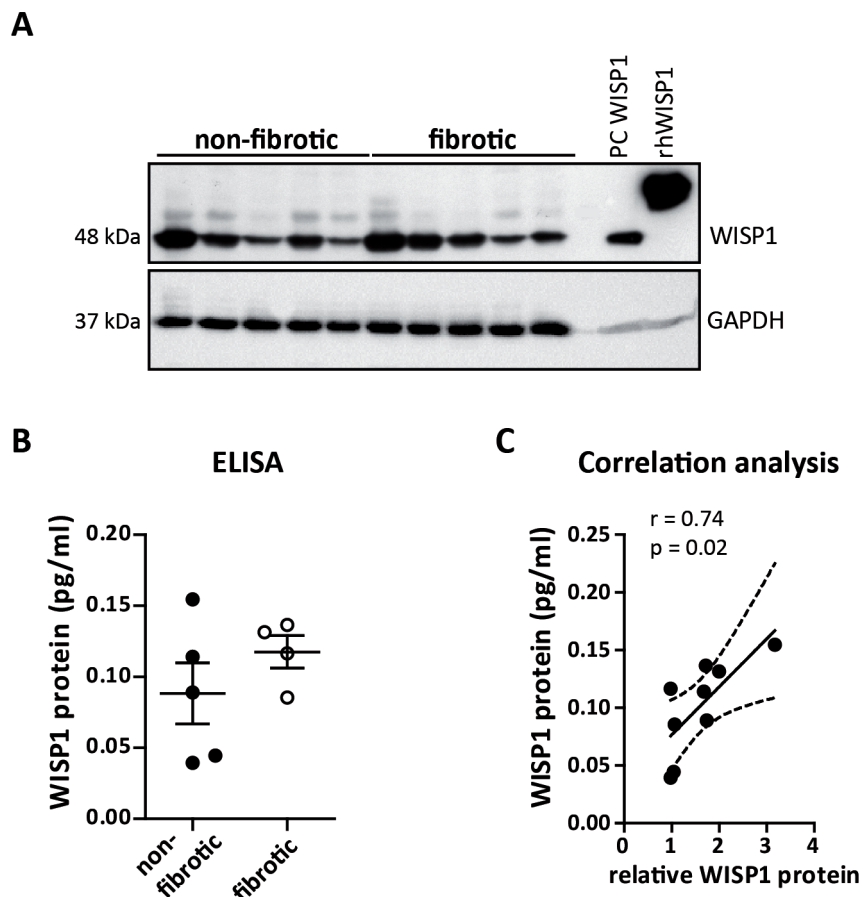
Figure 5.9: WISP1 protein expression in phFB from fibrotic patients.
A) Western Blot analysis for WISP1 of phFB cell lysates derived from non-fibrotic or fibrotic lungs. WISP1 controls are rhWISP1 protein (rhWISP1) and positive control WISP1 (PC WISP1: cell lysate from WISP1 overexpressing A549 cells). GAPDH served as loading control. B) WISP1 ELISA of cell supernatants collected from non-fibrotic or fibrotic phFB. Filled and open circles represent non-fibrotic and fibrotic phFB, respectively (n= 4-5 +/- SEM). C) WISP1 correlation analysis comparing Western Blot and ELISA data. Axis: x = WB protein, y = ELISA protein. The continuous line displays linear regression analysis; the dashed lines show the 95% confidence interval.

For the reason that WISP1 was upregulated in phFB, candidate miRNA expressions in fibrotic *versus* non-fibrotic phFB were investigated. Surprisingly, miR-30a and miR-30d tended to be even higher expressed in fibrotic cells than in non-fibrotic ones (mean +/- SD of relative miRNA levels for non-fibrotic *versus* fibrotic phFB: miR-30a -5.254 +/- 0.271 *versus* -4.470 +/- 0.983, miR-30d -4.918 +/- 0.255 *versus* -4.358 +/- 0.946,). Mean expression of miR-92a was similar for non-fibrotic and fibrotic fibroblasts (miR-92a relative expression mean +/- SD: -1.706 +/- 0.329 *versus* -1.612 +/- 0.877), and miR-203a was not detectable in human fibroblasts. Interestingly, correlation analysis revealed a strong negative correlation for miR-92a and *WISP1* mRNA (r=-0.830, p=0.0109, R^2=0.688, Figure 5.11 A), and also negative correlation for miR-92a and WISP1 protein (Western Blot data) (r=-0.684, p=0.042, R^2=0.468 Figure 5.11 B). However, WISP1 expression correlated neither with miR-30a nor miR-30d (data not shown).
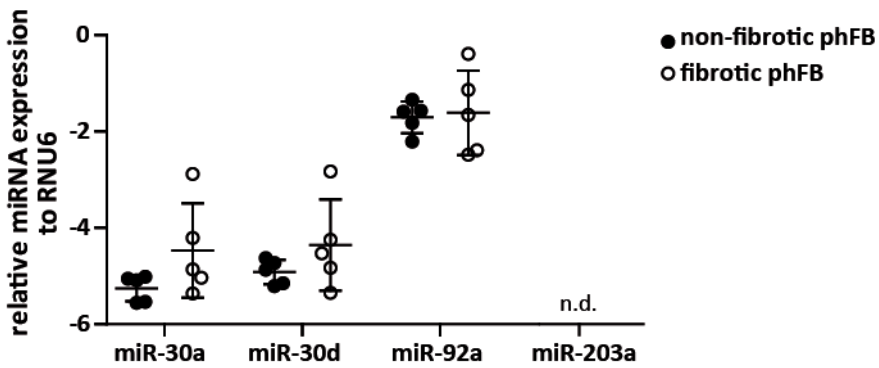
Figure 5.10: Candidate miRNA expression in fibrotic phFB.
MiR-30a, miR-30d, miR-92a and miR-203a expression levels were analysed in cell lysates from non-fibrotic and fibrotic phFB with qRT-PCR. MiRNA expression is depicted relative to the housekeeping gene RNU6. Filled and open circles represent non-fibrotic and fibrotic phFB, respectively (n.d.= not detectable).
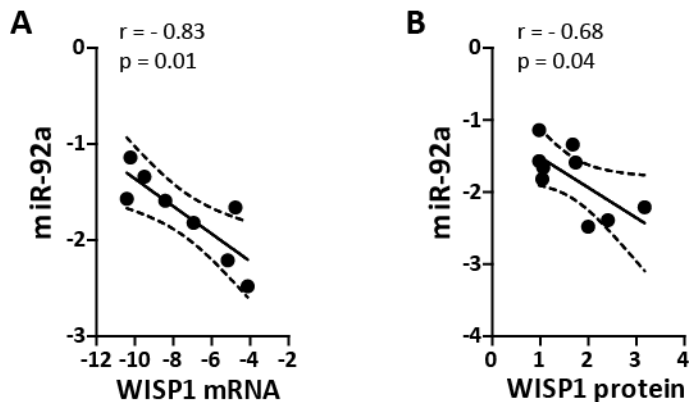
Figure 5.11: MiR-92a correlated negatively with WISP1 in phFB.
A) Pearson correlation analysis for miR-92a and *WISP1* mRNA of non-fibrotic and fibrotic phFBs, n=8, Pearson correlation factor r=-0.83, p=0.01. The continuous line displays linear regression analysis; the dashed lines show the 95% confidence interval. B) Pearson correlation analysis for miR-92a and WISP1 protein (Western Blot data) of non-fibrotic and fibrotic phFBs, n=9, Pearson correlation factor r=-0.68, p=0.04. The continuous line displays linear regression analysis; the dashed lines show the 95% confidence interval.

In summary, fibrotic phFB showed increased *WISP1* mRNA levels. On protein levels WISP1 was slightly increased with a high variability between individual samples. MiR-92a but not miR-30a/d correlated negatively with WISP1 expression in phFB.

5.2.2 Expression analysis of WISP1 and candidate miRNAs in murine samples

In addition to human samples, murine samples from bleomycin-induced fibrosis were investigated. Reasons for this are on the one hand verification analysis of the published data for miRNA expression and on the other hand minimization of the patient variability influence on data outcome. This was especially important, as WISP1 protein levels were highly patient dependent. Moreover no information about patients' genetic background, comorbidities and medication was available.

5.2.2.1 *Analysis of experimental fibrosis tissue*

Whole lung tissue samples were investigated for miRNA expression from control (ctrl) or bleomycin (BLEO)-treated mice at the indicated days after instillation. In general, miRNAs tended to be downregulated in experimental fibrosis, but the fold changes were smaller compared to the human data (Figure 5.6), and thus confirmed the results from the published data set (Figure 5.3) (mean +/- SEM of relative miRNA expression, miR-30a: 0.0625 +/- 0.08146 (ctrl) *versus* -0.5014 +/- 0.09237 (BLEO d7), -0.3588 +/- 0.1436 (BLEO d14), -0.3950 +/- 0.1949 (BLEO d21), miR-30d: -1.477 +/- 0.1239 (ctrl) *versus* -1.752 +/- 0.1275 (BLEO d7), -1.773 +/- 0.1080 (BLEO d14), -1.893 +/- 0.2274 (BLEO d21), miR-92a: -3.012 +/-0.1252 (ctrl) *versus* -3.139 +/- 0.09335 (BLEO d7), -3.336 +/- 0.1215 (BLEO d14), -3.030 +/- 0.1030 (BLEO d21), miR-203a: -5.326+/-0.7145 (ctrl) *versus* -6.345 +/- 0.09340 (BLEO d7), -6.609 +/-0.1501 (BLEO d14), -6.243 +/-0.2015 (BLEO d21), n=8 for ctrl, n=7 for BLEO d7, n=8 for BLEO d14 and n=3 for BLEO d21 samples, Figure 5.12). Note, that significant changes were detected for miR-30a comparing BLEO d7 and d14 with controls.
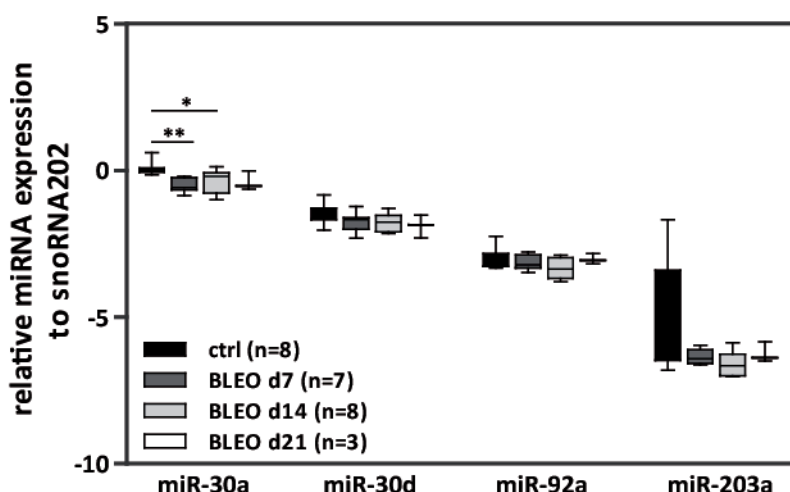
Figure 5.12: Candidate miRNA expression was downregulated in experimental fibrosis.
Analyses of candidate miRNAs in whole lung homogenate from bleomycin-instilled mice at *day 7* (d7), *day 14* (d14) and *day 21* (d21) as well as from ctrl (n=4 for saline-instilled mice, d14, and n=4 for untreated mice). Whisker Box Plots with 10th-90th percentile, one-way ANOVA with Dunnett's post-test * p<0.05, ** p<0.01.

Nevertheless, *Wisp1* was highly increased at the mRNA level comparing whole lung tissue from controls *versus* bleomycin-treated samples on *day 14* (mean +/- SD of *Wisp1* relative mRNA level: -3.305 +/- 0.3799 for ctrl *versus* -0.8791 +/- 0.3564 for bleomycin, n=3 t-test p=0.0013, Figure 5.13 A) corroborating earlier reports (Königshoff et al, 2009). Wisp1 protein increase was also detected in BALF (mean protein in pg/ml +/- SD: 57.43 +/- 52.32 for ctrl (n=16) *versus* 270.4 +/- 148.7 for BLEO (n=22), t-test with Welch's correction p<0.001, Figure 5.13 B).
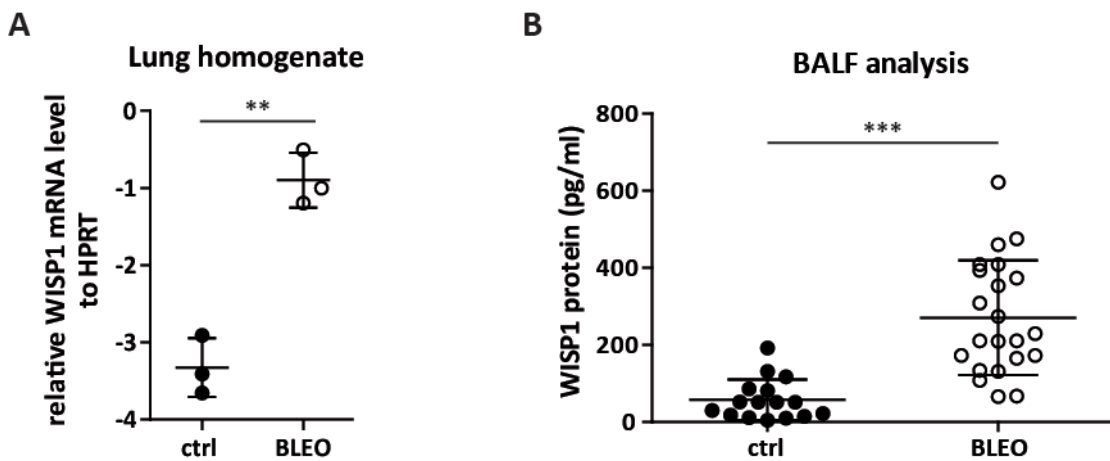
Figure 5.13: Wisp1 was increased in whole lung homogenate from bleomycin-instilled mice.
A) QRT-PCR analysis of whole murine lung homogenate from *day 14* after bleomycin instillation for WISP1 (n=3 +/- SD, t-test ** p<0.01). B) Wisp1 ELISA of BALF samples collected at d14 after bleomycin instillation (n=16 for ctrl and n=22 for BLEO +/- SD, t-test with Welch's correction *** p<0.001). Filled circles and ctrl represent control animals instilled with saline; open circles and BLEO represent fibrotic animals instilled with bleomycin.

5.2.2.2 *Analysis of murine alveolar epithelial cells*

In order to complete the picture for miRNA analysis for murine samples, cell specific analysis for primary murine ATII (pmATII) cells was performed. Primary murine fibroblasts (pmFB) were not analysed for miRNA expression, because *WISP1* was not differentially expressed in these cells (data not shown and (Königshoff et al, 2009), and because pmFB did not retain a fibrotic phenotype in our culture conditions. As it was reported previously and as shown in Figure 5.14, *Wisp1* was highly increased in freshly isolated pmATII cells at *day 14* after bleomycin instillation compared to control cells (relative *Wisp1* mRNA level +/- SD: -7.211 +/- 0.7755 for ctrl (n=3 for untreated mice and n=4 for saline-instilled mice and -2.305 +/- 0.5437 for BLEO mice (n=11), unpaired t-test p<0.0001).
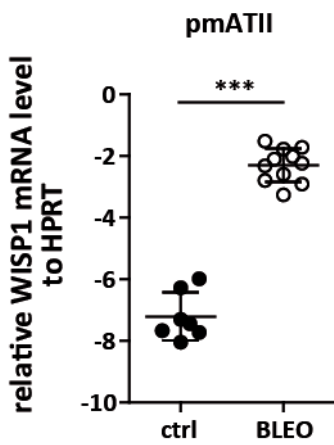
Figure 5.14: *Wisp1* mRNA was increased in pmATII cells from bleomycin treated mice.
QRT-PCR analysis was performed for WISP1 from pmATII cells. Freshly isolated cells from *day 14* after bleomycin instillation were examined. Relative mRNA levels compared to the housekeeping gene *HPRT* are shown (n=7 +/-SD for ctrl cells (filled circles) and n=11 +/- SD for bleomycin-diseased cells (open circles), t-test, *** p<0.001).

Therefore, candidate miRNAs were analysed in pmATIIs isolated from fibrotic mice (Figure 5.15). All miRNAs were lower expressed under fibrotic conditions in pmATII cells, the changes for miR-30d and miR-92a were significant (mean of relative miRNA levels +/- SD: miR-30a -0.4990 +/- 0.5157 (non-fibrotic) *versus* -0.9467 +/- 0.1833 (fibrotic), miR-30d -1.741 +/-0.4016 (non-fibrotic) *versus* -2.263 +/- 0.09465 (fibrotic), t-test p=0.0373; miR-92a -3.073 +/- 0.2922 (non-fibrotic) *versus* -3.572 +/- 0.02466 (fibrotic), t-test p=0.0145; and miR-203a -6.388 +/- 0.1949 (non-fibrotic) *versus* -6.783 +/- 0,4200 (fibrotic), n=5, for control mice (three cell isolations from untreated wild type mice and two from saline-instilled controls at *day 14*), and n=3 for BLEO pmATII cells).
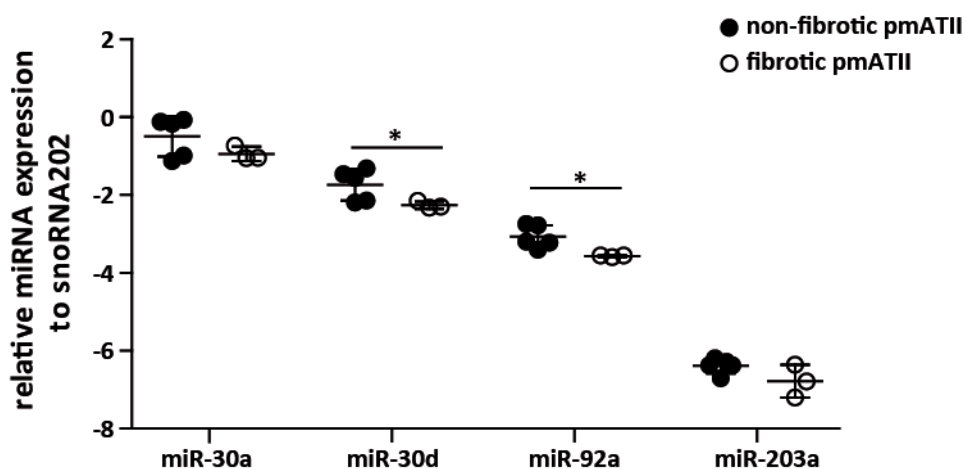
Figure 5.15: MiR-30d and miR-92a were downregulated in fibrotic pmATII cells.
Candidate miRNA levels were investigated by qRT-PCR in non-fibrotic (filled circles) and fibrotic (open circles) pmATII cells. Freshly isolated cells from *day 14* after bleomycin instillation were examined. Relative miRNA levels compared to the housekeeping gene snoRNA202 are depicted (n=5 +/-SD, three cell isolations from wild type and two from saline controls, were considered as non-fibrotic pmATII cells, n=3 +/- SD for fibrotic pmATIIs; one-tailed t-test * p<0.05).

In summary, downregulation of miR-30a, miR-30d, miR-92a and miR-203a was demonstrated in human and murine whole lung tissue specimens. It was newly described that human fibroblasts can be a source for WISP1 increase in IPF and miR-92a negatively correlates with WISP1 in fibroblasts derived from IPF patients. Furthermore, candidate miRNAs decrease may contribute to WISP1 increase in pmATII cells.

5.3 WISP1 3'UTR reporter gene analysis

WISP1 and candidate miRNAs expression was negatively correlated. To understand better the link between miRNA and WISP1 expression, binding analyses of miRNAs to the WISP1 3'UTR were performed. 3'UTR reporter assays are widely used to investigate post-transcriptional gene regulation by miRNAs. Therefore, WISP1 3'UTR reporter constructs were cloned and subsequently the influence of the candidate miRNAs was investigated.

5.3.1 Analysis of the whole WISP1 3'UTR

For reporter gene analysis, first an efficient and suitable transfection protocol was established. For WISP1 3'UTR analysis A549 cells were used. These cells were chosen, because they have low or no endogenous expression of the candidate miRNAs according to the Ambion miRNA research guide, what was corroborated by qRT-PCR (results not shown).

Transfection efficiency analyses of A549 cells were conducted with a GFP reporter plasmid. Immunofluorescence images were analysed for GFP positive cells compared with non-transfected cells after 24 h of transfection using the Imaris Software. The best efficiency was obtained using a 1:2 ratio of plasmid *versus* lipofectamine LTX, where the plasmid was preincubated with PLUS reagent in a 1:1 ratio. Thereby, transfection efficiency was 41.4% +/- 9.9. A representative image is depicted in Figure 5.16 A. In addition A549 cells were transfected with a red fluorescence Cy3-labeled miRNA mimic. After 24 h of transfection, immunofluorescence analysis showed that almost every cell was transfected using the same transfection protocol as for the GFP plasmid (Figure 5.16 B). From this, it was concluded, that cells transfected with GFP plasmid were most probably also transfected with miRNA mimics.
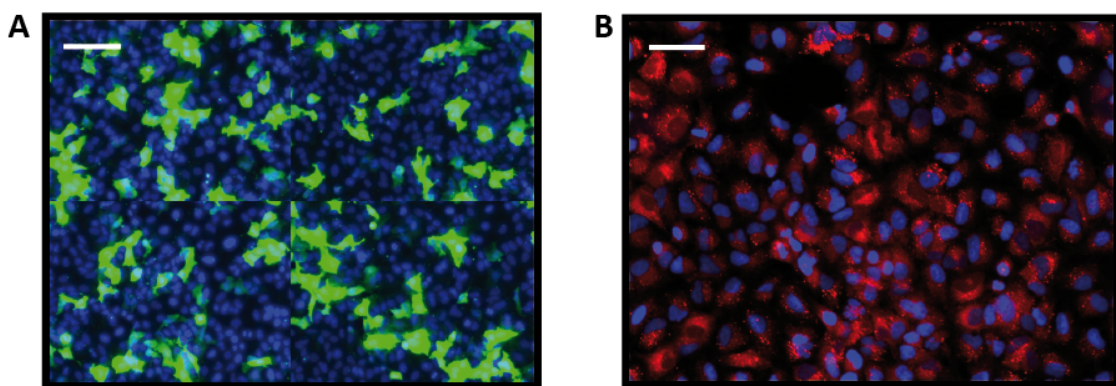
Figure 5.16: Transfection setup of A549 cells.
A) Representative image of A549 cells transfected with GFP reporter plasmid. Immunofluorescence analysis was performed after 24 h of transfection (blue: DAPI stained nuclei, green: ectopic GFP expression, scale bar: 100 μm). B) Representative image of A549 cells transfected with fluorescence labelled miRNA reporter mimics. Immunofluorescence analysis was performed after 24 h of transfection (blue: DAPI stained nuclei, red: miRNA mimics, scale bar: 50 μm).

The hWISP1 3'UTR was cloned into a luciferase reporter plasmid. The reporter plasmid applied was pmirGLO dual-luciferase miRNA target expression vector. It encodes two luciferase genes. The firefly luciferase gene (*luc2*) is the primary reporter gene under the control of the human phosphoglycerate kinase (PGK) promoter. The control reporter is a humanized *Renilla* luciferase neomycin fusion gene under the control of a SV40 early enhancer/promoter. The hWISP1 3'UTR was amplified by PCR from A549 gDNA with cloning primers containing a restriction site for either XhoI or NotI. This fragment was cloned into the pmirGLO vector resulting in a new vector, named pmirGLOW, with the hWISP1 3'UTR downstream of the firefly reporter gene. The complete sequence of the

pmirGLOW vector was verified by restriction digests as well as by sequencing the complete plasmid. Figure 5.17 shows a schematic picture of the pmirGLOW vector.
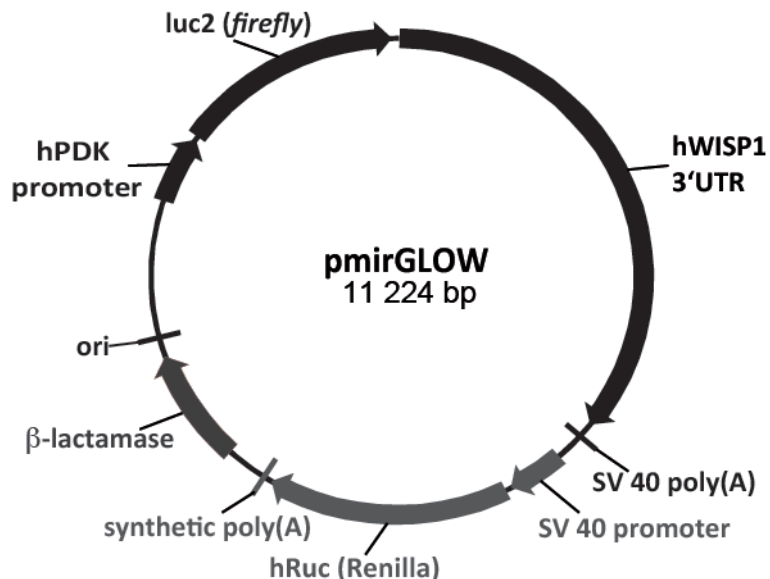
Figure 5.17: Schematic image of the WISP1 3'UTR reporter plasmid pmirGLOW.
The pmirGLOW plasmid is a dual luciferase reporter plasmid. Downstream of the primary reporter gene, firefly luciferase gene (luc2), the human WISP1 3'UTR is inserted. *Renilla* luciferase (*hRluc*) is encoded on the same plasmid and serves as control reporter for normalization.

A549 cells were co-transfected with pmirGLOW reporter plasmid and either negative control mimic or miRNA mimic in different concentrations (Figure 5.18 A and B, 5 pmol ≙ 20 nM and 50 pmol ≙ 200 nM miRNA mimic, respectively). MiRNA mimics are modified dsRNA oligonucleotids mimicking endogenous miRNA duplexes, and hence resemble overexpression of miRNAs. 48 h after co-transfection, firefly and *Renilla* luciferase activities were measured. Firefly luminescence values were divided by *Renilla* luminescence values and normalized to the M-miR-NCI transfected cell results. No significant difference was observed in firefly reporter luciferase activity comparing control transfected (M-miR-NCI) with candidate miRNA mimic transfected cells (M-miR-30a, -30d, -92a and 203a) (mean normalized ratio to cells transfected with M-miR-NCI +/- SD: M-miR-30a 87.81+/- 12.67, M-miR-30d 87.97+/- 6.488, M-miR-92a 111.9 +/- 11.83, M-miR-203a 96.16 +/- 7.430, one-way ANOVA with Dunnett's post-test (control = M-miR-NCI) no difference; similar data for 50 pmol: M-miR-30a 88.23 +/- 27.49, M-miR-30d 98.72 +/- 19.49, M-miR-92a 130.3 +/- 17.86, M-miR-203a 102.5 +/- 23.34.)
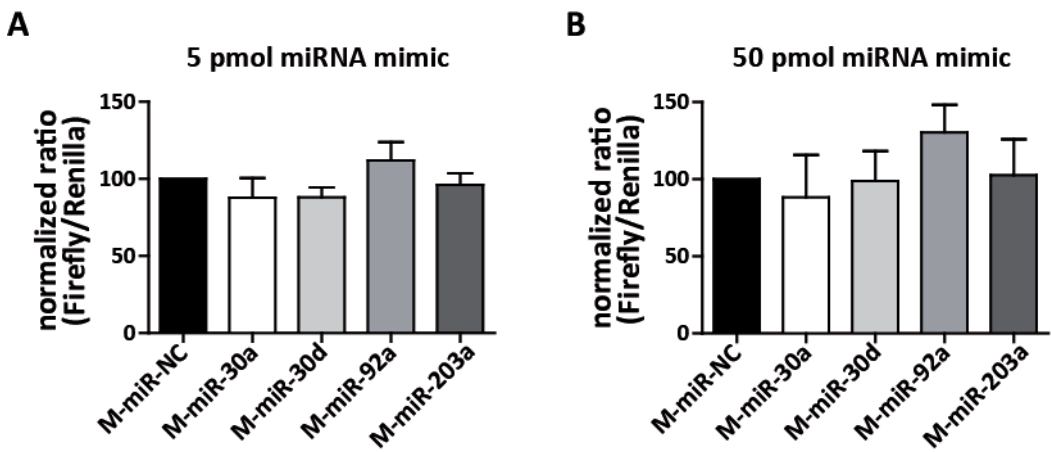
Figure 5.18: Luciferase analysis of A549 cells co-transfected with pmirGLOW and miRNA mimics.
A) A549 cells were transfected with pmirGLOW luciferase plasmid and with 5 pmol miRNA of either negative control mimics (M-miR-NC, black bar) or candidate miRNA mimics (M-miR-30a, open bar; M-miR-30d, light grey bar; M-miR-92a, grey bar and M-miR-203a dark grey bar). After 48 h cells were analysed for firefly and *Renilla* luminescence, the reporter and constant luciferase, respectively, n=3 +/- SD. B) Same analysis as in A) using 50 pmol miRNA mimic, n=2 +/- SD.

5.3.2 Analysis of truncated WISP1 3'UTR reporter plasmids

In order to rule out unspecific off-target effects of the miRNA mimics, co-transfections of miRNA mimics not only with pmirGLOW but also with the original vector pmirGLO were performed (Figure 5.19). No off-target effects were observed, as co-transfections of candidate miRNA mimics with pmirGLO did not alter luciferase ratios compared to negative control mimic. Interestingly, A549 cells co-transfected with the WISP1 3'UTR containing vector, pmirGLOW, and miRNA mimics, showed less firefly activity compared to the pmirGLO co-transfected ones. This suggested that the WISP1 3'UTR has regulatory properties alone on its own. However, miRNA mimics could not downregulated firefly luciferase in the pmirGLOW setup, as seen before in Figure 5.18. (Mean normalized ratio +/- SD for pmirGLO and co-transfected mimics: M-miR-30a 100.9 +/- 14.89, M-miR-30d 100.7 +/- 12.61, M-miR-92a 116.1 +/- 11.87, M-miR-203a 100.2 +/- 8.861; for pmirGLOW and co-transfected mimics: M-miR-NCI 34.45 +/- 7.641, M-miR-30a 29.89 +/- 6.047, M-miR-30d 30.23 +/- 6.868, M-miR-92a 38.03 +/- 5.778, M-miR-203a 32.99 +/- 7.157, One-way ANOVA with Dunnett's post-test (control pmirGLO + M-miR-NCI: p<0.0001 compared to all pmirGLOW co-transfected setups, Figure 5.19).
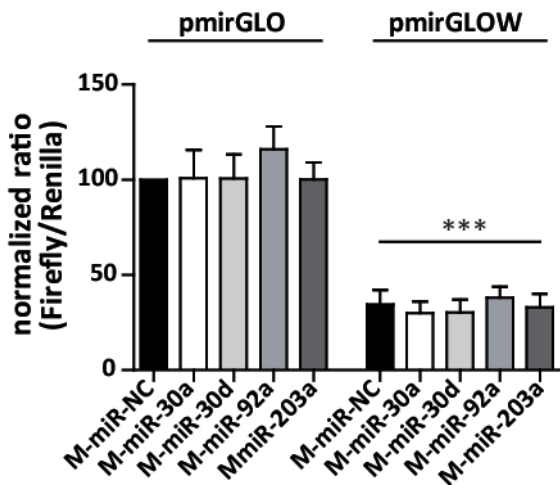
Figure 5.19: WISP1 3'UTR destabilized reporter luciferase.
A549 cells were either transfected with the pmirGLO, the unmodified reporter plasmid or with pmirGLOW, containing the WISP1 3'UTR between the firefly CDS and a synthetic poly(A) tail, and miRNA mimics (100 nM). After 48 h cells were analysed for luciferase activities, n=3 +/-SD, one-way ANOVA with Dunnett's post-test to pmirGLO + M-miR-NC transfected cells *** $p < 0.001$).

To further address this observation and to investigate, if shorter truncations of the WISP1 3'UTR show similar effects or may be detectably controllable by miRNAs, three additional WISP1 3'UTR luciferase reporters were constructed.

Figure 5.20 shows the 3'UTRs fragments chosen for the truncation constructs. PmirGLOW1 has incorporated about the first 1.1 kb from the WISP1 3'UTR from the 5' end containing only three miR-203a bindings sites (two 6mer (α, γ) and one 8mer) and no further candidate miRNA binding sites. The second truncated WISP1 3'UTR reporter, pmirGLOW2, contains about 0.9 kb ranging from 1.1 kb to 2 kb downstream from the WISP1 CDS. This fragment contained three binding sites for miR-30 (two 6mer (β, γ), one 7merβ) and two for miR-92a (one 6merγ and one 7merβ). The last truncation fragment contained the last part of the WISP1 3'UTR (about 2 kb) (pmirGLOW3). This region harboured predicted binding sites for all candidate miRNAs (nine in total, three miR-30 (two 6merα, one 7merβ), three miR-92a (two 6merβ, one 6merγ) and three miR-203 (two 6merα, one 6merβ)).
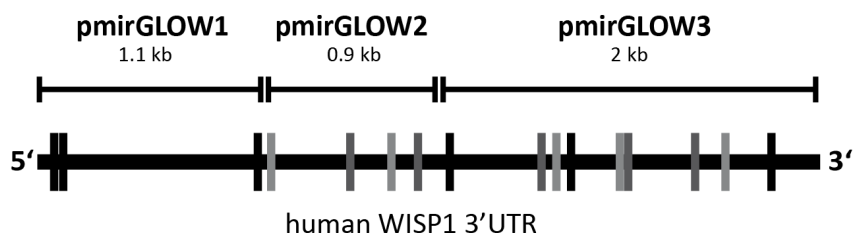
Figure 5.20: Schematic description of WISP1 3'UTR truncation constructs.
Three truncated WISP1 3'UTR fragments were cloned downstream of firefly luciferase resulting in pmirGLOW1-3. The pmirGLOW1 plasmid harbours the 5' end of the WISP1 3'UTR, where only miR-203a binding sites (black lines) are located. The pmirGLOW2 encodes the middle part of the WISP1 3'UTR with predicted miR-30 (light grey) and miR-92a (dark grey) binding sites. The pmirGLOW3 plasmid contains the 3' end of the 3'UTR with predicted binding sites for all candidate miRNAs.

First, A549 cells were transfected with the pmirGLO, pmirGLOW and pmiGLOW1-3 and luciferase activities were measured after 48 h. As observed before, pmirGLOW-transfected cells exhibited a decrease in firefly luciferase activity compared to pmirGLO-transfected cells (mean +/- SD 100 +/- 0 (pmirGLO) *versus* 36.58 +/- 2.768 (pmirGLOW). Using the new constructs, pmirGLOW1-3, a length and region dependent decrease in firefly luciferase activity was observed compared to pmirGLO (mean +/- SD: 62.04 +/- 5.899 (pmirGLOW1), 67.13 +/- 3.610 (pmirGLOW2), 46.04 +/- 6.625 (pmirGLOW3), n=3, one-way ANOVA with Dunnett's post-test (pmirGLO as control) *** $p<0.0001$, Figure 5.21 A). Interestingly, pmirGLOW3 reached similar low ratios as pmirGLOW. These results were confirmed in phFB (mean +/- SD compared to normalized ratio pmirGLO: 19.14 +/- 3.984 (pmirGLOW), 51.87 +/- 10.63 (pmirGLOW1), 70.28 +/- 8.718 (pmirGLOW2), 25.69+/- 0.1625 (pmirGLOW3), n=3, one-way ANOVA with Dunnett's post-test (pmirGLO as control) *** $p<0.0001$, Figure 5.21 B). Furthermore, co-transfections with truncated constructs and miRNA mimics were conducted. Here, no difference in luciferase activity was detected between transfections with and without miRNAs mimics. These results indicated that WISP1 3'UTR on its own is able to decrease reporter gene activity.

In summary, the incorporation of the WISP1 3'UTR led to decreased luciferase expression in a region and length dependent manner, but a further decrease in reporter activity after miRNA overexpression was not found.
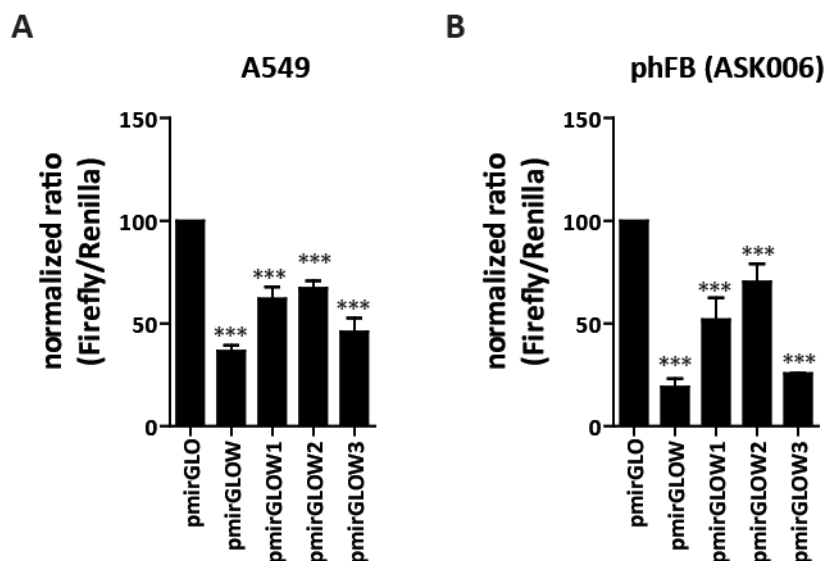
Figure 5.21: WISP1 3'UTR length and sequence influenced luciferase reporter expression in human lung cells.

A) A549 cells were transfected with pmirGLO and different 3'UTR WISP1 reporter plasmids (pmirGLOW, pmirGLOW1-3). Luciferase activities were measured after 48 h and are normalized to the pmirGLO transfected cells. (n=3 +/- SD, one-way ANOVA with Dunnett's post-test *** $p<0.0001$) B) Same setup as in A, but phFB (ASK006) were applied (n=3 +/- SD, one-way ANOVA with Dunnett's post-test *** $p<0.0001$).

5.3.3 MiRNA binding site reporter plasmids

As no significant miRNA dependent regulation of the different WISP1 3'UTR constructs was detected, two additional approaches were performed to ensure that these results are not artefacts of the applied method. Luciferase constructs specific for each candidate miRNA were cloned. Figure 5.22 gives an overview for the specific plasmids. Two the complementary sequences of the functional miRNA were included in tandem downstream of the firefly reporter sequence in the pmirGLO plasmid, resulting in pSi constructs (Figure 5.22 A). These constructs were used as proof of principle tools for miRNA studies, where the miRNAs function similar to siRNAs. Second, four pMI plasmids were designed. Here the sequences of the predicted miRNA binding sites were cloned downstream of the luciferase reporter CDS. In order to increase the chance for miRNA binding, the sequences were incorporated three times in a row, Figure 5.22 B.
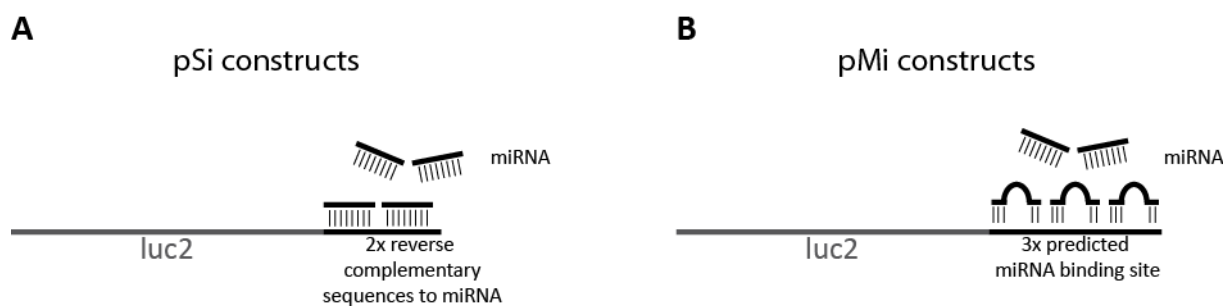
Figure 5.22: Schematic representation of pSi and pMi constructs.
Both vector types originate from the pmirGLO vector. A) The pSi construct harbours the reverse complement sequence of the respective miRNA two times downstream of the firefly coding sequence (luc2). B) The pMi construct harbours three predicted miRNA binding sites downstream of the firefly coding sequence (luc2). The miRNA binding sites are listed in the appendix.

In contrast to the luciferase reporter assays above, the pSi and pMi experiments were conducted with HEK cells. These cells were applied on the one hand as they are commonly used for reporter assay, as they are easy to transfect, and on the other hand because here no significant difference in firefly activity was observed between pmirGLO and pmirGLOW plasmids (ratio mean +/- SD 12.49 +/- 1.230 (pmirGLO) and 15.37 +/- 1.598 (pmirGLOW), n=3, Figure 5.23).
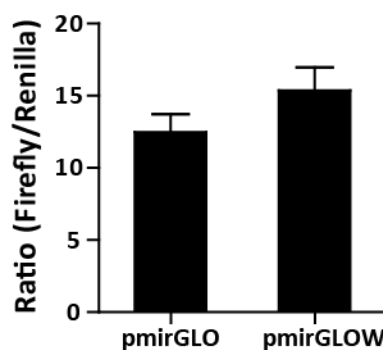
Figure 5.23: Firefly luciferase activity was not altered by WISP1 3'UTR in HEK cells.
Luciferase activities were analysed after 48 h of HEK cells transfection with either pmirGLO or pmirGLOW, n=3 +/- SD.

HEK cells were transfected with either pmirGLO, or the different pSi constructs in combination with no miRNA mimic (w/o), two different negative control mimics (M-miR-NCI and II) or the specific target miRNA mimics (for instance pSi30a plus M-miR-target = pSi30a plus M-miR-30a) (Figure 5.24). First, miRNA off-target effects due to miRNA overexpression were ruled out by comparing pmirGLO co-transfected with no mimic target, with control mimics or with miRNA mimics, as here no significant differences in luciferase activity were detected. Second, comparison analyses for each vector with the respective miRNA mimics and control mimics were carried out. Significant decrease was found for pSi30a in combination with M-miR-30a for firefly luciferase activity compared to only pSi30a vector transfected cells. However, there was no significant difference for control transfections (mean normalized ratio +/- SD, n=3 one-way ANOVA with Dunnett's post-test to pSi30a + w/o mimic: 84.07 +/- 8.47 (pSi30a +/- w/o), 81.99 +/- 19.10 (pSi30a + M-miR-NCI), 92.63 +/- 6.764 (pSi30a + M-miR-NCII), 54.64 +/- 24.41 (pSi30a + M-miR-30a, $p<0.05$). This data confirmed the proof of principle approach, as miRNA mimics were specifically able to decrease firefly activity in pSi-transfected cells. Similar results were obtained for pSi30d, but not for pSi92a and pSi203a. Of note, comparing the different vectors to each other, all pSi vectors had similar ratios except pSi92a (mean normalized ratio +/- SD, n=3 one-way ANOVA with Dunnett's post-test compared to pmirGLOW: 100 +/- 0.0 (pmirGLO), 84.07 +/- 8.47 (pSi30a), 79.94 +/- 11.72 (pSi30d), 37.28 +/- 8.27 (pSi92a ### $p<0.0001$), 87.96 +/- 11.58 (pSi203a)). For all pSi92a involved experiments, significant lower firefly activity was observed, and as for the pmirGLOW vectors firefly activity could not be further downregulated with miRNA overexpression (mean normalized ratio +/- SD, n=3: 37.28 +/- 8.27 (pSi92a +/- w/o), +/- 32.36 +/- 14.03 (pSi92a + M-miR-NCI), 40.74 +/- 10.31 (pSi92a + M-miR-NCII), 35.89 +/-10.42 (pSi92a + M-miR-92a)).
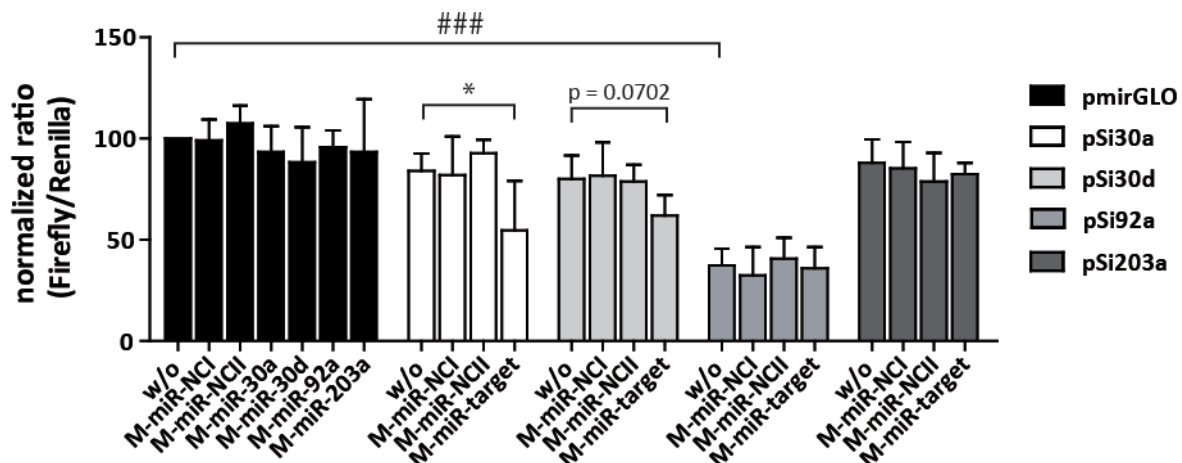
Figure 5.24: Firefly luciferase activity was regulated exogenously investigating pSi30a and pSi30d constructs and endogenously using pSi92a construct.
(Co-) transfections of HEK cells with pmirGLO (black bars) or pSi constructs and 100 nM miRNA mimics were performed and luciferase activities were measured after 48 h. Normalized ratios to pmirGLO transfected cells are displayed (pmirGLO without any miRNA mimics (w/o)). Open bars are HEK cells transfected with pSi30a construct and either no miRNA mimic (w/o), with negative control mimics I or II (M-miR-NCI or M-miR-NCII) or with the specific target mimic, here miRNA mimic for miR-30a (target); light grey bars represent pSi30d, grey bars pSi92a and dark grey bars pSi203a transfected cells (n=3 +/-SD; comparison between vectors w/o miRNA mimics: one-way ANOVA with Dunnett's post-test (w/o = only pmirGLO transfected cells) ### p<0.001; comparison between one group transfected with the same vector and w/o or different miRNA mimics: one-way ANOVA with Dunnett's post-test (w/o = only vector transfected cells) * p<0.05).

Analysis of the endogenous expression of candidate miRNAs in HEK cells (Figure 5.25) showed that miR-92a was the highest expressed one. MiR-30a and –d were expressed at similar levels and miR-203a was not detectable (mean of relative miRNA expression +/- SD, n=3: miR-30a -5.185 +/- 0.157, miR-30d -4.878 +/- 0.193, miR-92a 0.520 +/- 0.335).
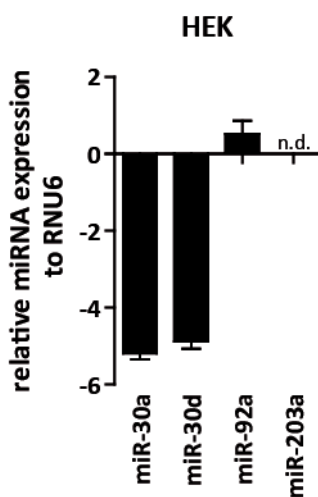
Figure 5.25: MiR-92a was the highest expressed miRNA among the candidate miRNAs in HEK cells.
Relative candidate miRNA levels compared to the housekeeping gene RNU6 in HEK cells are depicted, n=3 +/- SD, n.d. = not detectable.

The same experiments, as with the pSi constructs (Figure 5.24) were conducted with the pMi constructs (Figure 5.26). Similar results were obtained regarding off-target effects and luciferase activities for only vector controls. However, in contrast to pSi transfections, no change in firefly luciferase activity was measured for any target miRNA and pMi co-transfections.
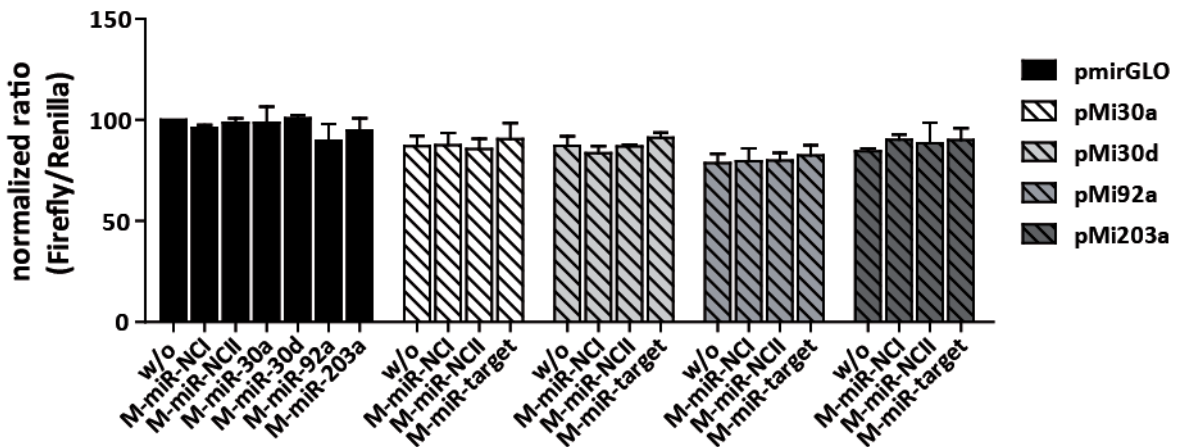
Figure 5.26: Firefly luciferase activity was not altered investigating pMi constructs.
(Co-) transfections of HEK cells with pmirGLO (black bars) or pMi constructs and miRNA mimics were performed and luciferase activities were measured after 48 h. Normalization was done to only pmirGLO transfected cells (pmirGLO without any miRNA mimics (w/o)). Open hatched bars are HEK cells transfected with pMi30a construct and either no miRNA mimic (w/o), with negative control mimics I or II (M-miR-NCI or M-miR-NCII) or with the specific target mimic, here miRNA mimic for miR-30a (target); light grey hatched bars represent pMi30d, grey hatched bars pMi92a and dark grey hatched bars pMi203a transfected cells (n=3 +/-SD).

To complete these experiments and to better assess the effect of endogenous miRNAs on the assay, miRNA inhibitors (I-miRs) were applied in combination with the pSi and pMi constructs and both luciferase activities were examined 48 h after transfection.

MiRIDIAN miRNA hairpin inhibitors, which are nucleic acid-based molecules, incorporate the reverse complement of the mature miRNA and are chemically modified to prevent RISC-induced cleavage and to enhance binding affinity to the mature miRNA. When delivered to a cell, binding of endogenous mature miRNAs to these complementary synthetic target sites is thought to be irreversible, thus these inhibitors are presumed to sequester the endogenous miRNA, making it unavailable for normal function. A decrease of the mature miRNA can be detected by qRT-PCR, and the miRNA-dependent regulated mRNA is diminished resulting in an upregulation of the mRNA and the respective protein. (Vermeulen et al, 2007). Inhibition of miR-203a was not performed, as this miRNA was not expressed in HEK cells. For the pSi and I-miR experiments, an increase for firefly luciferase was detected for pSi92a and I-miR-92a co-transfection corroborating previous results (mean ratio +/- SD, n=3, one-way ANOVA with Dunnett's post-test: 62.05 +/- 7.51 (pSi92a + w/o), 63.70 +/- 10.17 (pSi92a +/- I-miR-NCI), 113.0 +/- 9.11 (pSi92a +/- I-miR-92a, p<0.001), Figure 5.27). A similar trend was observed for pSi30a and I-miR-30a. However, no increase in luciferase activity was detected after co-transfection of the pMi constructs with their respective target inhibitor.
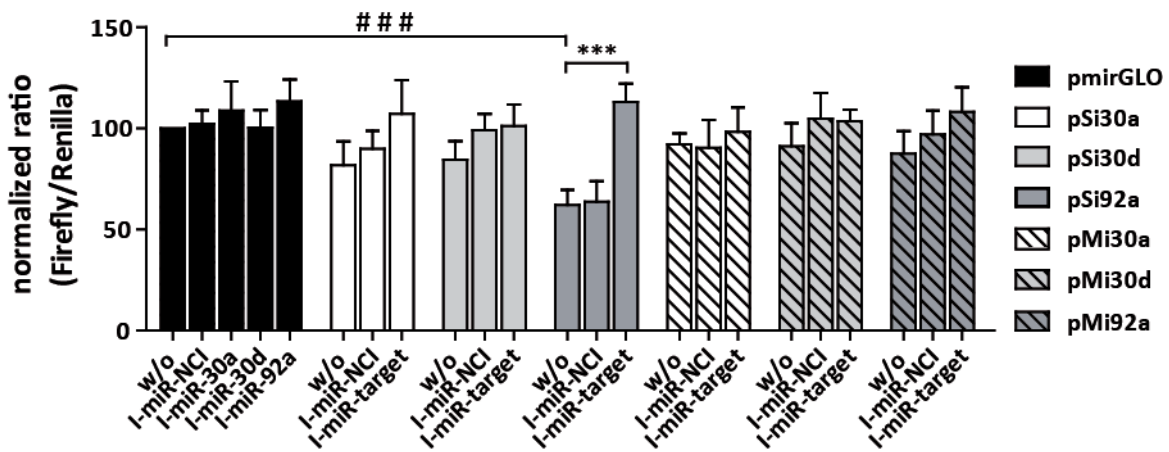
Figure 5.27: MiR-92a inhibition rescued firefly activity investigating pSi92a construct.
Candidate miRNA expressions were inhibited in HEK cells transfected with either pmirGLO (black bars), pSi (open bars) or pMi constructs (hatched bars) and luciferase activities were analysed after 48 h. W/o represents only vector transfected cells, I-miR-NCI the negative control inhibitor and I-miR-target the corresponding miRNA inhibitor, n=3 +/-SD; comparison between vectors w/o miRNA inhibitors: one-way ANOVA with Dunnett's post-test (control = only pmirGLO transfected cells) ### p<0.0001; comparison between one group transfected with the same vector and w/o or different miRNA inhibitors: one-way ANOVA with Dunnett's post-test (control = only vector transfected cells) *** p<0.001.

Altogether, from all luciferase experiments performed, it can be concluded that the WISP1 3'UTR itself already regulated reporter gene expression. Furthermore, the destabilizing effect of the WISP1 3'UTR was length dependent and observed for epithelial and mesenchymal lung cells. Additionally, neither WISP1 3'UTR reporter constructs (pmirGLOW, pmirGLOW1-3) nor candidate miRNA binding site reporter constructs (pMi30a, pMi30d, pMi92a and pMi203a) could be regulated any further by miRNA mimics under the applied experimental conditions.

5.4 Target miRNAs alterations *in vitro* and WISP1 expression analysis

5.4.1 Cell screen for *in vitro* experiments

In the artificial system using WISP1 3'UTR luciferase constructs, no candidate miRNA regulated the WISP1 reporter. Therefore it should be explored, if the endogenous WISP1 expression can be regulated by miRNAs. Candidate miRNAs inhibitions and overexpressions were performed with subsequent analysis of *WISP1* mRNA and protein expression.

To this end, it was first explored which cells were appropriate for such studies. In general, these cells should express WISP1 as well as the candidate miRNAs in order to be able to manipulate both. Epithelial and mesenchymal human lung cells were screened for WISP1 expression (Figure 5.28 A). Neither in A549 lung adenocarcinoma cells often used as model for ATII cells nor in bronchial epithelial cells (16HBE and phBEC) could *WISP1* expression be detected by qRT-PCR. In lung fibroblasts *WISP1* was higher expressed in foetal lung cell lines (HFL1 and MRC5) compared with adult phFB (here cells isolated from donor explant MLT003 tissue specimens) (mean WISP1 relative expression +/- SD, n=3: HFL1 -2.603 +/- 2.985, MRC5 -3,915 +/- 0.175, phFB (MLT003) -6.255 +/- 0.577). From the same cDNA

samples candidate miRNAs were investigated (Figure 5.28 B). MiR-203a was either not detectable or only poorly expressed in bronchial epithelial cells (16HBE and phBEC) where WISP1 was not detectable (mean miR-203a relative expression +/- SD, n=3: 16HBE -9.323+/- 0.303, phBEC -5.188 +/- 1.046). Furthermore, miR-92a was highest expressed among all cells analysed, and higher in epithelial cells compared with mesenchymal cells (mean miR-92a relative expression +/- SD, n=3: A659 -1.477 +/- 0.531, 16HBE -0.590 +/- 0.166, phBEC -1.650 +/- 0.0, HFL1 -2.343 +/- 1.486, MRC5 -4.073 +/- 0.364, phFB (MLT003) -2.393 +/- 0.909). MiR-30a and -30d were similar expressed in all cells (mean miR-30a relative expression +/- SD, n=3: A659 -4.493 +/- 0.586, 16HBE -3.255 +/- 0.048, phBEC -3.642 +/- 0.280, HFL1 -4.410 +/- 1.410, MRC5 -4.958 +/- 0.383, phFB (MLT003) -5.757 +/- 1,012; mean miR-30d relative expression +/- SD, n=3: A659 -4.870 +/- 0.533, 16HBE -3.6417 +/- 0.448, phBEC -4.510 +/- 0.062, HFL1 -4.183 +/- 1.369, MRC5 -5.137 +/- 0.290, phFB (MLT003) -5.360 +/- 0.944).

Considering this screening data, phFB were chosen for further experiments. Here, WISP1 as well as the candidate miRNAs, miR-30a/d and miR-92a, were expressed and could be detected reliably with qRT-PCR. WISP1 was even higher expressed in foetal lung fibroblasts, yet primary adult cells were considered for further experiments, as regulatory mechanisms may be different in foetal cells compared to adult ones.
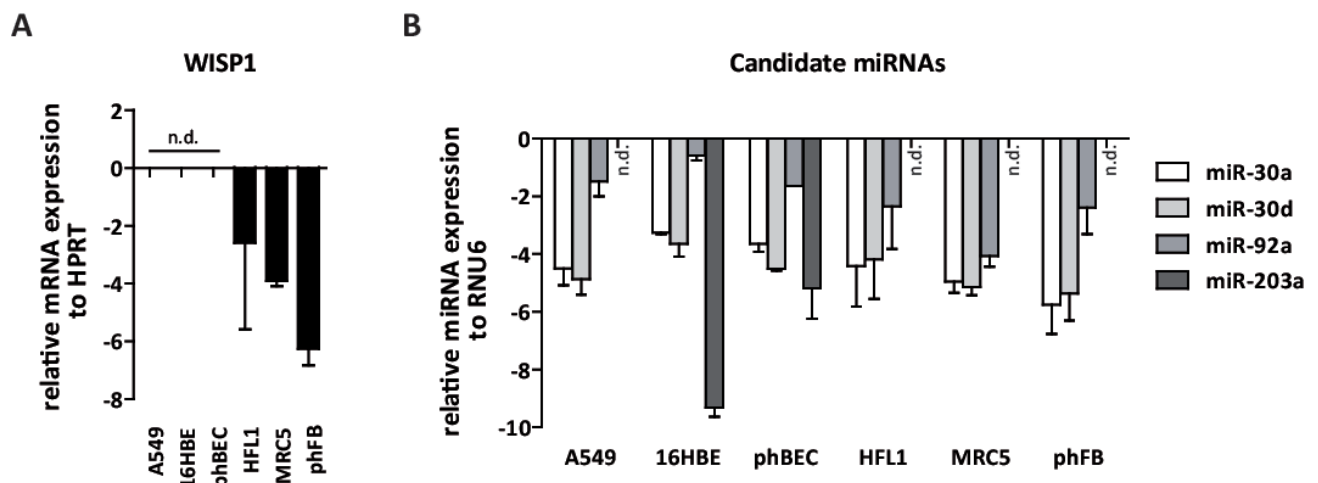
Figure 5.28: Human cell screen for WISP1 and candidate miRNA expression.
A) *WISP1* mRNA levels were investigated in human epithelial and mesenchymal cells and mRNA levels are depicted relative to the housekeeping gene *HPRT*. B) Candidate miRNAs levels were investigated in the same cells as in A). Relative miRNA levels are shown compared to the housekeeping gene RNU6 (n=3 +/- SD; n.d. = not detectable; A549: adenocarcinoma lung epithelial cell line, 16HBE: human bronchial epithelial cell line, phBEC: primary human bronchial epithelial cells; HFL1: human foetal lung fibroblasts, MRC5: human foetal lung fibroblast, phFB (MLT003): primary human lung fibroblasts).

MiRNAs target mostly the 3'UTR, and therefore, the binding predictions for the candidate miRNAs were performed for WISP1 3'UTR. In addition to *WISP1* mRNA expression in general, it was investigated, if the whole WISP1 3'UTR is present in *WISP1* mRNA level in phFB. WISP1 3'UTR PCR analysis was performed with lung fibroblast cDNA as input.

Agarose gel analysis of the PCR revealed that the whole WISP1 3'UTR (about 4 000 bp) exists in lung fibroblasts (Figure 5.29).
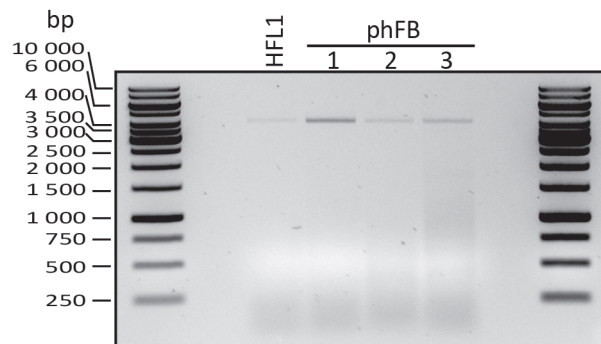

Figure 5.29: Whole WISP1 3'UTR was expressed in human fibroblasts.
PCR analysis for whole WISP1 3'UTR was performed using cDNAs from different human fibroblasts and analysed on a 1% agarose gel. HFL: cDNA from HFL cells, phFB 1, 2 and 3: cDNA from phFB MLT003, phFB ASK006 and phFB ASK006 treated with TGF-β1, respectively.

5.4.2 Inhibition of target miRNAs

As WISP1 was poorly expressed under normal cell culture conditions, first, inhibition of candidate miRNAs was conducted in order to see if this would be followed by *WISP1* mRNA increase. PhFB were transfected with miRNA inhibitors (I-miRs) and after 48 h of transfection, candidate miRNA levels were examined by qRT-PCR, as a decrease of the mature miRNA can be detected by qRT-PCR (Vermeulen et al, 2007). Figure 5.30 shows that the respective inhibitor downregulated the miRNAs in a concentration dependent manner (mean log fold change +/- SD, n=3: miR-30a -4.777 +/- 0.370 (100 nM), -3.115 +/- 0.472 (50 nM), -2.128 +/- 0.465 (25 nM), -1.233 +/- 0.882 (5 nM); miR-30d -5.008 +/-0.812 (100 nM), -4.608 +/- 1.087 (50 nM), -3.528 +/- 1.020 (25 nM), -1.730 +/-0.717 (5 nM); miR-92a -3.395 +/-0.113 (100 nM), -3.102 +/- 0.417 (50 nM), -2.673 +/- 0.634 (25 nM), -1.375 +/- 0.595 (5 nM)).

With 100 nM inhibitors, the highest downregulation of the miRNAs was achieved. In addition even the lowest concentration (5 nM) downregulated the candidate miRNAs. Therefore, these two concentrations were used in further experiments.
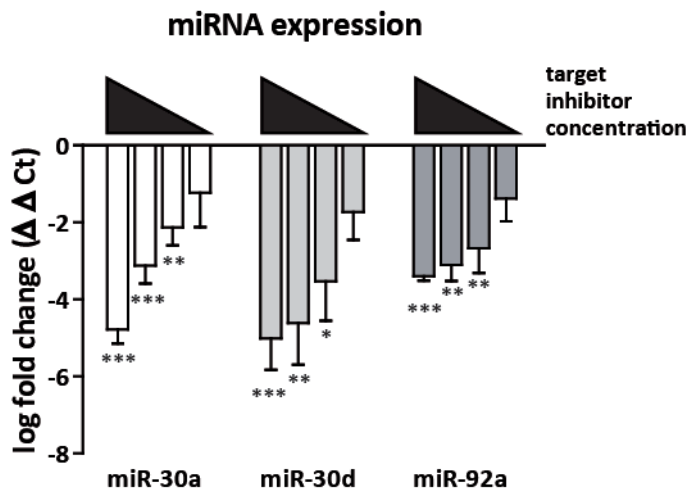
Figure 5.30: Candidate miRNA expression was inhibited in phFB in a miRNA inhibitor concentration dependent manner.
PhFB were transfected with different concentrations of miR-30a/d and -92a inhibitors (100 nM, 50 nM, 25 nM and 5 nM) and negative control miRNA inhibitor, and miRNA expression was analysed after 48 h of transfection. Log fold changes compared to concentration matched negative control inhibitor transfected cells are displayed, n=3 +/- SD, 2x MLT005 and 1x ASK013, one-way ANOVA with Dunnett's post-test to non-transfected cells * $p<0.05$, ** $p<0.01$, *** $p<0.001$.

After establishing the miRNA inhibition, miR-30a, miR-30d and miR-92a were inhibited with 100 nM and 5 nM miRNA inhibitor in phFB, and subsequently WISP1 expression was investigated. Again, the miRNA downregulation was verified by qRT-PCR (Figure 5.31 A). Here, two negative control miRNA inhibitors (I-miR-NCI and II) were used and log fold changes were compared to non-transfected cells. The I-miR-NCI and II transfection had no significant effect on candidate miRNA expression and similar decrease in candidate miRNA expression as reported above was observed with the respective inhibitor (mean miR-30a log fold change compared to non-transfected cells +/- SD: -4.045 +/- 0.4137 (100 nM I-miR-30a), 0.023 +/- 0.308 (100 nM I-miR-NCI), -0.348 +/- 0.447 (100 nM I-miR-NCII) and -1.084 +/- 0.433 (5 nM I-miR-30a), 0.280 +/- 0.310 (5 nM I-miR-NCI), -0.493 +/- 0.203 (5 nM I-miR-NCII); mean miR-30d log fold change compared to non-transfected cells +/- SD: -3.831 +/- 0.511 (100 nM I-miR-30d), 0.038 +/- 0.398 (100 nM I-miR-NCI), -0.456 +/- 0.333 (100 nM I-miR-NCII) and -1.080 +/- 0.750 (5 nM I-miR-30d), 0.198 +/-0.103 (5 nM I-miR-NCI), -0.430 +/- 0.132 (5 nM I-miR-NCII); mean miR-92a log fold change compared to non-transfected cells +/- SD: -2.876+/- 0.453 (100 nM I-miR-92a), 0.145 +/- 0.290 (100 nM I-miR-NCI), -0.520 +/- 0.215 (100 nM I-miR-NCII) and -1.034 +/- 0.908 (5 nM I-miR-92a), 0.423 +/- 0,018 (5 nM I-miR-NCI), -0.340 +/- 0.145 (5 nM I-miR-NCII)).

However, no increase or alteration in *WISP1* mRNA expression could be examined (mean WISP1 log fold change to non-transfected cells: 0.021 +/- 0.557 (100 nM I-miR-NCI), -0.679 +/- 0.308 (100 nM I-miR-NCII), -0.004 +/- 0.892 (100 nM I-miR-30a), -0.119 +/- 0.555 (100 nM I-miR-30d), -0.414 +/- 0.455 (100 nM I-miR-92a), -0.459 +/- 0.285 (5 nM I-miR-NCI), 0.120 +/- 0.412 (5 nM I-miR-NCII), -0.105 +/- 0.301 (5 nM I-miR-30a), -0.575 +/- 0.683 (5 nM I-miR-30d), 0.085 +/- 0.280 (5 nM I-miR-92a), Figure 5.31 B).
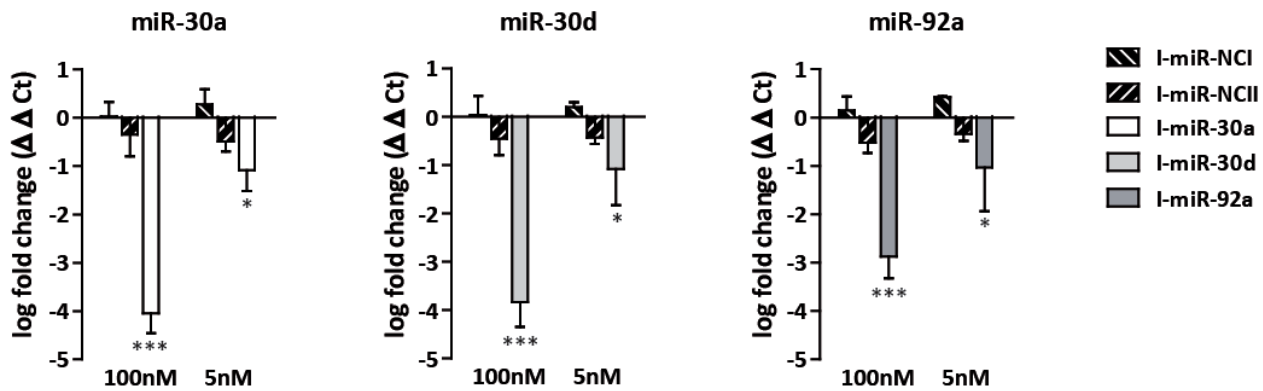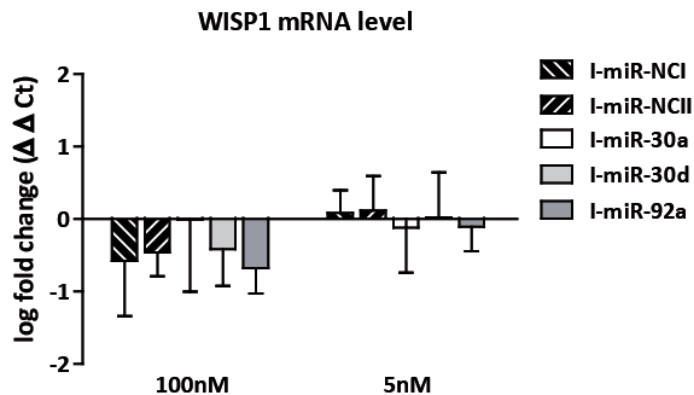
Figure 5.31: MiRNA inhibition in phFB did not alter *WISP1* mRNA expression.
A) MiRNA expression was inhibited in phFB (ASK013) with either 100 nM or 5 nM miRNA inhibitor and miR-30a, -30d and -92a inhibition was analysed after 48 h (indicated on top of each graph). Log fold changes to non-transfected cells are shown. Black bars with white lines represent either negative control inhibitor I (I-miR-NCI) or negative control inhibitor II (I-miR-NCII). Open bars represent miR-30a, light grey bars miR-30d inhibited, grey bars miR-92a inhibited cells, n=5 +/- SD for target inhibition and I-miR-NCI inhibition, n=4 +/- SD for I-miR-NCII; one-way ANOVA with Dunnett's post-test to non-transfected cells * $p<0.05$, *** $p<0.001$. B) WISP1 qRT-PCR from miR-inhibited samples was performed and log fold changes normalized to non-transfected cells are displayed.

MiRNAs function through destabilizing mRNA, but also through repressing translation (Fabian et al, 2010; Huntzinger & Izaurralde, 2011). Although no changes were observed on *WISP1* mRNA levels, still changes on protein levels could be induced by miRNAs. Hence, WISP1 protein levels were analysed by Western Blot and ELISA after 48 h of miRNA inhibition in phFB. Figure 5.32 A depicts a representative WISP1 Western Blot and Figure 5.32 B quantifications of five to nine experiments thereof (mean of relative WISP1 protein normalized to I-miR-NCI: 0.954 +/- 0.369 (100 nM I-miR-30a), 1.002 +/- 0.274 (100 nM I-miR-30d), 0.814 +/- 0.326 (100 nM I-miR-92a), 0.976 +/- 0.315 (5 nM I-miR-30a), 0.942 +/- 0.232 (5 nM I-miR-30d), 0.792 +/- 0.249 (5 nM I-miR-92a)), but no changes for WISP1 were observed. As WISP1 is a matricellular protein secreted from the cell, additionally cell supernatants were analysed using a WISP1 ELISA Figure 5.32 C). Again no WISP1 changes were detected (mean of relative WISP1 protein normalized to I-miR-NCI +/- SD, n=3: 0.933 +/- 0.295 (100 nM I-miR-NCII), 0.964 +/- 0.301 (100 nM I-miR-30a), 0.887 +/- 0.159 (100 nM I-miR-30d), 0.941 +/- 0.192 (100 nM I-miR-92a), 0.981 +/- 0.226 (5 nM I-miR-

NCII), 0.946 +/- 0.208 (5 nM I-miR-30a), 0.967 +/- 0.112 (5 nM I-miR-30d), 0.872 +/- 0.226 (5 nM I-miR-92a)).
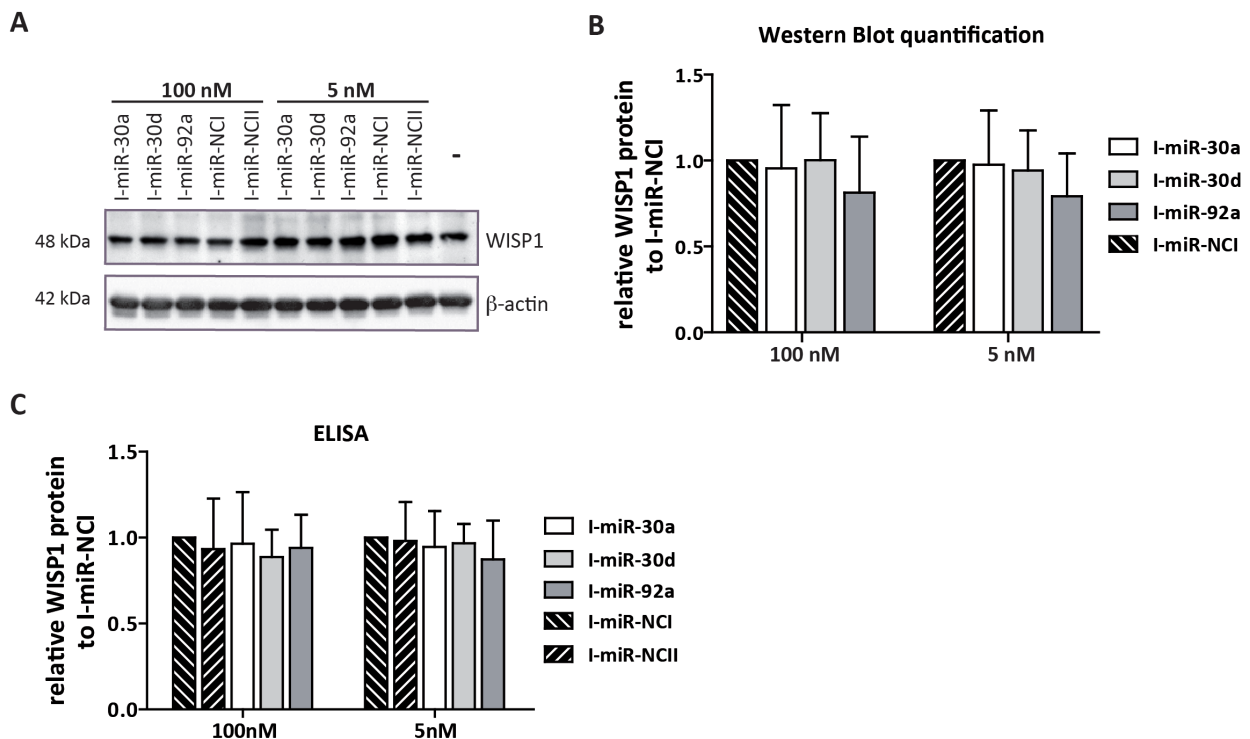

Figure 5.32: MiRNA inhibition in phFB did not alter WISP1 protein expression.
A) Representative WISP1 Western Blot analysis of phFB (ASK013) cell lysates after 48 h of miRNA inhibition with 100 nM and 5 nM inhibitors. As loading control β–actin was used. B) Densitometry of WISP1 Western Blots after 48 h miRNA inhibition normalized to loading control and miRNA negative control inhibitors (I-miR-NCI), n=9 +/-SD for 100 nM and n=5 +/- SD for 5 nM, black hatched bars represent I-miR-NCI transfection, open bars miR-30a, light grey bars miR-30d and grey bars miR-92a inhibition) C) WISP1 ELISA of phFB (ASK013) supernatants after candidate miRNA inhibition. Supernatants were collected after 48 h of inhibitor transfection, and were enriched for proteins for 24 h. WISP1 levels were compared to negative control inhibitor transfected cells (I-miR-NCI), n=3 +/-SD.

5.4.3 Overexpression of candidate miRNAs

As miRNA inhibition did not induce changes in WISP1 mRNA or protein levels, the opposite strategy, overexpression of miRNAs, was conducted. Overexpression of candidate miRNAs within phFB was achieved with miRNA mimic transfection. First, as for miRNA inhibition, the appropriate miRNA mimic concentration was evaluated. For this purpose a positive control mimic for a miRNA directed against GAPDH was used. A concentration row for both positive and negative control mimic was conducted in two different phFB isolates (Figure 5.33). The higher the concentration of the positive control mimic, the better the downregulation of GAPDH.
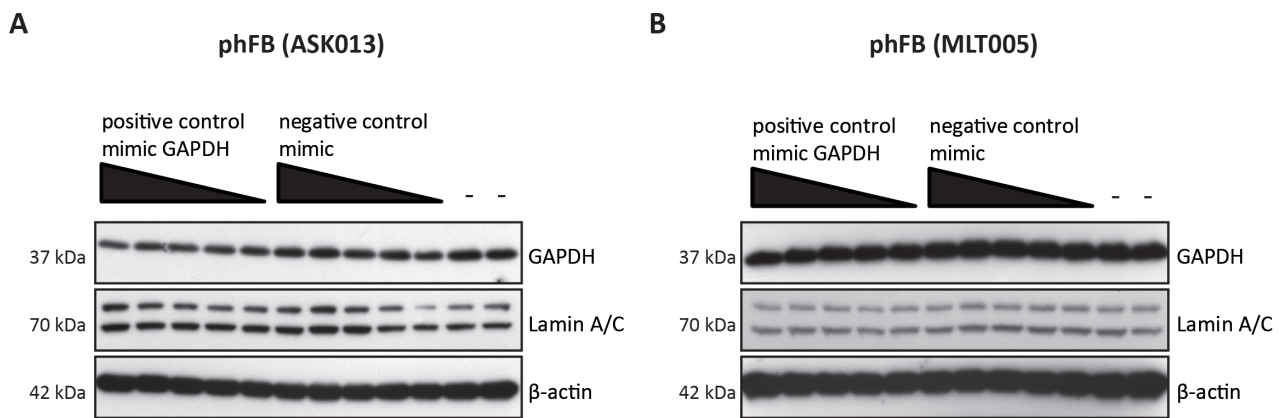
Figure 5.33: GAPDH was downregulated with positive control miRNA mimic in a concentration dependent manner in phFB.
A) PhFB (ASK013) were either transfected with a positive control mimic against GAPDH in different concentrations (100 nM, 50 nM, 25 nM, 10 nM and 5 nM) or with a negative control miRNA mimic in the same concentrations. GAPDH Western blot analysis was performed with cell lysates 48 h after transfection. Lamin A/C and β–actin served as loading controls. B) The same experiment as in A was performed with phFB (MLT005).

After the positive evaluation of miRNA mimic concentration, it was analysed, if it was possible to observe WISP1 downregulation in cell lysates in a RISC dependent manner. For this reason, phFB were transfected with 10 nM siRNA against WISP1. QRT-PCR was performed for all CCN family members after WISP1 siRNA transfection at 24 h, 48 h and 72 h (Figure 5.34 A). WISP1 was significantly downregulated over the whole time (mean WISP1 fold change +/- SD to scrambled siRNA transfected cells, n=3, paired t-test: 0.245 +/- 0.112 (24 h, p=0.0266), 0.304 +/- 0.092 (48 h, p=0.0243), 0.252 +/- 0.128 (72 h, p=0.0331)), slight increase was observed for WISP2 and no changes for CYR61, CTGF and NOV. From this, it could be concluded, that the siRNAs worked specifically in downregulating WISP1. WISP1 protein was also successfully decreased with 10 nM and 30 nM siRNA (Figure 5.34 B).

Figure 5.34: WISP1-specific siRNAs downregulated WISP1 levels.
A) CCN family proteins were investigated after transfection of 10 nM siRNAs against WISP1 at 24 h (open bars), 48 h (grey bars) and 72 h (dark grey bars) of transfection by qRT-PCR. Fold changes compared to 10 nM scrambled controls are shown, n=3 +/- SD, paired t-test, * p<0.05, n.d.=not detectable before and after siRNA transfection. B) Representative WISP1 Western Blot analysis after 24 h and 72 h of 10 nM or 30 nM siRNA transfection. GAPDH served as loading control (W= WISP1 siRNA and C= scrambled siRNA control).

After identifying 100 nM miRNA mimics as a valuable and effective working concentration and showing that WISP1 could be detectable downregulated in cell protein lysates, 100 nM candidate miRNA mimics were applied to overexpress miRNAs in phFB and subsequent WISP1 expression was analysed. First, phFB (ASK06), same as used in luciferase assays were investigated. After 48 h of miRNA mimic transfections a significant overexpression of the respective miRNAs was observed (mean log fold changes +/- SD, n=3, t-test: miR-30a 0.065 +/- 0.133 (M-miR-NCI) *versus* 12.46 +/- 0.56 (M-miR-30a, p<0.0001); miR-30d -0.08 +/- 0.43 (M-miR-NCI) *versus* 11.45 +/-0.52 (M-miR-miR-30d, p<0.0001); miR-92a -0,03333+/- 0,3370 (M-miR-NCI) *versus* 13,45 +/- 2,287 (M-miR-92a p<0.0001), Figure 5.35 A). *WISP1* mRNA expression was not altered after transfection with control mimic M-miR-NCI, but upregulated with miRNAs of the miR-30 family and downregulated overexpressing miR-92a (mean WISP1 log fold change +/- SD compared non-transfected cells, n=3: -0.21 +/- 0.40 (M-miR-NCI), 0.85 +/- 0.63 (M-miR-30a), 0.57 +/- 0.31 (M-miR-30d) and -1.09 +/- 0.55 (M-miR-92a)).

The same experiments were performed using phFB (ASK013) including a second negative control mimic, M-miR-NCII (Figure 5.35 B). Here, the miRNA overexpression was comparable to the previous experiment (mean miRNA log fold changes +/- SD compared to non-transfected cells, n=3, one-way ANOVA with Dunnett's post-test compared to M-miR-NCI transfected cells: miR-30a -0.27 +/- 0.29 (M-miR-NCI) *versus* 0.28 +/- 0.21 (M-miR-NCII) and 7.94 +/- 1.08 (M-miR-30a, p<0.0001), miR-30d -0.14 +/- 0.10 (M-miR-NCI) *versus* 0.24 +/- 0.12 (M-miR-NCII) and 8.38 +/- 0.54 (M-miR-30d, p<0.0001), miR-92a -0.05 +/- 0.28 (M-miR-NCI) *versus* 0.29 +/- 0.26 (M-miR-NCII) and 11.24 +/-1.11 (M-miR-92a, p<0.0001) Figure 5.35 B). However, *WISP1* mRNA levels scatter far more and show no significant change (mean WISP1 log fold change +/- SD compared non-transfected cells, n=3: +/- 0.23 +/- 0.11 (M-miR-NCI), 0.40 +/- 0.50 (M-miR-NCII), 1.35 +/- 0.52 (M-miR-30a), 0.93 +/- 0.90 (M-miR-30d) and 0.24 +/- 0.97 (M-miR-92a).
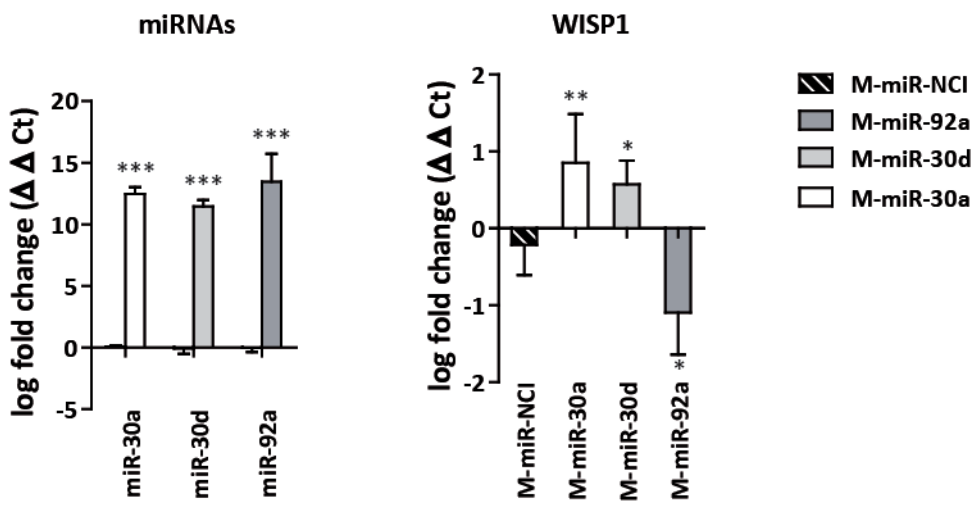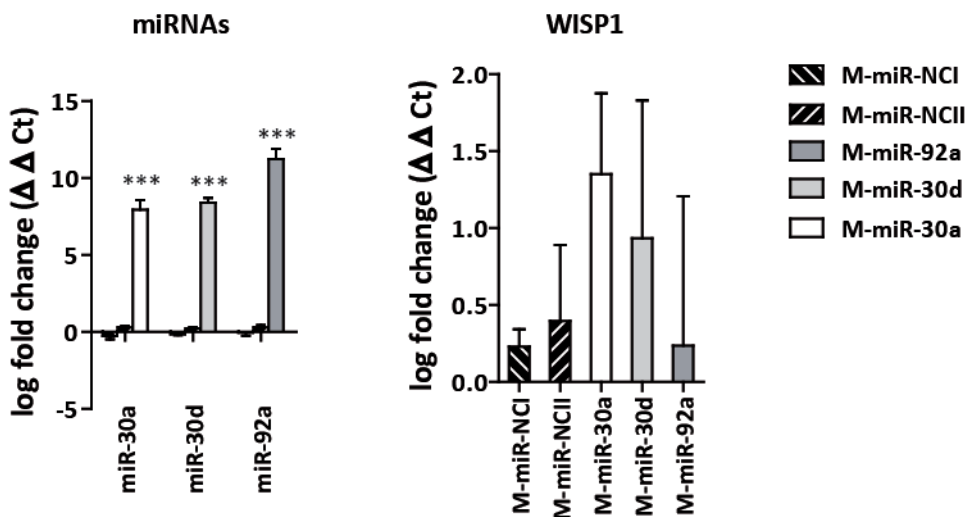
Figure 5.35: MiR-92a overexpression altered *WISP1* mRNA cell context dependent.
A) PhFB (ASK006) were transfected with 100 nM miRNA mimics and miRNA expression as well as *WISP1* mRNA levels were analysed after 48 h of transfection. Log fold change to non-transfected cells is shown. N=3 +/- SD, t-test for miRNA overexpression (*** p<0.0001), and one-way ANOVA with Dunnett's post-test compared to M-miR-NCI transfected cells for WISP1 analysis (* p<0.05, ** p<0.01). Black hatched bars represent negative control miRNA mimic transfected cells, open bars miR-30a mimic transfected cells analysed for miR-30a or WISP1 levels, light grey bars miR-30d transfected cells and grey bars miR-92a transfected cells. B) Same experiments as in A) with phFB (ASK013) including M-miR-NCII mimics (second black hatched bar), n=3, one-way ANOVA with Dunnett's post-test compared to M-miR-NCI transfected cells *** p<0.0001.

For this reason, the experiment was repeated in triplicates (Figure 5.36) with phFB (MLT005). Now, expression of all three miRNAs was analysed from all miRNA-overexpressing cells thus measuring not only specific but also unspecific overexpression. In addition, the miR-30a, miR-30d and miR-92a were combined in one transfection setup, named combinatorial approach. Candidate miRNA expression changes are depicted as log

fold changes compared to non-transfected cells (Figure 5.36 A). The miR-30a primer assay detected miR-30a overexpression in miR-30a and combinatorial transfected cells, but also in miR-30d transfected cells, suggesting that this primer assay detected additionally miR-30d if this miRNA is highly abundant. Induction of miR-30a expression by miR-30d overexpression could be also a reason (mean miR-30a log fold change +/- SD to non-transfected cells, n=3, one-way ANOVA with Dunnett's post-test: 1.01 +/- 0.40 (M-miR-NCI), 0.18 +/- 0.52 (M-miR-NCII), 9.66 +/- 1.02 (M-miR-30a, $p<0.001$), 7.05 +/- 0.26 (M-miR-30d, $p<0.001$), 0.76 +/- 1.12 (M-miR-92a), 7.59 +/- 0.32 (M-miR-combi, $p<0.001$)). These analyses were performed for miR-30d and miR-92a in addition, showing that these two primer assays were more specific and that both miRNAs were significantly overexpressed (mean miRNA log fold change +/- SD to non-transfected cells, n=3, one-way ANOVA with Dunnett's post-test compared to M-miR-NCI: miR-30d 0.51 +/- 0.30 (M-miR-NCI), -0.05 +/- 0.40 (M-miR-NCII), 2.51 +/- 0.45 (M-miR-30a, $p<0.01$), 8.27 +/- 0.23 (M-miR-30d, $p<0.001$), 0.40 +/- 0.93 (M-miR-92a), 7.47 +/- 0.15 (M-miR-combi, $p<0.001$), Figure 5.36 B; miR-92a -0.11 +/- 0.34 (M-miR-NCI), 0.01 +/- 0.57 (M-miR-NCII), 0.83 +/- 0.77 (M-miR-30a), 1.71 +/- 0.46 (M-miR-30d, $p<0.01$), 7.36 +/- 0.58 (M-miR-92a, $p<0.001$), 6.43 +/- 0.32 (M-30a, -30d and -92a, $p<0.001$), Figure 5.36 C).

WISP1 mRNA levels were explored from the same cDNA samples showing a slight WISP1 increase after miR-30a overexpression, which however was comparable in M-miR-NCII transfected cells. For miR-30d overexpression, a significant WISP1 downregulation was observed, and for miR-92a, WISP1 tended to decrease as well whereas no changes where detectable for the combinatorial approach (mean WISP1 log fold changes normalized to non-transfected cells, n=3, one-way ANOVA with Dunnett's post-test compared to M-miR-NCI: -0.14 +/- 0.21 (M-miR-NCI), 0.50+/- 0.39 (M-miR-NCII), 0.62 +/- 0.50 (M-miR-30a), -2.32 +/- 0.33 (M-miR-30d, $p<0.001$), -0.37 +/- 0.62 (M-miR-92a), 0.29 +/- 0.20 (M-miR-30a, -30d and -92a) Figure 5.36 D).

These miRNA and *WISP1* mRNA results after candidate miRNA overexpression indicate that miRNA overexpression was successful and independent from phFB origin, while the *WISP1* mRNA changes were cell origin dependent.
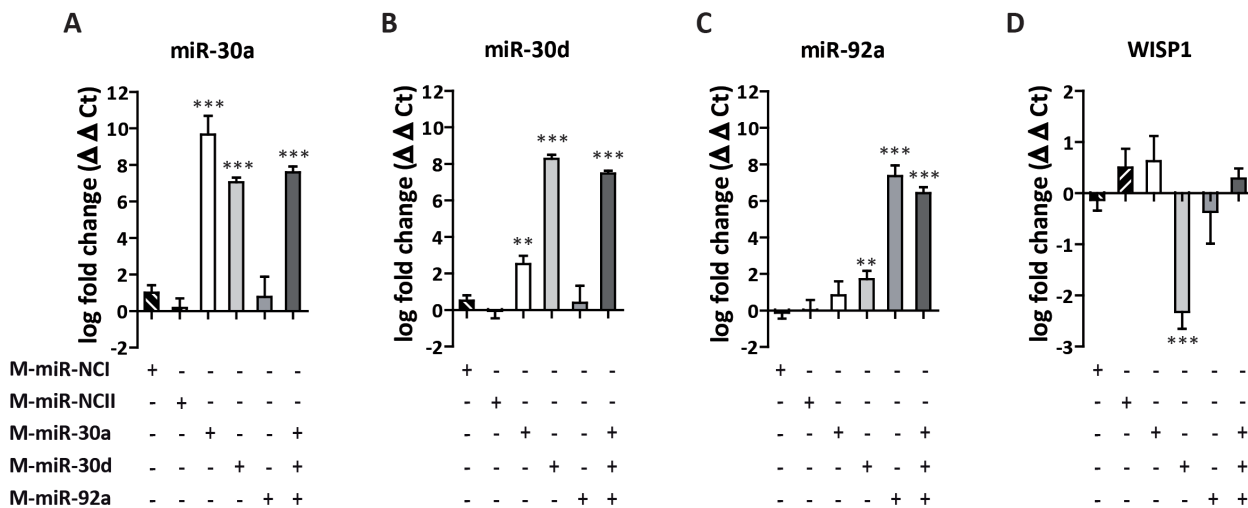
Figure 5.36: Effect of miRNA overexpression on miRNAs and WISP1 levels.
A-C) miR-30a, -30d and -92a miRNA levels were analysed after 48 h of miRNA overexpression with 100 nM miRNA mimic in phFB (MLT005). Log fold changes are depicted normalized to non-transfected cells (n=3 +/- SD; one-way ANOVA compared to M-miR-NCI ** $p<0.01$, *** $p<0.001$, black hatched bars represent cells transfected with negative control miRNA mimics (M-miR-NCI and NCII), open bars with miR-30a mimics, light grey bars with miR-30d mimics, grey bars with miR-92a and dark grey bars with a combination of all three miRNA mimics (50 nM M-miR-92a, 25 nM M-miR-30a and 25 nM M-miR-30d). D) *WISP1* mRNA levels were investigated from phFB samples shown in A-C.

Furthermore, WISP1 protein levels were investigated after candidate miRNA overexpression. Figure 5.37 A depicts a representative WISP1 Western Blot and Figure 5.37 B the quantification analysis thereof from three experiments performed in triplicates. After miR-92a overexpression, WISP1 protein levels decreased, supporting the mRNA results from phFB ASK006 cells (mean of normalized WISP1 protein levels +/- SD, n=3: 0.94 +/- 0.41 (scr siRNA), 0.90 +/- 0.36 (M-miR-NCI), 1.11 +/- 0.61 (M-miR-NCII), 1.19 +/- 0.21 (M-miR-30a), 1.09 +/- 0.29 (M-miR-30d) 0.63 +/- 0.28 (M-miR-92a), 1.03 +/- 0.51 (M-miR-30a, -30d and -92a)).

A

B

scr siRNA	−	+	−	−	−	−	−	−
M-miR-NCII	−	−	+	−	−	−	−	−
M-miR-NCI	−	−	−	+	−	−	−	−
M-miR-92a	−	−	−	−	+	+	−	−
M-miR-30d	−	−	−	−	+	−	+	−
M-miR-30a	−	−	−	−	+	−	−	+
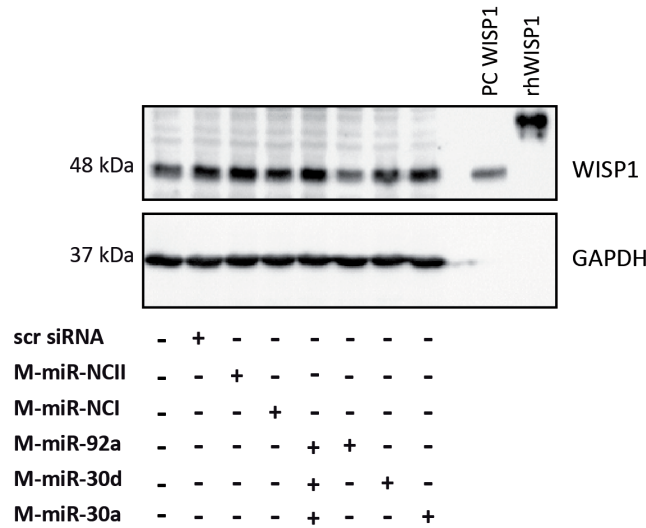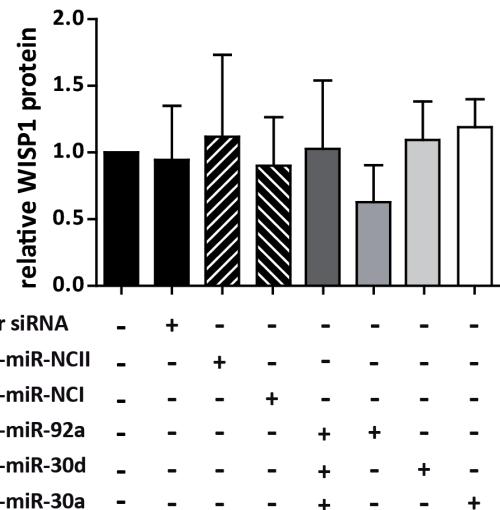
Figure 5.37: MiR-92a overexpression repressed WISP1 protein in phFB (MLT005).
A) Representative Western Blot picture of phFB (MLT005) cell lysates after 48 h of miRNA overexpression with 100 nM miRNA mimics or scrambled siRNA (scr siRNA). GAPDH served as loading control. Recombinant human WISP1 protein (rhWISP1) and cell lysate from WISP1 overexpressing A549 cells (PC WSP1) were loaded as WISP1 positive controls. B) WISP1 densitometry analysis of Western Blot analyses described in A (n=3 +/- SD).

In conclusion, for endogenous WISP1 regulation experiments, phFB were positively evaluated, as they express WISP1 and the candidate miRNAs except of miR-203a. Furthermore, endogenous miRNA expression was successfully modulated applying miRNA inhibitors and mimics for miRNA downregulation and upregulation, respectively. After miRNA inhibition, WISP1 expression was not altered. Notably, miR-92a overexpression led to WISP1 downregulation in phFB in a cell donor specific manner.

5.5 Regulation of WISP1 by miRNAs under profibrotic conditions

As pointed out above, miR-92a showed potential to regulate WISP1 *in vitro* and for this regulation to take place, possibly a certain microenvironment is a prerequisite. WISP1 is a matricellular protein, which is poorly expressed under homeostatic conditions, and its action most likely involves modulation by growth factor signalling, such as TGF-β1 signalling.

5.5.1 TGF-β1 induced WISP1 expression *in vitro*

In order to further analyse miRNA regulation of WISP1, TGF-β1 treated fibroblasts were used to mimic a profibrotic environment in vitro. TGF-β1 is one of the most potent profibrotic cytokines and is involved in key profibrotic processes, such as myofibroblast differentiation (Fernandez & Eickelberg, 2012a). PhFB morphology changed after TGF-β1 treatment.

Figure 5.38 shows control phFB (ctrl) and TGF-β1 treated phFB after 24 h. The cells acquired a myofibroblast-like phenotype, where they became flatter and contractile, and stress fibres were readily visible.
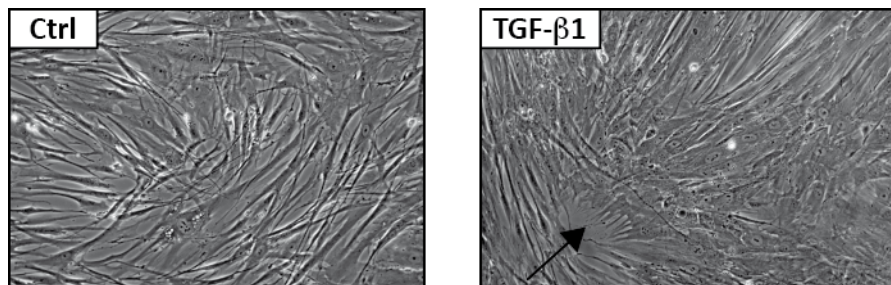

Figure 5.38: TGF-β1 treatment changed fibroblast morphology into myofibroblasts.
Representative images of non-treated (ctrl) and 2 ng/ml TGF-β1 treated phFB (MLT014) after 24 h are depicted (10x objective). Arrow indicates fibroblasts becoming myofibroblasts.

The influence of TGF-β1 on phFB was even better observed with immunofluorescence analysis. Immunofluorescence analysis of TGF-β1 treated phFB (MLT0014) revealed an increase for α-SMA, COL1A1 and FN1 protein after 24 h. Further, WISP1 appeared to be increased in addition.
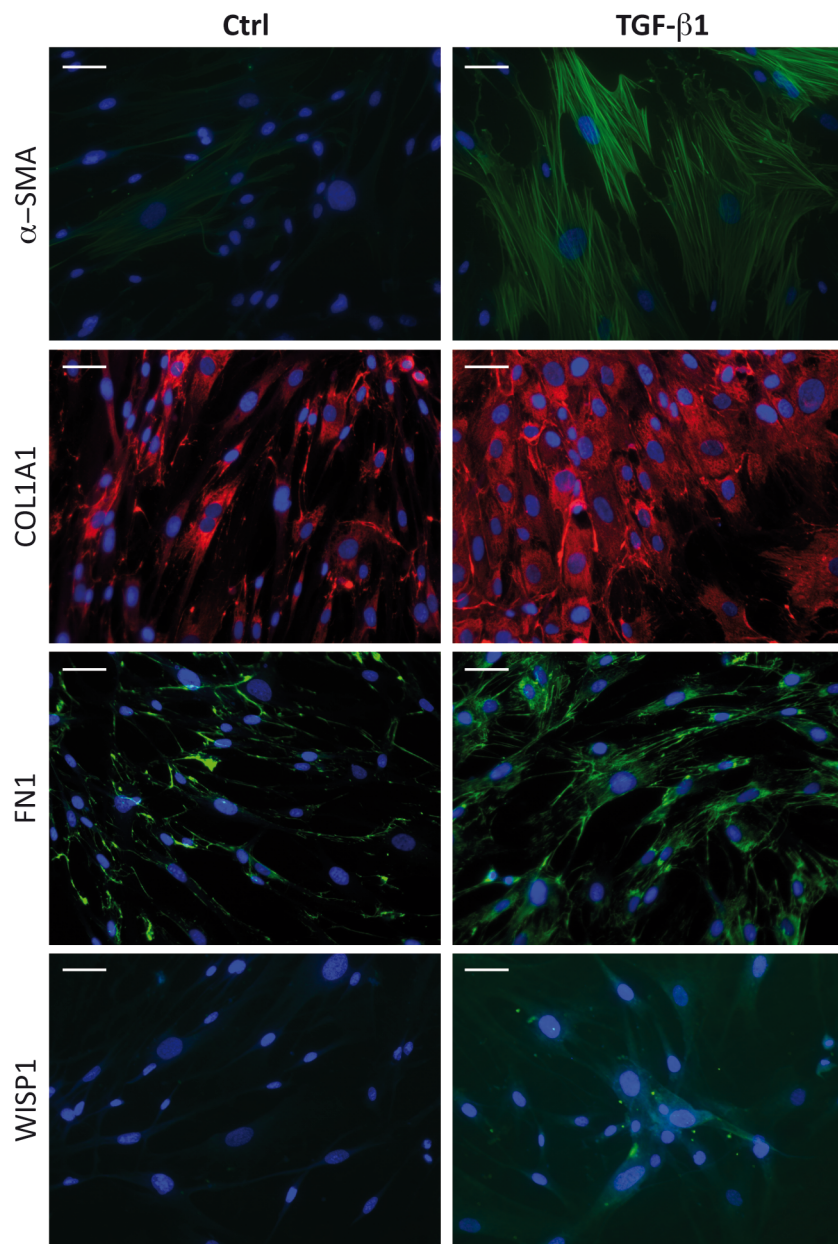
Figure 5.39: Immunofluorescence analysis of TGF-β1-treated fibroblasts.
Representative images are depicted of non-treated (ctrl) and 2 ng/ml TGF-β1 treated phFB (MLT014) after 24 h, stained for α-SMA (green), COL1A1 (red), FN1 (green) and WISP1 (green) expression. (blue: DAPI stained nuclei, scale bar 50 μm).

As WISP1 protein appeared to be increased in immunofluorescence analysis after TGF-β1 stimulation, this result was validated quantitatively with qRT-PCR analysis. *WISP1* mRNA was significantly increased in phFB after 24 h of TGF-β1 treatment (log fold change 1.6 +/- 0.1 SD, n=3, p=0.0012, Figure 5.40 A). This was accompanied by SERPINE1 upregulation, a known TGF-β1 target gene (log fold change 3.3 +/- 0.14 SD, p=0.0006 after 6 h and 3.9 +/- 0.13 SD, p=0.004 after 24 h.). Furthermore, WISP1 was upregulated at the protein level after 24 h and 48 h of TGF-β1 treatment as shown by Western Blotting. TGF-β1-dependent upregulation of α-SMA further indicated myofibroblast differentiation (Figure 5.40 B). Moreover, increased WISP1 protein was detected in supernatants of TGF-β1 treated phFB, by Western Blot analysis (Figure 5.40 C) and ELISA (Figure 5.40 D, mean +/- SD:

13.75 pg./ml +/- 2.64 (control 24 h), *versus* 65.04 pg./ml +/- 10.23 (TGF-β1 24 h), n=5, p<0.0001 and 10.70 pg./ml +/- 2.55 (control 48 h) *versus* 45.78 pg./ml +/- 21.31 (TGF-β1 48 h), n=5 p=0.0065). In sum, WISP1 mRNA and protein expression as well as a myofibroblast phenotype were induced by TGF-β1. The WISP1 increase was even better detectable in cell supernatants than in cell lysates.
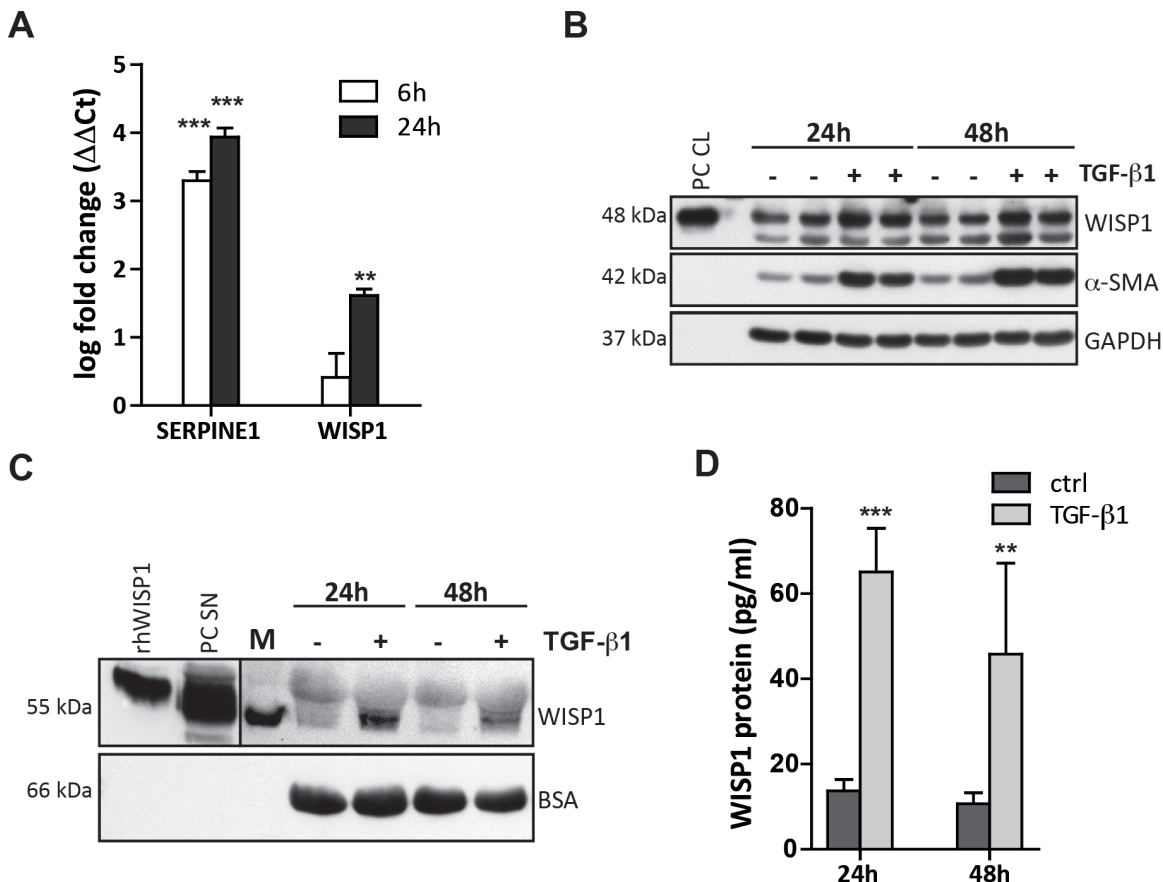

Figure 5.40: TGF-β1 induced WISP1 expression on mRNA and protein level in phFB.
A) QRT-PCR of 2 ng/ml TGF-β1 treated phFB (ASK013), n=3, paired t-test ** p<0.01 and *** p<0.001. B) WISP1 Western Blot analysis of phFB cell lysates treated with 2 ng/ml TGF-β1, shown n=2, PC CL= cell lysate of WISP1 overexpressing A549 cells; WISP1 is the upper band. α-SMA serves as a positive control for TGF-β1 treatment and GAPDH as loading control. C) Representative Western Blot of phFB supernatant after 2 ng/ml TGF-β1 stimulation. Supernatant of WISP1 overexpressing A549 cells and recombinant human WISP1 protein served as positive controls (PC SN). The upper band of the WISP1 Blot is bovine serum albumin (BSA) since TGF-β1 treatments were done with cell culture medium containing 0.1% FBS, and unspecific binding was observed. BSA served as a loading control. D) WISP1 ELISA from phFB supernatants treated with 2 ng/ml TGF-β1 (n=5 +/- SD, unpaired t–test compared to time matched controls ** p<0.01 and *** p<0.001).

5.5.2   TGF-β1 did not regulate target miRNAs *in vitro*

After demonstrating WISP1 induction by TGF-β1, miRNA levels were investigated in the same profibrotic environment. PhFB (ASK013) were stimulated with TGF-β1 for 6 h, 12 h and 24 h and miRNA levels were examined with qRT-PCR (Figure 5.41). Log fold changes to negative control transfected cells showed no significant miRNA changes (mean miRNA log fold change +/- SD to untreated cells: miR-30a 0.31 +/- 0.71 (6 h), -0.14 +/- 0.39 (12 h),

-0.30 +/- 0.47 (48 h); miR-30d 0.16 +/- 0.48 (6 h), -0.16 +/- 0.27 (12 h), -0.14 +/- 0.34 (48 h); miR-92a 0.14 +/- 0.21 (6 h), -0.019 +/- 0.35 (12 h), 0.07 +/- 0.29 (48 h)).
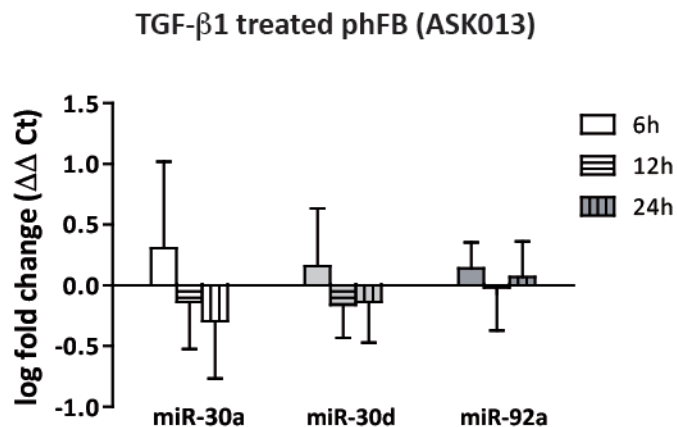

Figure 5.41: TGF-β1 did not regulate candidate miRNA levels in phFB.
QRT-PCR of 2 ng/ml TGF-β1 treated phFB (ASK013) after 6 h, 12 h and 24 h for candidate miRNAs. Log fold change values compared to untreated cells are depicted.

5.5.3 WISP1 expression under the influence of TGF-β1 and target miRNAs

To assess whether TGF-β1 induced WISP1 expression could be altered by miRNAs, candidate miRNAs miR-30a, miR-30d and miR-92a were overexpressed in phFB. Results of different phFB cells (ASK006, ASK013 and MLT013.1) were combined in order to rule out cell specific effects after TGF-β1 treatment. MiR-203a was not further analysed in this setup, as miR-203a was endogenously not expressed in phFB. As shown in Figure 5.42 A, all candidate miRNAs were significantly increased by transfection with the respective miRNA mimic (relative miRNA expression in TGF-β1 treated *versus* miRNA mimic transfected cells, mean +/- SEM, miR-30a: 0.35 +/- 0.16 *versus* 8.58 +/- 0.42 (p<0.0001); miR-30d: 0.41 +/- 0.19 *versus* 9.76 +/- 0.41 (p<0.0001), and miR-92a 0.21 +/- 0.30 *versus* 14.14 +/- 0.31 (p<0.001), n=9). Of note, miRNA mimics miR-30a and miR-30d were both detected by the miR-30a primer assay as seen before.

TGF-β1 alone induced *WISP1* expression to a similar level as shown in Figure 5.40 (log fold change 1.34 +/- 0.08 SEM, n=9, Figure 5.42 B). Transfection with M-miR-NCI did not significantly change the TGF-β1 induced upregulation of *WISP1* (log fold change 1.24 +/- 0.01 SEM, n=9). Importantly, miR-30a and miR-92a overexpression significantly reduced TGF-β1 induced *WISP1* mRNA level (log fold change +/- SEM, only TGF-β1 treated cells 1.34 +/- 0.08 *versus* 0.76 +/- 0.16 (p= 0.0064) and 1.02 +/- 0.11 (p=0.033) for miR-30a and miR-92a mimic, respectively, n=9), while miRNA 30d regulation of *WISP1* mRNA level did not reach statistical significance (log fold change 0.97 +/- 0.21 SEM). Moreover, combined overexpression of miR-30a, miR-30d and miR-92a, also counteracted TGF-β1 induced *WISP1* mRNA level (log fold change 0.76 +/- 0.05, n=6, p=0.0002 compared to only TGF-β1 treated cells 1.34 +/- 0.08). Additionally, the TGF-β1 target genes *SERPINE1* and *COL1A1* were explored demonstrating that their expression was induced by TGF-β1 (Figure 5.42 C-D). *SERPINE1* levels were altered by miR-30a, but *COL1A1* levels were not changed, as predicted by the TargetScan algorithm. Taken together, these data suggested that miR-30a

and miR-92a target TGF-β1-induced WISP1 specifically and may therefore be involved in WISP1 regulation in pulmonary fibrosis.
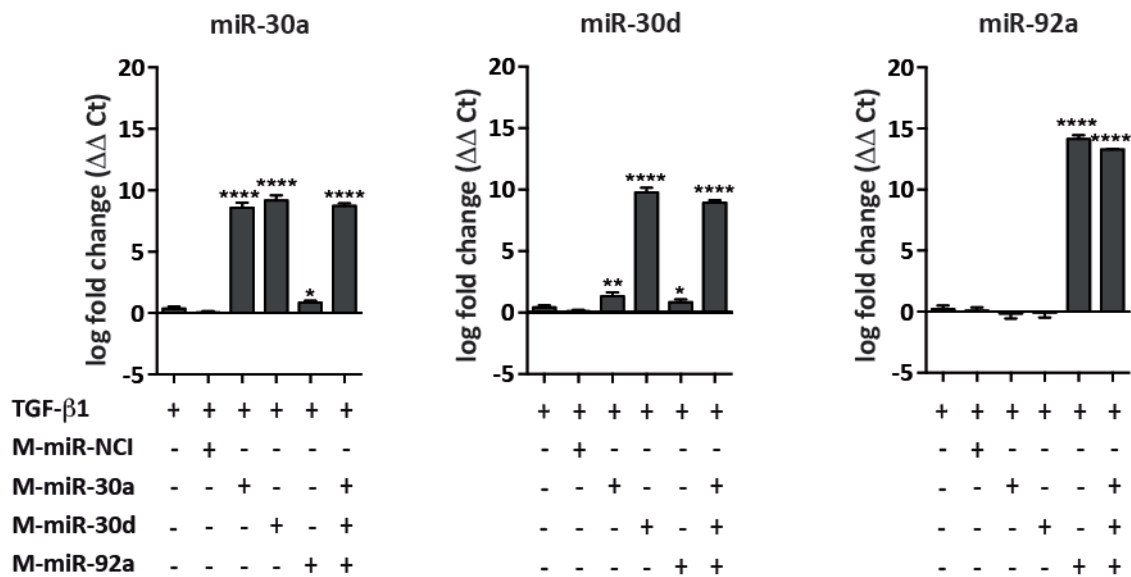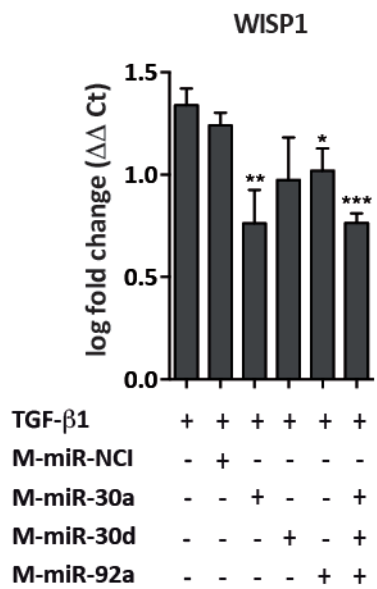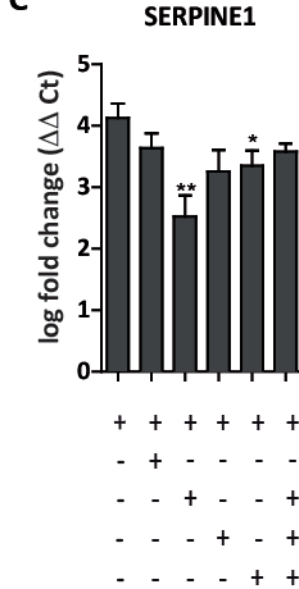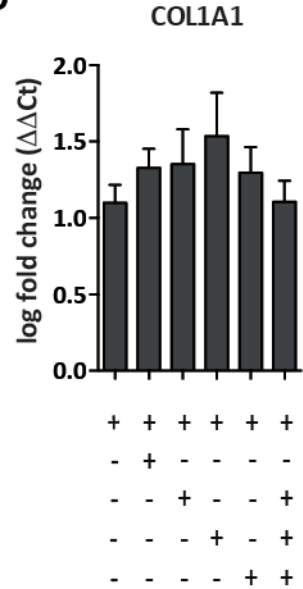

Figure 5.42: Candidate miRNAs reversed TGF-β1 effects on *WISP1* mRNA levels in phFB.
A) phFB (ASK006, ASK013, MLT013) were treated with 2 ng/ml TGF-β1 and transfected with 100 nM miRNA mimic as indicated. MiRNA levels were analysed after 24 h by qRT-PCR. Log fold changes normalized to RNU6 and untreated and non-transfected control cells are shown. B) - D) The same samples were analysed for *WISP1*, *SERPINE1* and *COL1A1* mRNA levels, respectively. Log fold change values are normalized to housekeeping gene *HPRT* and to non-transfected and untreated control cells after 24 h. (n=6-9 +/- SEM, unpaired t –test to TGF-β1 treated cells * p<0.05, ** p<0.01, *** p<0.001 and **** p<0.0001)

MiR-30a and miR-92a could reverse *WISP1* induction by TGF-β1 on mRNA level, and hereafter WISP1 protein levels were investigated. Western Blot analysis indicated comparable induction of WISP1 by TGF-β1 after 24 h (Figure 5.43 A) as shown before (Figure 5.40). However, a downregulation by miRNA overexpression could not be observed (Figure 5.43 B).
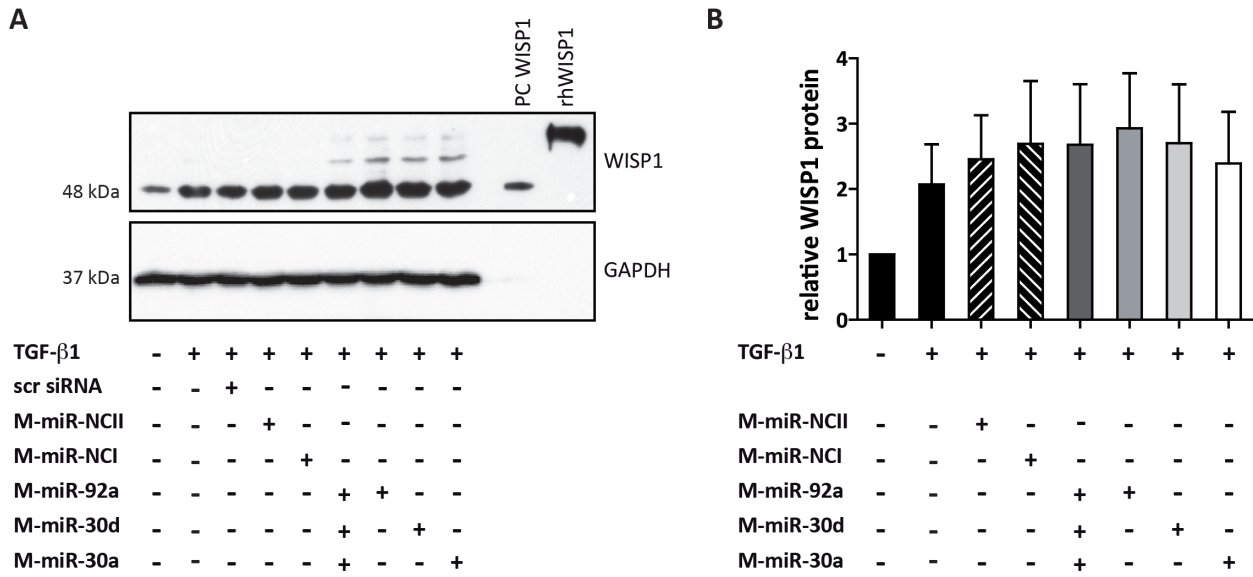
Figure 5.43: Candidate miRNAs did not alter TGF-β1 effects on WISP1 protein levels in phFB.
A) Representative WISP1 Western Blot of phFB (ASK006) after 24 h of TGF-β1 treatment and miRNA overexpression. Cell lysate from WISP1 overexpressing A549 cells (PC WISP1) and recombinant human WISP1 protein (rhWISP1) were loaded as WISP1 positive controls. B) WISP1 densitometry analysis of Western Blot analysis compared to untreated and non-transfected phFB. N=4 +/- SD, black bars represent control cells or TGF-β1 treated cells, black hatched bars cells transfected with negative control miRNA mimics (M-miR-NCI and NCII), dark grey bars with a combination of all three miRNA mimics (50 nM M-miR-92a, 25 nM M-miR-30a and 25 nM M-miR-30d), grey bars with miR-92a, light grey bars with miR-30d mimics and open bars with miR-30a mimics.

5.5.4 TGF-β1 regulated WISP1 and miRNAs *in vivo*

After successful evaluation of WISP1 regulation by miRNAs in a fibrotic environment *in vitro*, miRNA regulation of WISP1 was explored *in vivo*. Therefore, lung tissue homogenate from the TGF-β1-overexpressing rat lung fibrosis model was investigated (Sime et al, 1997) (Figure 5.44).

Lung tissue homogenate samples were analysed on *day 7* (d7) or *day 21* (d21) after viral overexpression of TGF-β1 in the rat lung. *Wisp1*, *Col1a1* and *Fn1* mRNAs were increased on d7 and d21 after TGF-β1 overexpression (mean +/- SD for relative mRNA level for ctrl d21 (n=3), TGF-β1 d14 (n=4) and TGF-β1 d21 (n=9) after viral infection, respectively: WISP1 -10.11 +/- 0.71, -7.52 +/- 1.88 and -8.29 +/- 1.68; *Col1a1* 3.34 +/- 0.47, 4.41 +/- 1.14, 4.96 +/- 1.22; *Fn1* -4.46 +/- 0.70, -1.48 +/- 1.53 (p<0.05), -2.70 +/- 0.87 (p<0.01), one-way ANOVA with Dunnett's post-test to ctrl d21, Figure 5.44 A-C). No significant changes were detected for miR-30a and miR-30d, while miR-92a was significantly downregulated on both days (mean +/- SD for relative miRNA level for ctrl d21 (n=3), TGF-β1 d14 (n=4) and TGF-β1 d21 (n=9) after viral infection, respectively: miR-30a -3.44 +/- 0.92, -3.37 +/- 1.51 and -2.64 +/- 0.32; miR-30d; -2.35 +/- 0.57, -3.43 +/- 1.06 and -2.46 +/- 0.30; miR-92a -1.23 +/- 0.20, -2.10 +/- 0.55 (p<0.05) and -2.08 +/- 0.39 (p<0.05), one-way ANOVA with Dunnett's post-test to ctrl d21, Figure 5.44 D-F).
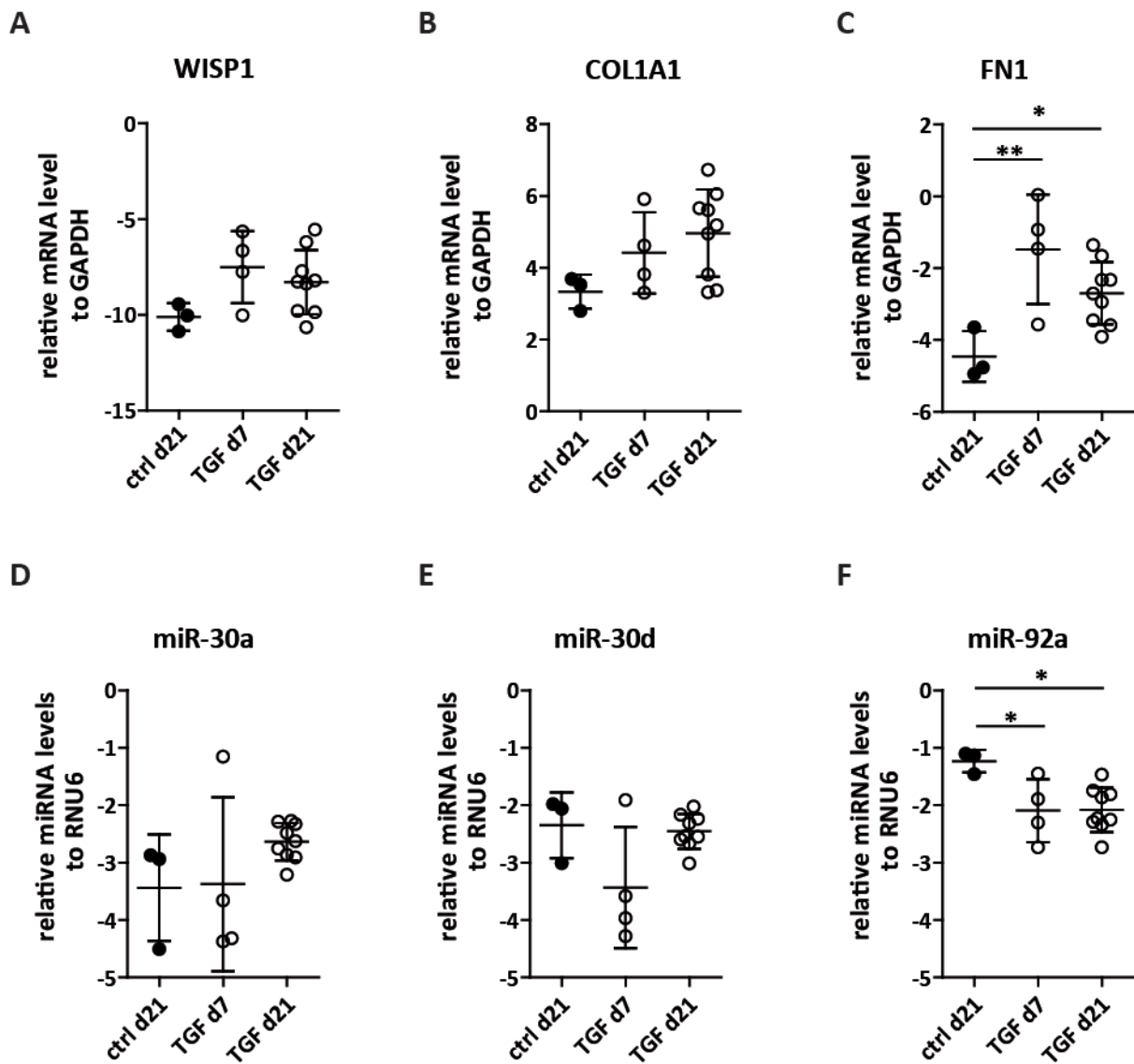
Figure 5.44: *WISP1* **mRNA was increased while miR-92a was decreased in a TGF-β1 overexpressing rat fibrosis model.**

A - C) QRT-PCR analyses were performed for *Wisp1*, *Col1a1* and *Fn1* from rat whole lung at day 7 (d7) and day 21 (d21) after infection with TGF-β1 expressing adenoviruses. Whole lung tissue from mock-infected rats at day 21 was used as control. Relative mRNA levels compared to the housekeeping gene *Gapdh* are shown. N=3 +/- SD for ctrl d21, n=7 +/- SD for TGF-β1 (TGF) d7 and n=9 +/- SD for d21; one-way ANOVA with Dunnett's post-test (control = control infected samples from day 21) * p<0.05, ** p<0.01. B) – F) QRT-PCR analyses were performed for miR-30a, miR-30d and miR-92a. Relative miRNA levels are shown to the housekeeping gene RNU6.

Moreover, levels of *Wisp1* mRNA and miR-92a exhibited a negative correlation, as analysed by Pearson correlation and linear regression analysis (r=-0.65, p=0.0061 and R^2=0.43, Figure 5.45). The same analyses were performed for miR-30a and miR-30d, but here no correlation with *Wisp1* was observed (data not shown).
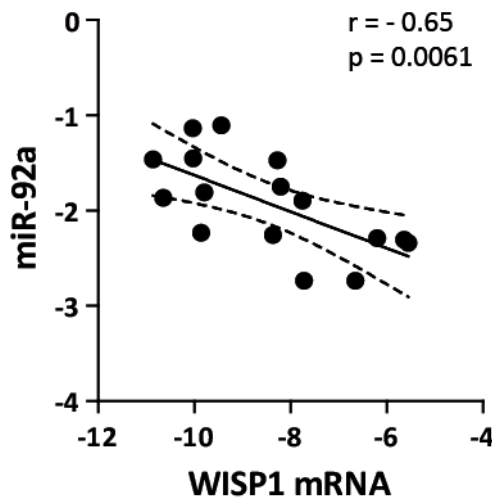
Figure 5.45: MiR-92a expression negatively correlates with WISP1 *in vivo*.
Pearson correlation analysis was performed for all samples shown in Figure 5.44 (n=16 r=-0.65, p=0.0061). The continuous line represents the linear regression analysis with the confidence interval of 95% shown in dashed lines.

In summary, these data provide for the first time evidence that miR-92a strongly negatively correlates with *Wisp1* expression in rat whole lung samples from TGF-β1 induced fibrosis. These data provide another strong point of evidence that miR-92a is involved in the regulation of WISP1. Furthermore miR-30a and -92a could counteract TGF-β1 induced increase of *WISP1* mRNA expression in phFB *in vitro*.

6 DISCUSSION

IPF is a lethal lung disease characterized by excessive connective tissue formation leading to disruption of normal lung architecture and respiratory failure. WISP1 was identified as a mediator of pulmonary fibrosis, but there is only limited knowledge how WISP1 is upregulated under diseased conditions and thus far, nothing is known about miRNA mediated WISP1 regulation. Several recent reports recognized that miRNAs, post-transcriptional gene regulators, are altered in lung diseases in general, and in pulmonary fibrosis in particular (Sessa & Hata, 2013). In the present study, miRNAs downregulated in three microarray data sets of pulmonary fibrosis that are predicted to bind to the human WISP1 3'UTR were identified. Downregulation of candidate miRNAs was accompanied by increased WISP1 protein expression in IPF samples and to some extend in two models of experimental fibrosis. Reporter gene assays did not reveal a direct interaction between miRNAs and WISP1, however indicated that the WISP1 3'UTR mediates translational repression by itself and therefore gene regulation. Cell screens identified phFB as a valid model for endogenous WISP1 regulations studies by miRNAs and endogenous WISP1 regulation depended on the cellular microenvironment. In addition, TGF-β1-induced WISP1 expression was demonstrated on mRNA and protein level in primary lung fibroblasts, as assessed in both cell lysates and supernatants. The candidate miRNAs, miR-30a and miR-92a, reversed TGF-β1-induced increase of WISP1 on mRNA level. An inverse relationship for *WISP1* mRNA and miR-92a was found in whole rat lung homogenate in a TGF-β1 dependent fibrosis model *in vivo*. Importantly, WISP1 mRNA and protein were significantly increased in phFB from IPF patients and negatively correlated with miR-92a levels. To the best of my knowledge, these data indicate for the first time a regulatory role of miR-30 and miR-92a for WISP1 expression in pulmonary fibrosis.

6.1 Target prediction evaluation of candidate miRNAs binding to WISP1

To predict the miRNA:mRNA interactions a novel SVM learning approach developed by Daniel Ellwanger was applied (unpublished data). The results of this prediction approach are shown for human WISP1 3'UTR and possible candidate miRNAs in Table 5.2 in the results section. Candidate miRNAs were chosen according to the following criteria: 1) downregulated in pulmonary fibrosis, 2) "long seed" sites (7mer or 8mer) on the WISP1 3'UTR and 3) more than one binding site in total.

The SVM was further developed during the time of the collaboration. Therefore, the used approach allowed later on not only the identification of the miRNA bindings site on the WISP1 3'UTR but also the prediction of regions, which are targeted preferentially by microRNA containing ribonucleoprotein particles (miRNP). This was achieved by analysing photoactivatable ribonucleoside-enhanced crosslinking and immunoprecipitation (PAR-CLIP) data from Kishore *et al.* for AGO transcriptome-wide binding sites (Kishore et al, 2011). Thus, the advantage of this applied binding sites prediction method over existing tools is the classification of mRNA transcript segments into preferable AGO binding sites

(AGO⁺) independent of any miRNA sequence. AGO⁺ sites were found for the "longest seed" miRNA binding sites of the candidate miRNAs miR-92a and miR-30a/d using the Ensembl annotated WISP1 3'UTR sequence ENST00000250160 (as shown Table 6.1). In addition, for miR-92a the 6merβ site at position 2583 is located in an AGO⁺ region. For miR-203a, two AGO⁺ regions were predicted for the binding sites at position 78 and 125 on the WISP1 3'UTR, but none for the "longest seed" site.

Altogether, these data corroborate that the chosen miRNAs possess functional sites on the WISP1 3'UTR.

Table 6.1: List of AGO sites for candidate miRNAs on the human WISP1 3'UTR

Symbol	Position in 3'UTR	Seed type	AGO⁺	ΔG_{hybrid} (kcal/mol)
hsa-miR-92a	1600	7merα	1	-13.30
hsa-miR-203a	125	6merγ	1	-12.30
hsa-miR-203a	78	6merα	1	-10.50
hsa-miR-92a	2583	6merβ	1	-8.70
hsa-miR-30a-5p	1811	7merβ	1	-8.26
hsa-miR-30d	1811	7merβ	1	-5.86
hsa-miR-30a-5p	1183	6merβ	0	-16.20
hsa-miR-30d	1183	6merβ	0	-15.50
hsa-miR-30a-5p	1194	6merγ	0	-13.39
hsa-miR-30d	1194	6merγ	0	-13.29
hsa-miR-203a	1125	8merα	0	-9.92
hsa-miR-203a	2109	6merβ	0	-9.46
hsa-miR-92a	1947	6merγ	0	-7.83

The energy (ΔG_{hybrid}), which is released upon miRNA:mRNA binding, is listed in Table 6.1. The higher the absolute value the more energy gets released upon binding. Comparing the calculated values among the candidate miRNAs, miR-92a binds most strongly to the 1 600 binding site, as the most energy gets released. In addition, this site lies in an AGO⁺ region, which makes miR-92a a good potential candidate.

A basic biological principle is that important mechanisms are conserved between the genomes of different species. This also holds true for miRNA binding sites. For instance by comparing five different genomes (human, mouse, rat, dog and chicken), the ratio for predicting positive to false-positive targets is 3.5:1 when conserved 7 nt motifs are chosen over non-conserved ones (Lewis et al, 2005). As conservation plays a critical role in miRNA targeting and target repression, a murine data set was analysed in addition in the present study. Here, a decrease of miR-30a/d, miR-92a and miR-203a was observed in an experimental lung fibrosis model. Their binding sites on the murine WISP1 3'UTR were predicted by the SVM developed by Daniel Ellwanger. However, the number and positions of the binding sites differ from the human ones, as listed in Table 6.2.

Table 6.2: Candidate miRNA binding sites on the murine WISP1 3'UTR

Symbol	Position on 3'UTR	Seed type
mmu-miR-30	1132	6merα
	2644	6merγ
	3708	8mer
mmu-miR-92a	3729	6merα
mmu-miR-203a	87	6merβ
	633	7merβ
	1620	6merα
	3246	6merβ
	3354	6merγ

In addition to the prediction by the SVM, the WISP1 3'UTR was analysed with the prediction algorithm TargetScan (Friedman et al, 2009), a stringent miRNA prediction tool, which is widely used (Tan Gana et al, 2012). The longest binding sites for miR-30, miR-92a and miR-203a were verified, but classified as poorly conserved. This is in consistence with observation of the present study comparing the candidate miRNA binding sites on the human and mouse WISP1 3'UTR.

Besides seed type and conservation criteria, miRNA binding position on the 3'UTR, the target site accessibility and the proximity to other miRNA binding sites influence the efficacy of the miRNA-mediated regulation (Bartel, 2009). MiRNA binding sites, which are located within 15 nt after the stop codon, exhibit poor efficacy. For this, binding competition of the translation and silencing machinery to the mRNA may be responsible (Grimson et al, 2007). However, this does not apply to any predicted target site of the candidate miRNAs. It is further reported that binding sites in the middle of UTR's are less functional as they may be less accessible due to secondary RNA structures. Gimson *et al*. report that this effect was most pronounced for UTRs longer than 1 300 nt (Grimson et al, 2007). The analysed WISP1 3'UTR is around 4 000 nt long and in the first quartile only miR-203a bindings sites were predicted. In the last quartile, there are several binding sites predicted, however, only with a 6mer seed. Thus, most predicted, favourable long seed binding sites are in the two middle quartiles. Therefore, it cannot be excluded that secondary structures of the WISP1 3'UTR disturb the candidate miRNAs' bindings and their regulation capacity.

Another determinant of miRNA efficiency is the number of binding sites. Multiple miRNA binding sites are associated with greater mRNA destabilization (Doench & Sharp, 2004; Grimson et al, 2007). The repressive effect of two sites matches the effect anticipated by multiplying the repression from two single sites indicating an independent silencing action. Interestingly, Gimson *et al.* reported that two sites in close proximity (100 nt) repressed to a greater extend than expected from two independent single sites, suggesting a cooperative action mode (Grimson et al, 2007; Saetrom et al, 2007). Close proximity can be found for the predicted binding sites miR-203a at position 78 and 125, for miR-30 at position 1183 and 1194, for miR-30 and miR-92a at 2982 and 3027, respectively.

Taking all these features (seed type, AGO$^+$ region, conservation, accessibility and position on the 3'UTR) into account, the candidate miRNAs have a strong possibility to affect WISP1 expression. All candidate miRNAs' longest seed sites lay in an AGO$^+$ region except miR-203a. Additionally, for miR-92a strong binding affinity and high hybridization energy with the WISP1 3'UTR were predicted. Furthermore, binding sites were reported to be in close proximity, which might enhance their effect. Uncertainties lie in the facts that for all candidate miRNAs except for miR-203a all binding sites are located in the central region of the 3'UTR and are poorly conserved. Thus altogether, the selected miRNAs represent the most likely ones emerging from this present analysis to bind to the WISP1 3'UTR.

Besides these evaluated candidate miRNAs, miR-29 would be an interesting candidate to look at. Even though this miRNA did not come up in the present analysis of the human miRNA data sets, it is widely shown that miR-29 is downregulated in fibrosis (Cushing et al, 2011; Qin et al, 2011; Roderburg et al, 2011; Xiao et al, 2012). According to TargetScan prediction, the human WISP1 3'UTR possesses two conserved miR-29 sites and one lays in close proximity to the stop codon. Furthermore, a miR-29 dependent regulation for CTGF is known (Xiao et al, 2012) and miR-29a can potentiate Wnt signalling during osteoblast differentiation by directly regulating Wnt inhibitors DKK1, Kremen2, and sFRP2 (Kapinas et al, 2010). However, miR-29 was not analysed during this study, as in this present analysis of the miRNA data sets, miR-29 was not significantly decreased. In sum, this indicates the miR-29 family as an interesting additional future target to look at in the context of WISP1 regulation and fibrosis.

6.2 The occurrence and function of the candidate miRNAs

In this study the focus was on miR-30s, miR-92a and miR-203a, as these miRNAs are a) downregulated in IPF, and b) predicted to bind to the WISP1 3'UTR, thus might contribute to high WISP1 expression in IPF.

It has been known that miR-30 family negatively regulates mesenchymal gene transcripts like VIM and SNAIL1 in primary human pancreatic epithelial cells and thereby controls EMT of these primary cultures. MiR-30 overexpression retained the epithelia cell character of the primary cultures while miR-30 inhibition promoted transition to a mesenchymal cell phenotype. Interestingly, miR-30 family expression was decreased in fibrotic compared to non-fibrotic regions of pancreatitis tissue samples in the same study (Joglekar et al, 2009). Later, similar studies with thyroid carcinoma cells, non-small cell lung cancer cells, hepatocytes and prostate cancer cells confirmed VIM and SNAIL1 as a miR-30 target and that miR-30 represses EMT (Braun et al, 2010; Kao et al, 2014; Kumarswamy et al, 2012; Zhang et al, 2012). As miR-30 was downregulated in IPF and as WISP1 fosters also EMT of ATII cells (Königshoff et al, 2009), in addition to all bioinformatics criteria, miR-30 has been an interesting candidate and the role of miR-30 in WISP1 regulation was further investigated.

Additionally, TGF-β1 was capable of downregulating miR-30s in podocytes (Shi et al, 2013), and in another study miR-30 regulated TGF-β1 signalling by downregulating Smad2, whereas here TGF-β1 did not influence miR-30 expression (Braun et al, 2010). Milosevic *et al.* performed TGF-β1 stimulation of normal lung fibroblasts and found miR-30a-3p significantly downregulated among the miR-30 family (Milosevic et al, 2012). Furthermore, miR-30b was decreased in systemic sclerosis, another fibrotic disease involving skin, lung, heart and the digestive system, and TGF-β1 downregulated miR-30b in dermal fibroblasts. Here, it was shown that miR-30b targets PDGFRA, COL1A2 and ACTA (Tanaka et al, 2013). However, in the present study no direct influence of TGF-β1 on miR-30 expression was observed *in vitro*. In the described studies above, different TGF-β1 concentrations were used from the one applied in this work suggesting that TGF-β1 induces miR-30 in a cell type- and concentration-dependent manner.

Interestingly, the miR-30 family has been shown to regulate other CCN protein family members, such as CTGF (Duisters et al, 2009). CTGF is upregulated both, *in vitro* in lung fibroblasts by TGF-β1 (Lasky et al, 1998) and *in vivo* in pulmonary fibrosis (Pan et al, 2001). Hence, it can be speculated that miR-30 may regulate CTGF and WISP1, and loss of these miRNAs under profibrotic conditions may lead to an upregulation of these profibrotic matricellular proteins, thereby contributing to disease development.

Furthermore, miR-92a was identified as a candidate miRNA downregulated in IPF. MiR-92a is transcribed with six other miRNAs (miR-17-5p and -3p, miR-18a, miR19a, miR-19b and miR-20a) from the polycistronic miRNA cluster 17~92. The miR-17~92 cluster is primarily linked to cancer pathogenesis (Mendell, 2008). Loss of function of this cluster resulted in postnatal death of knock out animals, which was likely due to hypoplastic lungs and ventricular septal defects (Ventura et al, 2008). Further, the miR-17~92 cluster was expressed in epithelial lung progenitor cells promoting their proliferative and undifferentiated phenotype (Lu et al, 2007). Together, these data suggest an important role for miR-17~92 cluster in lung development and homeostasis. In mammals, two miR-17~92 cluster paralogues, miR-106b~25 and miR-106a~363, exist. The mature miR-92a sequence can arise from either the miR-17~92 or the miR-106b~25 cluster. However, from these clusters only miR-25 and miR-363 have the same seed as miR-92a, which are both not decreased in the present analysis of the fibrotic data sets.

Among candidate miRNAs, miR-92a was the most abundantly expressed in all analysed human cells, like lung cancer cells and normal epithelial cells as well as fibroblasts. In whole human lung tissue homogenate, it was second highest expressed after miR-30a/d. However, other cluster members were not analysed, as they were not decreased in the present analysis of the published data sets and more importantly do not target the WISP1 3'UTR.

Interestingly, a recent report by Dakhlallah *et al.* described downregulation of miR-92a in IPF tissue and IPF derived fibroblasts, which is in agreement with the presented findings (Dakhlallah et al, 2013). They further report that miR-17~92 was silenced due to enhanced DNA methylation, and that fibrotic genes such as *COL13A*, *COL1A* and *CTGF* are regulated by

this miRNA cluster in IPF fibroblasts, but not by miR-92a explicitly. Li *et al.* further reported the regulation of collagen synthesis by the miR-17~92 cluster in palatal shelves (Li et al, 2012b). However, not miR-19a/b and miR-92a, but miR-17, miR-18a and miR-20a interfered with the TGF-β1-induced collagen production from palatal mesenchymal cells. Similarly, in the present study no changes of *COL1A1* after miR-92a overexpression could be observed in normal lung fibroblasts upon TGF-β1 stimulation. Thus, miR-92a is highly expressed in IPF fibroblasts and lung cancer cells but is not directly involved in increased collagen expression. These data further highlight target specificity of single miRNAs originating from the same cluster.

MiR-203a, the third candidate has been thus far known to be involved in skin development. During skin development, miR-203a expression highly increases when epidermal differentiation occurs by restricting the proliferation potential of basal cells due to downregulation of p63 (Yi et al, 2008). In contrast, miR-203a expression was lost due to promoter hypermethylation in various cancers (Taube et al, 2013; Zhu et al, 2013). In this context, loss of miR-203a expression was associated with EMT induction. MiR-203a was mainly expressed in epithelial, non-cancerous cells and expression in mesenchymal cells compromises cell migration and invasion (Taube et al, 2013). Besides miR-203a epigenetic regulation, miR-203a was repressed by SNAIL2 induction upon TGF-β1 stimulation of mammary epithelial cells (Ding et al, 2013). As for the other miRNAs, a direct regulation of miR-203a upon TGF-β1 treatment could not be found in phFB in the present study.

In the lung, miR-203a was poorly expressed in my analysis. A miR-203a expression screen in several organs showed that miR-203a is highly and almost exclusively expressed in the skin and only poorly in in the lung (Sonkoly et al, 2007). Furthermore, in the cell screen conducted in the present study miR-203a was only detectable in primary bronchial epithelial cells and not in A549 lung cancer cells confirming literature reports identifying miR-203a as an epithelial miRNA being downregulated in cancerous tissue and cells (Jin et al, 2013; Wang et al, 2013).

In context with Wnt signalling, LEF1, a transcription factor involved in canonical Wnt signalling, is a target of miR-203a in zebra fish (Thatcher et al, 2008). Moreover, in mammary epithelial cells high miR-203a levels are associated with high levels of Dkk1, an inhibitor of Wnt signalling, and low levels of β-catenin suggesting inhibition of Wnt signalling (Taube et al, 2013).

Altogether, miR-203 is involved in skin differentiation and loss of miR-203 accompanied EMT and tumour cell invasion. WISP1 induces EMT of ATII cells as well as cell migration and invasion, and therefore the interplay between miR-203a and WISP1 in the context of pulmonary fibrosis was chosen to be studied.

6.3 The candidate miRNAs are downregulated in several fibrotic data sets

The decrease of the candidate miRNAs was evaluated in whole IPF tissue and in IPF derived fibroblasts as well as in the experimental lung fibrosis model and pmATII cells, thereof.

The miR-30 family has been found to be downregulated in pulmonary fibrosis in several independent data sets, which was further confirmed for miR-30a/d in IPF tissue homogenates in the present study (Cho et al, 2011; Liu et al, 2010; Pandit et al, 2010). Recently, Schulz *et al*. identified miR-30d to be downregulated in lung development and in IPF (Schulz et al, 2013). Corroborating results were shown by Milosevic *et al.,* comparing 13 IPF *versus* 12 control tissue samples for miR-30a/d and miR-203a expressions (Milosevic et al, 2012).

As mentioned above, miR-92a can originate from two different miRNA clusters. The current analysis of the *GSE13316* and the *GSE21394* profile revealed exclusively miR-92a as downregulated (Cho et al, 2011; Pandit et al, 2010). Dakhlallah *et al.* reported significant downregulation for all miRNAs of the miR17~92 cluster in IPF and IPF-derived fibroblasts (Dakhlallah et al, 2013). Furthermore, miR-92a and other members of the cluster were reported as being downregulated in the different datasets of IPF cohorts provided by Schulz *et al.* (Schulz et al, 2013). In the study from Oak *et al.* miR-92a was found increased in IPF tissue while other cluster members (miR-17, miR-19a/b, miR-18a and miR-20a) were decreased (Oak et al, 2011). Interestingly, miR-92a was increased in skin fibroblasts treated with TGF-β1 and fibroblasts from scleroderma patients, which is an autoimmune disorder with cutaneous and visceral fibrosis (Sing et al, 2012). Although the miR-17~92 cluster is transcribed as one primary transcript, several studies indicate that the different members of the cluster are differentially regulated (Heinrich et al, 2013).

In sum, the candidate miRNAs (miR-30a/d, miR-203 and miR-92a) are significantly decreased in most IPF cohorts analysed, which is in line with other investigations. For miR-92a it is not finally clear whether the whole cluster or the single miRNA is regulated in pulmonary fibrosis. However, the current findings support the notion that miR-92a is regulated independently in fibrosis. Furthermore, the decrease of the candidate miRNAs could be confirmed in whole tissue from the bleomycin model proving that these animal models exhibit the same miRNA phenotype as the human disease. Additionally, a significant decrease of miR-92a in another experimental fibrosis model was reported here for the first time, indicating that a decrease in miR-92a during fibrosis is an important hallmark of fibrosis.

Beyond the decrease of candidate miRNAs, increased WISP1 levels were identified as previously reported in IPF tissue specimens (Königshoff et al, 2009; Selman et al, 2006). In addition, increased WISP1 levels from IPF-derived fibroblasts could be reported for the first time. This shows that mesenchymal cells in addition to epithelial cells can be a source for WISP1 in IPF. Moreover, miR-92a expression negatively correlated with WISP1 in phFB suggesting a WISP1 regulation by miR-92a in these cells. No correlation was found for the other candidate miRNAs. This might be due to lack of WISP1regulation by miR-30 or due to

other mechanisms interfering and regulating both expression of miRNAs and WISP1 resulting in no noticeably relation.

6.4 Reporter assays for WISP1 regulation by candidate miRNAs

In order to verify the miRNA binding sites on the WISP1 3'UTR, luciferase reporter assays were performed, which is the most commonly used approach (van Rooij, 2011).

First, the complete WISP1 3'UTR sequence according to the UCSC genome browser was tested in order to determine whether the WISP1 3'UTR was susceptible to candidate miRNA regulation. The whole WISP1 3'UTR was incorporated, as distal regions may enhance or inhibit miRNA binding and truncated sequence versions may provide inappropriate accessibility to a given miRNA binding site, and hence influence gene regulation (Bartel, 2009; van Rooij, 2011). In this study, a combined transfection approach of miRNA mimics and luciferase reporter was applied. First it was demonstrated that a GFP plasmid reporter can be transfected with efficiency as high as 41%, and that nearly every cell was transfected with a fluorescent dye-labelled miRNA reporter, indicating high transfection efficiency. Therefore, it was assumed that in every cell transfected with a reporter plasmid the target miRNA amount also increased.

As control experiments, co-transfections of the reporter vector pmirGLOW with non-targeting miRNA mimics (M-miR-NCI and NCII) were performed. A reduction in luciferase expression could neither be observed for the control experiments nor for the co-transfections with targeting candidate mimics. Therefore, it was concluded that the candidate miRNAs do not affect luciferase expression in the applied setups. This could be due to lack of binding of the miRNAs to the 3'UTR or lack of regulation of luciferase expression by miRNA binding to the 3'UTR. Further conventional controls like reporter vectors containing the 3'UTR in the reverse orientation or mutated miRNA-binding sites were not necessary, as these initial experiments showed no regulation.

However, another control experiment comparing the reporter vectors with and without WISP1 3'UTR revealed a decrease in reporter gene expression using the WISP1 3'UTR tagged reporter compared to the untagged one. In general, 3'UTRs serve not only as binding element for miRNAs but also for regulatory proteins (reviewed by (Barrett et al, 2012)). Furthermore, secondary RNA structures as well as 3'UTR length can influence mRNA accessibility and stability (Barrett et al, 2012). In 1996, Tanguay and colleagues reported that increasing the length of the 3'UTR from 19 nt to 156 nt decreased expression around 45-fold, independently of the orientation, gene or sequence (Tanguay, 1996). Even though the whole WISP1 3'UTR as well as the truncated fragments are much longer, a similar observation was made in this study. The insertion of the whole WISP1 3'UTR repressed reporter expression the most, followed by fragment 3, containing a 2 kb insert, fragment 1 (1.1 kb) and fragment 2 (0.9 kb). In general, for the transfection setup, the different molculare weights of the constructs have not been taken into accout. However, the *Renilla* luciferase gene was always encoded on the same plasmid as a control, and therefore an effect due to transfection efficiency and the different molecular weights of the

different reporter plasmids can be ruled out. A simple explanation for this observed effect could be that the longer the UTR the more miRNA and protein binding sites and regulatory *cis* elements it can possess. Interestingly, the 3'UTR of CYR61, another protein of the CCN family, was recently investigated. Nakagawa and colleagues recognized a stable secondary structure in the proximal part of the CYR61 3'UTR responsible for translational repression. In addition miR-181 regulation of CYR61 was investigated but no miRNA dependent regulation was observed (Nakagawa et al, 2013). By the same group, a minimal RNA element named CESAR within the 3'UTR of CTGF, which belongs also to the CCN protein family was reported to play a role in protein expression regulation (Kubota et al, 2000). For the WISP1 3'UTR no *cis* elements are known to be involved in expression regulation, however the WISP1 3'UTR forms various secondary structures as analysed with the VIENNA package (Hofacker, 2003) (data not shown). Therefore, it seems plausible that the WISP1 3'UTR itself has an effect on luciferase expression which cannot or not any further be regulated by overexpressing the candidate miRNAs. The conducted luciferase assays indicate a possible impact of the WISP1 3'UTR itself on gene expression. However, further studies would need to be conducted to elucidate the role of 3'UTR RNA secondary structures for the WISP1 expression.

To shed light on the role of the candidate miRNAs without the influence of the 3'UTR effects described above, luciferase assays with so-called pSi and pMi reporters were performed. This served on the one hand as a proof of principle approach using the pSi constructs which have ideal binding capacity to the miRNAs. On the other hand it omits the influence of the long 3'UTR investigating only the predicted miRNA binding sites using the pMi constructs. Both reporters, pSi and pMi constructs, possessed either twice or three times the target site, respectively, in order to increase the statistical binding possibility, and no additional inter-site spacers were included.

The proof of principle successfully worked for instance for the pSi30a approach and demonstrated that in general the experimental setup was established correctly, assuming that the canonical RNAi pathway led to cleavage and degradation of perfectly complementary RNA targets. Considering the results from the pSi proof of principle study (Figure 5.24) and the candidate miRNA expression screen in HEK cells (Figure 5.25), it seems plausible that pSi92a is already regulated by endogenous miR-92a. MiR-92a mimics could not further modify this quite extensive effect, so the miRNA-dependent regulation system seemed to be already at its limits.

All cloned miRNA binding sites for pMi constructs, are the ones with the longest seed and are located in an AGO[+] region, except pMi203a, where the site with the longest seed is not identical with the AGO[+] site. However no change in luciferase was detected for the pMi constructs. Either the predicted and cloned binding sites are not functional or they are not sufficient to foster regulation. It was shown that identical miRNA sites could mediate repression in some UTRs but not in others (Bartel, 2009; Brennecke et al, 2005).

In general, reporter assays have limitations, as the natural regulatory context is lost, both at the level of the target sequence within its mRNA and at the level of cellular context (Pasquinelli, 2012). Here, lung cells but also HEK cells were applied for reporter gene

experiments. HEK cells were applied, because they are easy to transfect and the endogenous downregulating effect of the whole 3'UTR could not be observed here. In order to be able to verify the predicted candidate miRNA binding sites as being functional, other methods like AGO and/or miRNA pull-down (Nonne et al, 2010) would need to be applied. In the present study, the focus was further on endogenous WISP1 regulation by miRNAs and the influence of the cellular microenvironment on this process, as Duisters *et al.* showed that the cellular microenvironment could influence miRNA regulation (Duisters et al, 2009).

6.5 WISP1 regulation by microRNAs depends on the cellular microenvironment

The reporter gene analysis of the WISP1 3'UTR revealed that the length of the UTR has an influence on reporter gene expression, but cannot be further regulated by the candidate miRNAs. Therefore, endogenous WISP1 expression was investigated if it is susceptible to miRNA regulation. For this, various human lung cells were screened for WISP1 and miRNA expression. WISP1 expression was low but clearly detectable in mesenchymal cells. Moreover, here it was reported for the first time that WISP1 expression was increased also in IPF-derived fibroblasts. Altogether, this suggests that also mesenchymal cells are a source for WISP1 under homeostasis and contribute to increased WISP1 levels after injury. This is an interesting observation, as WISP1 was reported to be highly increased in human and murine epithelial cells after lung injury (Königshoff et al, 2009; Li et al, 2012a; Zemans et al, 2013). However, Knobloch *et al.* detected WISP1 expression only in human airway smooth muscle, but not in bronchial epithelial cells (Knobloch et al, 2013), corroborating the cell screen data of the present study.

MiR-30a/d possessed similar expression levels in all cells tested, but with the highest levels in bronchial epithelial cells. MiR-92a was the highest expressed candidate miRNA, with higher occurrence in epithelial cells than in mesenchymal cells. Of note, miR-203a was only detectable in bronchial epithelial cells, but here WISP1 was not detectable (Figure 5.28). This expression data are in line with published data as outlined above in detail. In general, primary adult cells may resemble the *in vivo* situation better than HFL1 and MRC5 cells, as these are of foetal origin. Hence, phFB were chosen to investigate endogenous WISP1 regulation by miRNAs, as these cells express WISP1 and most of the candidate miRNAs.

In addition to WISP1 expression, the existence of the whole WISP1 3'UTR was positively evaluated, since alternative poly(A) sites can occur and be involved in gene regulation. Hence, it should be examined that the whole 3'UTR exists in these cells and all predicted binding sites could represent a target site of candidate miRNA regulation.

First, endogenous regulation was investigated by downregulation of candidate miRNAs applying miRNA inhibitors, as WISP1 is poorly expressed and this approach should lead to WISP1 upregulation. The candidate miRNAs could be downregulated in a concentration dependent manner. Subsequent 100 nM and 5 nM inhibitor were chosen for further investigations, as the highest concentration caused the highest downregulation and even

the lowest concentration showed a decrease in miRNA levels, but may cause no or less off target effects. However, no change in WISP1 mRNA and protein levels could be observed after successful candidate miRNA downregulation. Reasons therefore might be mRNA and protein stability and only slight effects by miRNAs, which are beyond the detection limit or due to lack of regulation with the applied settings.

Second, candidate miRNAs were overexpressed applying miRNA mimic transfection to phFB. Here, a GAPDH specific positive control was utilized to elaborate a working concentration for the miRNA mimics. 100 nM GAPDH-specific miRNA mimics downregulated *GAPDH* mRNA the most, and hence this concentration was used for candidate miRNA overexpression. In addition, siRNA experiments against WISP1 were performed in order to demonstrate that WISP1 could be downregulated by small RNAs, and this downregulation can be observed on protein level. As miRNAs act on mRNA levels and not only on protein abundance (Guo et al, 2010), first *WISP1* mRNA levels were investigated. Downregulation of *WISP1* mRNA by miR-92a overexpression was observed in two out of three donor lines and miR-30d decreased *WISP1* mRNA in phFB from MLT005. However, in another phFB batch, miR-30 had the opposite effects and increased *WISP1* mRNA levels. AT the protein level, miR-92a showed a trend to decrease WISP1. In summary, candidate miRNA inhibition and overexpression was successfully set up. MiR-92a appeared to influence WISP1 levels on mRNA and protein levels in a cell donor-specific way, and therefore under a certain microenvironment.

One reason for this observed effect might be the occurrence of alternative WISP1 3'UTRs. Even though the whole WISP1 3'UTR existed in phFB, it cannot be excluded that alternative poly(A) sites result in shorter WISP1 3'UTRs. Alternative poly(A) sites are predicted for the human *WISP1* mRNA, for instance by PolyAPred (Ahmed et al, 2009), and one of the predictions is in agreement with the annotated human WISP1 3'UTR, only 2634 nt long, in the Ensembl database. These alternative 3'UTR may avoid to be regulated by certain miRNAs, as the binding site is missing. However, its existence in phFB would need to be verified experimentally, for instance using RACE-PCR. Even if the candidate miRNAs downregulate the mRNA with the long 3'UTR, WISP1 protein can originate from mRNAs with shorter 3'UTRs where the miRNA in question may not bind. As it is reported that miRNAs have a modest impact on protein output (around 50%) (Baek et al, 2008; Selbach et al, 2008), one can speculate that if the protein arises from more than one mRNA, that the miRNA-dependent regulation may not be detectable. In addition, AU rich elements can influence mRNA stability (Barrett et al, 2012). These elements could be another 3'UTR length-dependent regulatory factor and hence, interfere with miRNA-mediated gene regulation.

In general, mRNA and protein levels are tightly regulated by several mechanisms and the correlation of their levels is rather poor for non-housekeeping genes (Schwanhausser et al, 2011). Even though the correlation for WISP1 mRNA and protein was rather good under steady state levels, miRNA transfection in addition to TGF-β1 treatment may represent a strong perturbation, leading to a misbalance of WISP1 mRNA and protein levels. Therefore, miRNA induced changes may only be detectable at mRNA but not on protein levels.

Therefore, next WISP1 regulation by miRNAs was assessed in a disease relevant profibrotic environment.

6.6 WISP1 is regulated by miRNAs in a profibrotic environment

WISP1 is only modestly expressed under tissue homeostasis and in cell culture. Therefore, WISP1 modulation by microRNAs may be rather difficult to be observed. As WISP1 was increased under profibrotic conditions, WISP1 regulation by miRNAs was aimed to be studied in a profibrotic environment *in vitro*. In order to do so, phFB were treated with TGF-β1, a potent profibrotic cytokine and inducer of WISP1 (Blaauboer et al, 2013; Fernandez & Eickelberg, 2012a; Tatler & Jenkins, 2012). Under this conditions, miR-30a, miR-92a, and a combination thereof, significantly reduced WISP1 at the mRNA level. However, a reduction at the protein level could not be detected. This expression might be due to WISP1 protein stability, faster protein production than degradation or detection limitations.

Interestingly, in addition to WISP1 regulation by miR-30a and miR-92a in the presence of TGF-β1 *in vitro*, a strong negative correlation for WISP1 and miR-92a *in vivo* in a TGF-β1-dependent fibrosis model was reported in this study. Altogether, this indicates that miR-92a is involved in WISP1 regulation under fibrotic conditions.

While Figure 5.42 indicates that miR-30a and miR-92a directly target WISP1, miR-30a in addition reduces SERPINE1, a known TGF-β1 target. TargetScan predicts one conserved miR-30 binding site in the human SERPINE1 3'UTR. Furthermore, in human endothelial cells it was shown that miR-30c regulates SERPINE1 (Marchand et al, 2012), which is in line with the presented data.

However, it cannot be excluded that not only WISP1 expression itself but also that of other members of the TGF-β1 and/or Wnt/β–catenin pathways are modified by miR-30 and miR-92a in the applied setting as well as in fibrosis, also contributing to changes in WISP1 expression. Several components of the Wnt and TGF signalling cascade are predicted to harbour candidate miRNA binding sites. (TargetScan prediction for miR-30: FZD3 and 2, Kremen1, LRP6, Vangl1 and WNT7b as well as Smad2; for miR-92a: DKK3 (Haug et al, 2011), FZD10 as well as TGIF1, Smad7 and Smurf1). Interestingly, in neuroblastoma the miR-17~92 cluster is associated with the regulation of TGF-β1 pathway components (Mestdagh et al, 2010) and similarly, miR-30 repressed Smad2 expression in thyroid carcinoma cells (Braun et al, 2010), supporting the notion that regulation of WISP1 by miRNAs is not only due to direct targeting but also due to targeting of WISP1 upstream effectors.

As mentioned in the introduction and in sections above, miRNA expression is tightly regulated for instance by promoter hypermethylation, as reported for the miR-17~92 cluster in IPF (Dakhlallah et al, 2013). In general miRNA expression can be regulated at the transcriptional level as well as during various processing steps. In fibrogenesis, TGF-β1 influence on miRNA expression was reported among others for miR-29, let-7d and miR-21 (reviewed in (Bowen et al, 2013; Pandit et al, 2011)). At the transcriptional level, Smad3

binding to either the miR-29 or let-7d promoter represses their expression (Pandit et al, 2010; Qin et al, 2011). Moreover, miR-21 was regulated at the post-transcriptional level. The pri-miR-21 has a putative Smad response element in its hairpin, and Smad binding promotes miR-21 processing and expression increases (Davis et al, 2010). In addition, regulation of miR-30 by TGF-β1 was reported as mentioned in paragraph 6.2. However, a direct TGF-β1 regulation of miR-30, as well as of the other candidate miRNAs could not be observed in the applied cell system in the present study (Figure 5.41). In summary, miRNAs can be regulated by members of the TGF signalling pathway but also by promoter hypermethylation. Reciprocally, the candidate miRNAs may regulate WISP1 by modulating components of TGF-β1 or Wnt signalling cascade. Therefore, TGF-β1 treatment might enhance WISP1 expression by altering miRNA levels and WISP1 regulation can be conveyed by direct miRNA effects or by changes of their upstream effectors.

6.7   WISP1 regulation by cytokines

Besides WISP1 regulation by miRNAs, an increase in WISP1 transcript expression was shown in this study in TGF-β1-treated lung fibroblasts *in vitro*, which is in agreement with a recent report (Blaauboer et al, 2013). Blaauboer *et al.* further reported that increased WISP1 levels were associated with *de novo* collagen synthesis in bleomycin-induced lung fibrosis (Blaauboer et al, 2013). Here, elevated WISP1 protein expression and secretion was detected upon exposure of pulmonary cells to TGF-β1 *in vitro* as well as *in vivo* suggesting that WISP1 is able to exhibit autocrine and paracrine functions within the epithelial-mesenchymal unit in IPF. Furthermore, WISP1 induction by TGF-β1 was known in osteoblasts and in hepatocytes (Lukowski et al, 2012; Parisi et al, 2006), indicating a major role for TGF-β1-dependent WISP1 regulation.

In addition to TGF-β1, WISP1 is a known Wnt target gene (Königshoff et al, 2009; Pennica et al, 1998). Notably, Wnt/β–catenin and TGF-β1 signalling interplay has recently been demonstrated in experimental and human pulmonary fibrosis (Akhmetshina et al, 2012; Ulsamer et al, 2012; Zhou et al, 2012). Furthermore, increased IL-1β and TNF-α levels are associated with fibrotic lung diseases (Wynn, 2011). Both cytokines are describted to induce WISP1 expression in several different cells (Colston et al, 2007; Knobloch et al, 2013; Liu et al, 2013a; Venkatachalam et al, 2009). This shows that WISP1 regulation by TGF-β1 or other cytokines in both epithelial as well as mesenchymal cells might be an important step in the progression of fibrosis. Therefore, it would be interesting to furthermore evaluate the potential of IL-1β and TNF-α for WISP1 induction in the context of pulmonary fibrosis.

6.8 Conclusion

This study revealed disease-relevant miR-30a/d, miR-203a and miR-92a target sites in the human WISP1 3'UTR. Furthermore, phFB were established as valid cell culture model to study WISP1 expression and regulation. WISP1 is increased in lung specimens from IPF patients and it was further demonstrated that the profibrotic protein TGF-β1 functions as potent WISP1 inducer. Interestingly, both miR-30a and miR-92a reversed TGF-β1-induced WISP1 expression *in vitro*. Importantly, correlation studies in lung tissue homogenate *in vivo* and phFB from IPF patients *ex vivo* further corroborate the inverse relation of WISP1 and miR-92a. However, reporter assays could not underpin miRNA binding to the WISP1 3'UTR. As the WISP1 3'UTR is rather long, WISP1 3'UTR length- and sequence-dependent reporter gene downregulation was observed. This insights might help to further explore the influence of the WISP1 3'UTR on WISP1 expression and contribution to its low levels under tissue homeostasis. In summary, evidence is provided for WISP1 regulation by miR-92a in pulmonary fibrosis, which further highlights the potential role of miRNAs as novel therapeutic targets for pulmonary fibrosis.

7   REFERENCES

Abreu JG, Ketpura NI, Reversade B, De Robertis EM (2002) Connective-tissue growth factor (CTGF) modulates cell signalling by BMP and TGF-beta. *Nat Cell Biol* **4:** 599-604

Ahmed F, Kumar M, Raghava GP (2009) Prediction of polyadenylation signals in human DNA sequences using nucleotide frequencies. *In silico biology* **9:** 135-148

Akhmetshina A, Palumbo K, Dees C, Bergmann C, Venalis P, Zerr P, Horn A, Kireva T, Beyer C, Zwerina J, Schneider H, Sadowski A, Riener MO, MacDougald OA, Distler O, Schett G, Distler JH (2012) Activation of canonical Wnt signalling is required for TGF-beta-mediated fibrosis. *Nature communications* **3:** 735

Alder JK, Chen JJ, Lancaster L, Danoff S, Su SC, Cogan JD, Vulto I, Xie M, Qi X, Tuder RM, Phillips JA, 3rd, Lansdorp PM, Loyd JE, Armanios MY (2008) Short telomeres are a risk factor for idiopathic pulmonary fibrosis. *Proc Natl Acad Sci U S A* **105:** 13051-13056

Armanios MY, Chen JJ, Cogan JD, Alder JK, Ingersoll RG, Markin C, Lawson WE, Xie M, Vulto I, Phillips JA, 3rd, Lansdorp PM, Greider CW, Loyd JE (2007) Telomerase mutations in families with idiopathic pulmonary fibrosis. *The New England journal of medicine* **356:** 1317-1326

B BM, Lawson WE, Oury TD, Sisson TH, Raghavendran K, Hogaboam CM (2013) Animal models of fibrotic lung disease. *American journal of respiratory cell and molecular biology* **49:** 167-179

Baek D, Villen J, Shin C, Camargo FD, Gygi SP, Bartel DP (2008) The impact of microRNAs on protein output. *Nature* **455:** 64-71

Barrett LW, Fletcher S, Wilton SD (2012) Regulation of eukaryotic gene expression by the untranslated gene regions and other non-coding elements. *Cell Mol Life Sci* **69:** 3613-3634

Bartel DP (2009) MicroRNAs: target recognition and regulatory functions. *Cell* **136:** 215-233

Bauer M, Su G, Casper C, He R, Rehrauer W, Friedl A (2010) Heterogeneity of gene expression in stromal fibroblasts of human breast carcinomas and normal breast. *Oncogene* **29:** 1732-1740

Berendsen AD, Fisher LW, Kilts TM, Owens RT, Robey PG, Gutkind JS, Young MF (2011) Modulation of canonical Wnt signaling by the extracellular matrix component biglycan. *Proc Natl Acad Sci U S A* **108:** 17022-17027

Berschneider B, Königshoff M (2011) WNT1 inducible signaling pathway protein 1 (WISP1): a novel mediator linking development and disease. *The international journal of biochemistry & cell biology* **43:** 306-309

Blaauboer ME, Emson CL, Verschuren L, van Erk M, Turner SM, Everts V, Hanemaaijer R, Stoop R (2013) Novel combination of collagen dynamics analysis and transcriptional

profiling reveals fibrosis-relevant genes and pathways. *Matrix biology : journal of the International Society for Matrix Biology* **32:** 424-431

Blom AB, Brockbank SM, van Lent PL, van Beuningen HM, Geurts J, Takahashi N, van der Kraan PM, van de Loo FA, Schreurs BW, Clements K, Newham P, van den Berg WB (2009) Involvement of the Wnt signaling pathway in experimental and human osteoarthritis: prominent role of Wnt-induced signaling protein 1. *Arthritis Rheum* **60:** 501-512

Bolstad BM, Irizarry RA, Astrand M, Speed TP (2003) A comparison of normalization methods for high density oligonucleotide array data based on variance and bias. *Bioinformatics* **19:** 185-193

Bonniaud P, Margetts PJ, Kolb M, Schroeder JA, Kapoun AM, Damm D, Murphy A, Chakravarty S, Dugar S, Higgins L, Protter AA, Gauldie J (2005) Progressive transforming growth factor beta1-induced lung fibrosis is blocked by an orally active ALK5 kinase inhibitor. *Am J Respir Crit Care Med* **171:** 889-898

Bowen T, Jenkins RH, Fraser DJ (2013) MicroRNAs, transforming growth factor beta-1, and tissue fibrosis. *J Pathol* **229:** 274-285

Braun J, Hoang-Vu C, Dralle H, Huttelmaier S (2010) Downregulation of microRNAs directs the EMT and invasive potential of anaplastic thyroid carcinomas. *Oncogene* **29:** 4237-4244

Brennecke J, Stark A, Russell RB, Cohen SM (2005) Principles of microRNA-target recognition. *PLoS biology* **3:** e85

Brigstock DR, Goldschmeding R, Katsube KI, Lam SC, Lau LF, Lyons K, Naus C, Perbal B, Riser B, Takigawa M, Yeger H (2003) Proposal for a unified CCN nomenclature. *Mol Pathol* **56:** 127-128

Busch A, Richter AS, Backofen R (2008) IntaRNA: efficient prediction of bacterial sRNA targets incorporating target site accessibility and seed regions. *Bioinformatics* **24:** 2849-2856

Calvisi DF, Conner EA, Ladu S, Lemmer ER, Factor VM, Thorgeirsson SS (2005) Activation of the canonical Wnt/beta-catenin pathway confers growth advantages in c-Myc/E2F1 transgenic mouse model of liver cancer. *J Hepatol* **42:** 842-849

Cavazza A, Rossi G, Carbonelli C, Spaggiari L, Paci M, Roggeri A (2010) The role of histology in idiopathic pulmonary fibrosis: an update. *Respir Med* **104 Suppl 1:** S11-22

Cervello M, Giannitrapani L, Labbozzetta M, Notarbartolo M, D'Alessandro N, Lampiasi N, Azzolina A, Montalto G (2004) Expression of WISPs and of their novel alternative variants in human hepatocellular carcinoma cells. *Ann N Y Acad Sci* **1028:** 432-439

Chambers RC, Scotton CJ (2012) Coagulation cascade proteinases in lung injury and fibrosis. *Proceedings of the American Thoracic Society* **9:** 96-101

Chang W, Wei K, Jacobs SS, Upadhyay D, Weill D, Rosen GD (2010) SPARC suppresses apoptosis of idiopathic pulmonary fibrosis fibroblasts through constitutive activation of beta-catenin. *J Biol Chem* **285:** 8196-8206

Chen CC, Lau LF (2009) Functions and mechanisms of action of CCN matricellular proteins. *The international journal of biochemistry & cell biology* **41:** 771-783

Chen K, Rajewsky N (2007) The evolution of gene regulation by transcription factors and microRNAs. *Nature reviews Genetics* **8:** 93-103

Chen PP, Li WJ, Wang Y, Zhao S, Li DY, Feng LY, Shi XL, Koeffler HP, Tong XJ, Xie D (2007) Expression of Cyr61, CTGF, and WISP-1 correlates with clinical features of lung cancer. *PLoS One* **2:** e534

Chi SW, Hannon GJ, Darnell RB (2012) An alternative mode of microRNA target recognition. *Nature structural & molecular biology* **19:** 321-327

Chi SW, Zang JB, Mele A, Darnell RB (2009) Argonaute HITS-CLIP decodes microRNA-mRNA interaction maps. *Nature* **460:** 479-486

Chilosi M, Poletti V, Zamo A, Lestani M, Montagna L, Piccoli P, Pedron S, Bertaso M, Scarpa A, Murer B, Cancellieri A, Maestro R, Semenzato G, Doglioni C (2003) Aberrant Wnt/beta-catenin pathway activation in idiopathic pulmonary fibrosis. *Am J Pathol* **162:** 1495-1502

Cho JH, Gelinas R, Wang K, Etheridge A, Piper MG, Batte K, Dakhallah D, Price J, Bornman D, Zhang S, Marsh C, Galas D (2011) Systems biology of interstitial lung diseases: integration of mRNA and microRNA expression changes. *BMC Med Genomics* **4:** 8

Chuang JY, Chang AC, Chiang IP, Tsai MH, Tang CH (2013) Apoptosis signal-regulating kinase 1 is involved in WISP-1-promoted cell motility in human oral squamous cell carcinoma cells. *PLoS One* **8:** e78022

Clevers H (2006) Wnt/beta-catenin signaling in development and disease. *Cell* **127:** 469-480

Coker RK, Laurent GJ, Jeffery PK, du Bois RM, Black CM, McAnulty RJ (2001) Localisation of transforming growth factor beta1 and beta3 mRNA transcripts in normal and fibrotic human lung. *Thorax* **56:** 549-556

Coker RK, Laurent GJ, Shahzeidi S, Lympany PA, du Bois RM, Jeffery PK, McAnulty RJ (1997) Transforming growth factors-beta 1, -beta 2, and -beta 3 stimulate fibroblast procollagen production in vitro but are differentially expressed during bleomycin-induced lung fibrosis. *Am J Pathol* **150:** 981-991

Colston JT, de la Rosa SD, Koehler M, Gonzales K, Mestril R, Freeman GL, Bailey SR, Chandrasekar B (2007) Wnt-induced secreted protein-1 is a prohypertrophic and profibrotic growth factor. *Am J Physiol Heart Circ Physiol* **293:** H1839-1846

Cushing L, Kuang PP, Qian J, Shao F, Wu J, Little F, Thannickal VJ, Cardoso WV, Lu J (2011) miR-29 is a major regulator of genes associated with pulmonary fibrosis. *American journal of respiratory cell and molecular biology* **45:** 287-294

Dakhlallah D, Batte K, Wang Y, Cantemir-Stone CZ, Yan P, Nuovo G, Mikhail A, Hitchcock CL, Wright VP, Nana-Sinkam SP, Piper MG, Marsh CB (2013) Epigenetic regulation of miR-17~92 contributes to the pathogenesis of pulmonary fibrosis. *Am J Respir Crit Care Med* **187:** 397-405

Davies SR, Watkins G, Mansel RE, Jiang WG (2007) Differential expression and prognostic implications of the CCN family members WISP-1, WISP-2, and WISP-3 in human breast cancer. *Ann Surg Oncol* **14:** 1909-1918

Davis BN, Hilyard AC, Nguyen PH, Lagna G, Hata A (2010) Smad proteins bind a conserved RNA sequence to promote microRNA maturation by Drosha. *Molecular cell* **39:** 373-384

Degryse AL, Lawson WE (2011) Progress toward improving animal models for idiopathic pulmonary fibrosis. *Am J Med Sci* **341:** 444-449

Desnoyers L (2004) Structural basis and therapeutic implication of the interaction of CCN proteins with glycoconjugates. *Curr Pharm Des* **10:** 3913-3928

Desnoyers L, Arnott D, Pennica D (2001) WISP-1 binds to decorin and biglycan. *J Biol Chem* **276:** 47599-47607

Ding X, Park SI, McCauley LK, Wang CY (2013) Signaling between transforming growth factor beta (TGF-beta) and transcription factor SNAI2 represses expression of microRNA miR-203 to promote epithelial-mesenchymal transition and tumor metastasis. *J Biol Chem* **288:** 10241-10253

Doench JG, Sharp PA (2004) Specificity of microRNA target selection in translational repression. *Genes Dev* **18:** 504-511

Duisters RF, Tijsen AJ, Schroen B, Leenders JJ, Lentink V, van der Made I, Herias V, van Leeuwen RE, Schellings MW, Barenbrug P, Maessen JG, Heymans S, Pinto YM, Creemers EE (2009) miR-133 and miR-30 regulate connective tissue growth factor: implications for a role of microRNAs in myocardial matrix remodeling. *Circ Res* **104:** 170-178, 176p following 178

Ellwanger DC, Buttner FA, Mewes HW, Stumpflen V (2011) The sufficient minimal set of miRNA seed types. *Bioinformatics* **27:** 1346-1350

Fabian MR, Sonenberg N, Filipowicz W (2010) Regulation of mRNA translation and stability by microRNAs. *Annual review of biochemistry* **79:** 351-379

Feng XH, Derynck R (2005) Specificity and versatility in tgf-beta signaling through Smads. *Annual review of cell and developmental biology* **21:** 659-693

Fernandez IE, Eickelberg O (2012a) The impact of TGF-beta on lung fibrosis: from targeting to biomarkers. *Proceedings of the American Thoracic Society* **9:** 111-116

Fernandez IE, Eickelberg O (2012b) New cellular and molecular mechanisms of lung injury and fibrosis in idiopathic pulmonary fibrosis. *Lancet* **380:** 680-688

Finnegan EF, Pasquinelli AE (2013) MicroRNA biogenesis: regulating the regulators. *Crit Rev Biochem Mol Biol* **48:** 51-68

Flicek P, Amode MR, Barrell D, Beal K, Brent S, Carvalho-Silva D, Clapham P, Coates G, Fairley S, Fitzgerald S, Gil L, Gordon L, Hendrix M, Hourlier T, Johnson N, Kahari AK, Keefe D, Keenan S, Kinsella R, Komorowska M, Koscielny G, Kulesha E, Larsson P, Longden I, McLaren W, Muffato M, Overduin B, Pignatelli M, Pritchard B, Riat HS, Ritchie GR, Ruffier M, Schuster M, Sobral D, Tang YA, Taylor K, Trevanion S, Vandrovcova J, White S, Wilson M, Wilder SP, Aken BL, Birney E, Cunningham F, Dunham I, Durbin R, Fernandez-Suarez XM, Harrow J, Herrero J, Hubbard TJ, Parker A, Proctor G, Spudich G, Vogel J, Yates A, Zadissa A, Searle SM (2012) Ensembl 2012. *Nucleic acids research* **40:** D84-90

French DM, Kaul RJ, D'Souza AL, Crowley CW, Bao M, Frantz GD, Filvaroff EH, Desnoyers L (2004) WISP-1 is an osteoblastic regulator expressed during skeletal development and fracture repair. *Am J Pathol* **165:** 855-867

Friedman RC, Farh KK, Burge CB, Bartel DP (2009) Most mammalian mRNAs are conserved targets of microRNAs. *Genome Res* **19:** 92-105

Gibson GJ, Loddenkemper R, Sibille Y, Lundback B. (2013) The European Lung White Book Respiratory Health and Disease in Europe. European Respiratory Society, Sheffield.

Goodwin A, Jenkins G (2009) Role of integrin-mediated TGFbeta activation in the pathogenesis of pulmonary fibrosis. *Biochemical Society transactions* **37:** 849-854

Grimson A, Farh KK, Johnston WK, Garrett-Engele P, Lim LP, Bartel DP (2007) MicroRNA targeting specificity in mammals: determinants beyond seed pairing. *Molecular cell* **27:** 91-105

Gross TJ, Hunninghake GW (2001) Idiopathic pulmonary fibrosis. *The New England journal of medicine* **345:** 517-525

Guo H, Ingolia NT, Weissman JS, Bartel DP (2010) Mammalian microRNAs predominantly act to decrease target mRNA levels. *Nature* **466:** 835-840

Hafner M, Landthaler M, Burger L, Khorshid M, Hausser J, Berninger P, Rothballer A, Ascano M, Jr., Jungkamp AC, Munschauer M, Ulrich A, Wardle GS, Dewell S, Zavolan M, Tuschl T (2010) Transcriptome-wide identification of RNA-binding protein and microRNA target sites by PAR-CLIP. *Cell* **141:** 129-141

Hagimoto N, Kuwano K, Inoshima I, Yoshimi M, Nakamura N, Fujita M, Maeyama T, Hara N (2002) TGF-beta 1 as an enhancer of Fas-mediated apoptosis of lung epithelial cells. *Journal of immunology* **168:** 6470-6478

Hashimoto Y, Shindo-Okada N, Tani M, Nagamachi Y, Takeuchi K, Shiroishi T, Toma H, Yokota J (1998) Expression of the Elm1 gene, a novel gene of the CCN (connective tissue

growth factor, Cyr61/Cef10, and neuroblastoma overexpressed gene) family, suppresses In vivo tumor growth and metastasis of K-1735 murine melanoma cells. *J Exp Med* **187:** 289-296

Haug BH, Henriksen JR, Buechner J, Geerts D, Tomte E, Kogner P, Martinsson T, Flaegstad T, Sveinbjornsson B, Einvik C (2011) MYCN-regulated miRNA-92 inhibits secretion of the tumor suppressor DICKKOPF-3 (DKK3) in neuroblastoma. *Carcinogenesis* **32:** 1005-1012

Heinrich EM, Wagner J, Kruger M, John D, Uchida S, Weigand JE, Suess B, Dimmeler S (2013) Regulation of miR-17-92a cluster processing by the microRNA binding protein SND1. *FEBS letters* **587:** 2405-2411

Heise RL, Stober V, Cheluvaraju C, Hollingsworth JW, Garantziotis S (2011) Mechanical stretch induces epithelial-mesenchymal transition in alveolar epithelia via hyaluronan activation of innate immunity. *J Biol Chem* **286:** 17435-17444

Henderson WR, Jr., Chi EY, Ye X, Nguyen C, Tien YT, Zhou B, Borok Z, Knight DA, Kahn M (2010) Inhibition of Wnt/beta-catenin/CREB binding protein (CBP) signaling reverses pulmonary fibrosis. *Proc Natl Acad Sci U S A* **107:** 14309-14314

Hofacker IL (2003) Vienna RNA secondary structure server. *Nucleic acids research* **31:** 3429-3431

Hou CH, Chiang YC, Fong YC, Tang CH (2011) WISP-1 increases MMP-2 expression and cell motility in human chondrosarcoma cells. *Biochemical pharmacology* **81:** 1286-1295

Hou CH, Tang CH, Hsu CJ, Hou SM, Liu JF (2013) CCN4 induces IL-6 production through alphavbeta5 receptor, PI3K, Akt, and NF-kappaB singling pathway in human synovial fibroblasts. *Arthritis Res Ther* **15:** R19

Huang Y, Zou Q, Song H, Song F, Wang L, Zhang G, Shen X (2010) A study of miRNAs targets prediction and experimental validation. *Protein & cell* **1:** 979-986

Huntzinger E, Izaurralde E (2011) Gene silencing by microRNAs: contributions of translational repression and mRNA decay. *Nature reviews Genetics* **12:** 99-110

Inkson CA, Ono M, Bi Y, Kuznetsov SA, Fisher LW, Young MF. (2009) The potential functional interaction of biglycan and WISP-1 in controlling differentiation and proliferation of osteogenic cells. *Cells Tissues Organs*, Vol. 189, pp. 153-157.

Inkson CA, Ono M, Kuznetsov SA, Fisher LW, Robey PG, Young MF (2008) TGF-beta1 and WISP-1/CCN-4 can regulate each other's activity to cooperatively control osteoblast function. *J Cell Biochem* **104:** 1865-1878

Jenkins G (2008) The role of proteases in transforming growth factor-beta activation. *The international journal of biochemistry & cell biology* **40:** 1068-1078

Jin J, Deng J, Wang F, Xia X, Qiu T, Lu W, Li X, Zhang H, Gu X, Liu Y, Cao W, Shao W (2013) The expression and function of microRNA-203 in lung cancer. *Tumour biology : the journal of the International Society for Oncodevelopmental Biology and Medicine* **34:** 349-357

Joglekar MV, Patil D, Joglekar VM, Rao GV, Reddy DN, Mitnala S, Shouche Y, Hardikar AA (2009) The miR-30 family microRNAs confer epithelial phenotype to human pancreatic cells. *Islets* **1:** 137-147

Kao CJ, Martiniez A, Shi XB, Yang J, Evans CP, Dobi A, deVere White RW, Kung HJ (2014) miR-30 as a tumor suppressor connects EGF/Src signal to ERG and EMT. *Oncogene* **33:** 2495-2503

Kapinas K, Kessler C, Ricks T, Gronowicz G, Delany AM (2010) miR-29 modulates Wnt signaling in human osteoblasts through a positive feedback loop. *J Biol Chem* **285:** 25221-25231

Kasper M, Haroske G (1996) Alterations in the alveolar epithelium after injury leading to pulmonary fibrosis. *Histol Histopathol* **11:** 463-483

Katzenstein AL, Myers JL (1998) Idiopathic pulmonary fibrosis: clinical relevance of pathologic classification. *Am J Respir Crit Care Med* **157:** 1301-1315

Kawaki H, Kubota S, Suzuki A, Suzuki M, Kohsaka K, Hoshi K, Fujii T, Lazar N, Ohgawara T, Maeda T, Perbal B, Takano-Yamamoto T, Takigawa M (2011) Differential roles of CCN family proteins during osteoblast differentiation: Involvement of Smad and MAPK signaling pathways. *Bone* **49:** 975-989

Kent WJ, Sugnet CW, Furey TS, Roskin KM, Pringle TH, Zahler AM, Haussler D (2002) The human genome browser at UCSC. *Genome Res* **12:** 996-1006

Khor TO, Gul YA, Ithnin H, Seow HF (2006) A comparative study of the expression of Wnt-1, WISP-1, survivin and cyclin-D1 in colorectal carcinoma. *Int J Colorectal Dis* **21:** 291-300

Kim KK, Kugler MC, Wolters PJ, Robillard L, Galvez MG, Brumwell AN, Sheppard D, Chapman HA (2006) Alveolar epithelial cell mesenchymal transition develops in vivo during pulmonary fibrosis and is regulated by the extracellular matrix. *Proc Natl Acad Sci U S A* **103:** 13180-13185

Kim TH, Kim SH, Seo JY, Chung H, Kwak HJ, Lee SK, Yoon HJ, Shin DH, Park SS, Sohn JW (2011) Blockade of the Wnt/beta-catenin pathway attenuates bleomycin-induced pulmonary fibrosis. *The Tohoku journal of experimental medicine* **223:** 45-54

King TE, Pardo A, Selman M (2011) Idiopathic pulmonary fibrosis. *The Lancet* **378:** 1949-1961

Kishore S, Jaskiewicz L, Burger L, Hausser J, Khorshid M, Zavolan M (2011) A quantitative analysis of CLIP methods for identifying binding sites of RNA-binding proteins. *Nature methods* **8:** 559-564

Klingberg F, Hinz B, White ES (2013) The myofibroblast matrix: implications for tissue repair and fibrosis. *J Pathol* **229:** 298-309

Knobloch J, Lin Y, Konradi J, Jungck D, Behr J, Strauch J, Stoelben E, Koch A (2013) Inflammatory responses of airway smooth muscle cells and effects of endothelin receptor antagonism. *American journal of respiratory cell and molecular biology* **49:** 114-127

Kolb M, Margetts PJ, Sime PJ, Gauldie J (2001) Proteoglycans decorin and biglycan differentially modulate TGF-beta-mediated fibrotic responses in the lung. *American journal of physiology Lung cellular and molecular physiology* **280:** L1327-1334

Königshoff M, Balsara N, Pfaff EM, Kramer M, Chrobak I, Seeger W, Eickelberg O (2008) Functional Wnt signaling is increased in idiopathic pulmonary fibrosis. *PLoS One* **3:** e2142

Königshoff M, Kramer M, Balsara N, Wilhelm J, Amarie OV, Jahn A, Rose F, Fink L, Seeger W, Schaefer L, Gunther A, Eickelberg O (2009) WNT1-inducible signaling protein-1 mediates pulmonary fibrosis in mice and is upregulated in humans with idiopathic pulmonary fibrosis. *J Clin Invest* **119:** 772-787

Korfei M, Ruppert C, Mahavadi P, Henneke I, Markart P, Koch M, Lang G, Fink L, Bohle RM, Seeger W, Weaver TE, Guenther A (2008) Epithelial endoplasmic reticulum stress and apoptosis in sporadic idiopathic pulmonary fibrosis. *Am J Respir Crit Care Med* **178:** 838-846

Kozomara A, Griffiths-Jones S (2014) miRBase: annotating high confidence microRNAs using deep sequencing data. *Nucleic acids research* **42:** D68-73

Krol J, Loedige I, Filipowicz W (2010) The widespread regulation of microRNA biogenesis, function and decay. *Nature reviews Genetics* **11:** 597-610

Kubota S, Kondo S, Eguchi T, Hattori T, Nakanishi T, Pomerantz RJ, Takigawa M (2000) Identification of an RNA element that confers post-transcriptional repression of connective tissue growth factor/hypertrophic chondrocyte specific 24 (ctgf/hcs24) gene: similarities to retroviral RNA-protein interactions. *Oncogene* **19:** 4773-4786

Kumarswamy R, Mudduluru G, Ceppi P, Muppala S, Kozlowski M, Niklinski J, Papotti M, Allgayer H (2012) MicroRNA-30a inhibits epithelial-to-mesenchymal transition by targeting Snai1 and is downregulated in non-small cell lung cancer. *International journal of cancer Journal international du cancer* **130:** 2044-2053

Lal A, Navarro F, Maher CA, Maliszewski LE, Yan N, O'Day E, Chowdhury D, Dykxhoorn DM, Tsai P, Hofmann O, Becker KG, Gorospe M, Hide W, Lieberman J (2009) miR-24 Inhibits cell proliferation by targeting E2F2, MYC, and other cell-cycle genes via binding to "seedless" 3'UTR microRNA recognition elements. *Molecular cell* **35:** 610-625

Lasky JA, Ortiz LA, Tonthat B, Hoyle GW, Corti M, Athas G, Lungarella G, Brody A, Friedman M (1998) Connective tissue growth factor mRNA expression is upregulated in bleomycin-induced lung fibrosis. *Am J Physiol-Lung C* **275:** L365-L371

Lee CG, Cho SJ, Kang MJ, Chapoval SP, Lee PJ, Noble PW, Yehualaeshet T, Lu B, Flavell RA, Milbrandt J, Homer RJ, Elias JA (2004) Early growth response gene 1-mediated apoptosis is essential for transforming growth factor beta1-induced pulmonary fibrosis. *J Exp Med* **200:** 377-389

Lee HC, Chen CY, Au LC (2011) Systemic comparison of repression activity for miRNA and siRNA associated with different types of target sequences. *Biochem Biophys Res Commun* **411:** 393-396

Lewis BP, Burge CB, Bartel DP (2005) Conserved seed pairing, often flanked by adenosines, indicates that thousands of human genes are microRNA targets. *Cell* **120:** 15-20

Li HH, Li Q, Liu P, Liu Y, Li J, Wasserloos K, Chao W, You M, Oury TD, Chhinder S, Hackam DJ, Billiar TR, Leikauf GD, Pitt BR, Zhang LM (2012a) WNT1-inducible signaling pathway protein 1 contributes to ventilator-induced lung injury. *American journal of respiratory cell and molecular biology* **47:** 528-535

Li L, Shi JY, Zhu GQ, Shi B (2012b) MiR-17-92 cluster regulates cell proliferation and collagen synthesis by targeting TGFB pathway in mouse palatal mesenchymal cells. *J Cell Biochem* **113:** 1235-1244

Li P, Zhao GQ, Chen TF, Chang JX, Wang HQ, Chen SS, Zhang GJ (2013) Serum miR-21 and miR-155 expression in idiopathic pulmonary fibrosis. *The Journal of asthma : official journal of the Association for the Care of Asthma* **50:** 960-964

Li Y, Jiang D, Liang J, Meltzer EB, Gray A, Miura R, Wogensen L, Yamaguchi Y, Noble PW (2011) Severe lung fibrosis requires an invasive fibroblast phenotype regulated by hyaluronan and CD44. *J Exp Med* **208:** 1459-1471

Liu G, Friggeri A, Yang Y, Milosevic J, Ding Q, Thannickal VJ, Kaminski N, Abraham E (2010) miR-21 mediates fibrogenic activation of pulmonary fibroblasts and lung fibrosis. *J Exp Med* **207:** 1589-1597

Liu H, Dong W, Lin Z, Lu J, Wan H, Zhou Z, Liu Z (2013a) CCN4 regulates vascular smooth muscle cell migration and proliferation. *Molecules and cells* **36:** 112-118

Liu JF, Hou SM, Tsai CH, Huang CY, Hsu CJ, Tang CH (2013b) CCN4 induces vascular cell adhesion molecule-1 expression in human synovial fibroblasts and promotes monocyte adhesion. *Biochimica et biophysica acta* **1833:** 966-975

Liu T, Ullenbruch M, Young Choi Y, Yu H, Ding L, Xaubet A, Pereda J, Feghali-Bostwick CA, Bitterman PB, Henke CA, Pardo A, Selman M, Phan SH (2013c) Telomerase and telomere length in pulmonary fibrosis. *American journal of respiratory cell and molecular biology* **49:** 260-268

Liu ZJ, Li Y, Tan Y, Xiao M, Zhang J, Radtke F, Velazquez OC (2012) Inhibition of fibroblast growth by Notch1 signaling is mediated by induction of Wnt11-dependent WISP-1. *PLoS One* **7:** e38811

Longo KA, Kennell JA, Ochocinska MJ, Ross SE, Wright WS, MacDougald OA (2002) Wnt signaling protects 3T3-L1 preadipocytes from apoptosis through induction of insulin-like growth factors. *J Biol Chem* **277:** 38239-38244

Loomis-King H, Flaherty KR, Moore BB (2013) Pathogenesis, current treatments and future directions for idiopathic pulmonary fibrosis. *Current opinion in pharmacology* **13:** 377-385

Lorda-Diez CI, Montero JA, Diaz-Mendoza MJ, Garcia-Porrero JA, Hurle JM (2011) Defining the earliest transcriptional steps of chondrogenic progenitor specification during the formation of the digits in the embryonic limb. *PLoS One* **6:** e24546

Lu Y, Thomson JM, Wong HY, Hammond SM, Hogan BL (2007) Transgenic over-expression of the microRNA miR-17-92 cluster promotes proliferation and inhibits differentiation of lung epithelial progenitor cells. *Developmental biology* **310:** 442-453

Lukowski S, Weng H, Gu X, Li Q, Gao C, Dooley S, Ilkavets I (2012) TGF-beta induced hepatocellular Wisp1 is expressed in hepatocellular carcinoma and drives proliferation of epithelial-type cancer cells. *Zeitschrift für Gastroenterologie* **50:** P5_32

Maher TM, Evans IC, Bottoms SE, Mercer PF, Thorley AJ, Nicholson AG, Laurent GJ, Tetley TD, Chambers RC, McAnulty RJ (2010) Diminished prostaglandin E2 contributes to the apoptosis paradox in idiopathic pulmonary fibrosis. *Am J Respir Crit Care Med* **182:** 73-82

Marchand A, Proust C, Morange PE, Lompre AM, Tregouet DA (2012) miR-421 and miR-30c inhibit SERPINE 1 gene expression in human endothelial cells. *PLoS One* **7:** e44532

Mendell JT (2008) miRiad roles for the miR-17-92 cluster in development and disease. *Cell* **133:** 217-222

Mendell JT, Olson EN (2012) MicroRNAs in stress signaling and human disease. *Cell* **148:** 1172-1187

Mestdagh P, Bostrom AK, Impens F, Fredlund E, Van Peer G, De Antonellis P, von Stedingk K, Ghesquiere B, Schulte S, Dews M, Thomas-Tikhonenko A, Schulte JH, Zollo M, Schramm A, Gevaert K, Axelson H, Speleman F, Vandesompele J (2010) The miR-17-92 microRNA cluster regulates multiple components of the TGF-beta pathway in neuroblastoma. *Molecular cell* **40:** 762-773

Milosevic J, Pandit K, Magister M, Rabinovich E, Ellwanger DC, Yu G, Vuga LJ, Weksler B, Benos PV, Gibson KF, McMillan M, Kahn M, Kaminski N (2012) Profibrotic role of miR-154 in pulmonary fibrosis. *American journal of respiratory cell and molecular biology* **47:** 879-887

Moeller A, Rodriguez-Lecompte JC, Wang L, Gauldie J, Kolb M (2006) Models of pulmonary fibrosis. *Drug Discovery Today: Disease Models* **3:** 243-249

Moore BB, Hogaboam CM (2008) Murine models of pulmonary fibrosis. *American journal of physiology Lung cellular and molecular physiology* **294:** L152-160

Nakagawa Y, Minato M, Sumiyoshi K, Maeda A, Hara C, Murase Y, Nishida T, Kubota S, Takigawa M (2013) Regulation of CCN1 via the 3'-untranslated region. *Journal of cell communication and signaling* **7:** 207-217

Nielsen CB, Shomron N, Sandberg R, Hornstein E, Kitzman J, Burge CB (2007) Determinants of targeting by endogenous and exogenous microRNAs and siRNAs. *RNA* **13:** 1894-1910

Nogee LM, Dunbar AE, 3rd, Wert SE, Askin F, Hamvas A, Whitsett JA (2001) A mutation in the surfactant protein C gene associated with familial interstitial lung disease. *The New England journal of medicine* **344:** 573-579

Nonne N, Ameyar-Zazoua M, Souidi M, Harel-Bellan A (2010) Tandem affinity purification of miRNA target mRNAs (TAP-Tar). *Nucleic acids research* **38:** e20

Oak SR, Murray L, Herath A, Sleeman M, Anderson I, Joshi AD, Coelho AL, Flaherty KR, Toews GB, Knight D, Martinez FJ, Hogaboam CM (2011) A micro RNA processing defect in rapidly progressing idiopathic pulmonary fibrosis. *PLoS One* **6:** e21253

Ono M, Inkson CA, Kilts TM, Young MF (2011) WISP-1/CCN4 regulates osteogenesis by enhancing BMP-2 activity. *J Bone Miner Res* **26:** 193-208

Ono M, Inkson CA, Sonn R, Kilts TM, de Castro LF, Maeda A, Fisher LW, Robey PG, Berendsen AD, Li L, McCartney-Francis N, Brown AC, Crawford NP, Molinolo A, Jain A, Fedarko NS, Young MF (2013) WISP1/CCN4: a potential target for inhibiting prostate cancer growth and spread to bone. *PLoS One* **8:** e71709

Pan LH, Yamauchi K, Uzuki M, Nakanishi T, Takigawa M, Inoue H, Sawai T (2001) Type II alveolar epithelial cells and interstitial fibroblasts express connective tissue growth factor in IPF. *The European respiratory journal* **17:** 1220-1227

Pandit KV, Corcoran D, Yousef H, Yarlagadda M, Tzouvelekis A, Gibson KF, Konishi K, Yousem SA, Singh M, Handley D, Richards T, Selman M, Watkins SC, Pardo A, Ben-Yehudah A, Bouros D, Eickelberg O, Ray P, Benos PV, Kaminski N (2010) Inhibition and role of let-7d in idiopathic pulmonary fibrosis. *Am J Respir Crit Care Med* **182:** 220-229

Pandit KV, Milosevic J, Kaminski N (2011) MicroRNAs in idiopathic pulmonary fibrosis. *Translational research : the journal of laboratory and clinical medicine* **157:** 191-199

Parisi MS, Gazzerro E, Rydziel S, Canalis E (2006) Expression and regulation of CCN genes in murine osteoblasts. *Bone* **38:** 671-677

Pasquinelli AE (2012) MicroRNAs and their targets: recognition, regulation and an emerging reciprocal relationship. *Nature reviews Genetics* **13:** 271-282

Pennica D, Swanson TA, Welsh JW, Roy MA, Lawrence DA, Lee J, Brush J, Taneyhill LA, Deuel B, Lew M, Watanabe C, Cohen RL, Melhem MF, Finley GG, Quirke P, Goddard AD, Hillan KJ, Gurney AL, Botstein D, Levine AJ (1998) WISP genes are members of the connective tissue growth factor family that are up-regulated in wnt-1-transformed cells and aberrantly expressed in human colon tumors. *Proc Natl Acad Sci U S A* **95:** 14717-14722

Pottier N, Maurin T, Chevalier B, Puissegur MP, Lebrigand K, Robbe-Sermesant K, Bertero T, Lino Cardenas CL, Courcot E, Rios G, Fourre S, Lo-Guidice JM, Marcet B, Cardinaud B, Barbry

P, Mari B (2009) Identification of keratinocyte growth factor as a target of microRNA-155 in lung fibroblasts: implication in epithelial-mesenchymal interactions. *PLoS One* **4:** e6718

Qin W, Chung AC, Huang XR, Meng XM, Hui DS, Yu CM, Sung JJ, Lan HY (2011) TGF-beta/Smad3 signaling promotes renal fibrosis by inhibiting miR-29. *J Am Soc Nephrol* **22:** 1462-1474

Raghu G, Collard HR, Egan JJ, Martinez FJ, Behr J, Brown KK, Colby TV, Cordier JF, Flaherty KR, Lasky JA, Lynch DA, Ryu JH, Swigris JJ, Wells AU, Ancochea J, Bouros D, Carvalho C, Costabel U, Ebina M, Hansell DM, Johkoh T, Kim DS, King TE, Jr., Kondoh Y, Myers J, Muller NL, Nicholson AG, Richeldi L, Selman M, Dudden RF, Griss BS, Protzko SL, Schunemann HJ, Fibrosis AEJACoIP (2011) An official ATS/ERS/JRS/ALAT statement: idiopathic pulmonary fibrosis: evidence-based guidelines for diagnosis and management. *Am J Respir Crit Care Med* **183:** 788-824

Raghu G, Weycker D, Edelsberg J, Bradford WZ, Oster G (2006) Incidence and prevalence of idiopathic pulmonary fibrosis. *Am J Respir Crit Care Med* **174:** 810-816

Reddy VS, Valente AJ, Delafontaine P, Chandrasekar B (2011) Interleukin-18/WNT1-inducible signaling pathway protein-1 signaling mediates human saphenous vein smooth muscle cell proliferation. *J Cell Physiol* **226:** 3303-3315

Ritchie ME, Silver J, Oshlack A, Holmes M, Diyagama D, Holloway A, Smyth GK (2007) A comparison of background correction methods for two-colour microarrays. *Bioinformatics* **23:** 2700-2707

Roderburg C, Urban GW, Bettermann K, Vucur M, Zimmermann H, Schmidt S, Janssen J, Koppe C, Knolle P, Castoldi M, Tacke F, Trautwein C, Luedde T (2011) Micro-RNA profiling reveals a role for miR-29 in human and murine liver fibrosis. *Hepatology* **53:** 209-218

Roy S, Khanna S, Hussain SR, Biswas S, Azad A, Rink C, Gnyawali S, Shilo S, Nuovo GJ, Sen CK (2009) MicroRNA expression in response to murine myocardial infarction: miR-21 regulates fibroblast metalloprotease-2 via phosphatase and tensin homologue. *Cardiovascular research* **82:** 21-29

Ryan RM, Mineo-Kuhn MM, Kramer CM, Finkelstein JN (1994) Growth factors alter neonatal type II alveolar epithelial cell proliferation. *Am J Physiol* **266:** L17-22

Saetrom P, Heale BS, Snove O, Jr., Aagaard L, Alluin J, Rossi JJ (2007) Distance constraints between microRNA target sites dictate efficacy and cooperativity. *Nucleic acids research* **35:** 2333-2342

Sambrook J, Russell DW (2001) *Molecular cloning : a laboratory manual*, 3rd edn. Cold Spring Harbor, N.Y.: Cold Spring Harbor Laboratory Press.

Schulz MH, Pandit KV, Lino Cardenas CL, Ambalavanan N, Kaminski N, Bar-Joseph Z (2013) Reconstructing dynamic microRNA-regulated interaction networks. *Proc Natl Acad Sci U S A* **110:** 15686-15691

Schwanhausser B, Busse D, Li N, Dittmar G, Schuchhardt J, Wolf J, Chen W, Selbach M (2011) Global quantification of mammalian gene expression control. *Nature* **473:** 337-342

Seibold MA, Wise AL, Speer MC, Steele MP, Brown KK, Loyd JE, Fingerlin TE, Zhang W, Gudmundsson G, Groshong SD, Evans CM, Garantziotis S, Adler KB, Dickey BF, du Bois RM, Yang IV, Herron A, Kervitsky D, Talbert JL, Markin C, Park J, Crews AL, Slifer SH, Auerbach S, Roy MG, Lin J, Hennessy CE, Schwarz MI, Schwartz DA (2011) A common MUC5B promoter polymorphism and pulmonary fibrosis. *The New England journal of medicine* **364:** 1503-1512

Selbach M, Schwanhausser B, Thierfelder N, Fang Z, Khanin R, Rajewsky N (2008) Widespread changes in protein synthesis induced by microRNAs. *Nature* **455:** 58-63

Selman M, King TE, Pardo A (2001) Idiopathic pulmonary fibrosis: Prevailing and evolving hypotheses about its pathogenesis and implications for therapy. *Annals of Internal Medicine* **134:** 136-151

Selman M, Pardo A, Barrera L, Estrada A, Watson SR, Wilson K, Aziz N, Kaminski N, Zlotnik A (2006) Gene expression profiles distinguish idiopathic pulmonary fibrosis from hypersensitivity pneumonitis. *Am J Respir Crit Care Med* **173:** 188-198

Selman M, Pardo A, Kaminski N (2008) Idiopathic pulmonary fibrosis: aberrant recapitulation of developmental programs? *PLoS medicine* **5:** e62

Sessa R, Hata A (2013) Role of microRNAs in lung development and pulmonary diseases. *Pulmonary circulation* **3:** 315-328

Shanmugam P, Valente AJ, Prabhu SD, Venkatesan B, Yoshida T, Delafontaine P, Chandrasekar B (2011) Angiotensin-II type 1 receptor and NOX2 mediate TCF/LEF and CREB dependent WISP1 induction and cardiomyocyte hypertrophy. *J Mol Cell Cardiol* **50:** 928-938

Shao H, Cai L, Grichnik JM, Livingstone AS, Velazquez OC, Liu ZJ (2011) Activation of Notch1 signaling in stromal fibroblasts inhibits melanoma growth by upregulating WISP-1. *Oncogene* **30:** 4316-4326

Sharma S, Tantisira K, Carey V, Murphy AJ, Lasky-Su J, Celedon JC, Lazarus R, Klanderman B, Rogers A, Soto-Quiros M, Avila L, Mariani T, Gaedigk R, Leeder S, Torday J, Warburton D, Raby B, Weiss ST (2010) A role for Wnt signaling genes in the pathogenesis of impaired lung function in asthma. *Am J Respir Crit Care Med* **181:** 328-336

Shi S, Yu L, Zhang T, Qi H, Xavier S, Ju W, Bottinger E (2013) Smad2-dependent downregulation of miR-30 is required for TGF-beta-induced apoptosis in podocytes. *PLoS One* **8:** e75572

Sime PJ, Xing Z, Graham FL, Csaky KG, Gauldie J (1997) Adenovector-mediated gene transfer of active transforming growth factor-beta1 induces prolonged severe fibrosis in rat lung. *J Clin Invest* **100:** 768-776

Sing T, Jinnin M, Yamane K, Honda N, Makino K, Kajihara I, Makino T, Sakai K, Masuguchi S, Fukushima S, Ihn H (2012) microRNA-92a expression in the sera and dermal fibroblasts increases in patients with scleroderma. *Rheumatology (Oxford)* **51:** 1550-1556

Sisson TH, Mendez M, Choi K, Subbotina N, Courey A, Cunningham A, Dave A, Engelhardt JF, Liu X, White ES, Thannickal VJ, Moore BB, Christensen PJ, Simon RH (2010) Targeted injury of type II alveolar epithelial cells induces pulmonary fibrosis. *Am J Respir Crit Care Med* **181:** 254-263

Sonkoly E, Wei T, Janson PC, Saaf A, Lundeberg L, Tengvall-Linder M, Norstedt G, Alenius H, Homey B, Scheynius A, Stahle M, Pivarcsi A (2007) MicroRNAs: novel regulators involved in the pathogenesis of psoriasis? *PLoS One* **2:** e610

Soon LL, Yie TA, Shvarts A, Levine AJ, Su F, Tchou-Wong KM (2003) Overexpression of WISP-1 down-regulated motility and invasion of lung cancer cells through inhibition of Rac activation. *J Biol Chem* **278:** 11465-11470

Su F, Overholtzer M, Besser D, Levine AJ (2002) WISP-1 attenuates p53-mediated apoptosis in response to DNA damage through activation of the Akt kinase. *Genes Dev* **16:** 46-57

Tan Gana NH, Victoriano AF, Okamoto T (2012) Evaluation of online miRNA resources for biomedical applications. *Genes Cells* **17:** 11-27

Tanaka S, Sugimachi K, Kameyama T, Maehara S, Shirabe K, Shimada M, Wands JR, Maehara Y (2003) Human WISP1v, a member of the CCN family, is associated with invasive cholangiocarcinoma. *Hepatology* **37:** 1122-1129

Tanaka S, Sugimachi K, Saeki H, Kinoshita J, Ohga T, Shimada M, Maehara Y, Sugimachi K (2001) A novel variant of WISP1 lacking a Von Willebrand type C module overexpressed in scirrhous gastric carcinoma. *Oncogene* **20:** 5525-5532

Tanaka S, Suto A, Ikeda K, Sanayama Y, Nakagomi D, Iwamoto T, Suzuki K, Kambe N, Matsue H, Matsumura R, Kashiwakuma D, Iwamoto I, Nakajima H (2013) Alteration of circulating miRNAs in SSc: miR-30b regulates the expression of PDGF receptor beta. *Rheumatology (Oxford)* **52:** 1963-1972

Tanguay (1996) Translational efficiency is regulated by the length of the 3' untranslated region. *Mol Cell Biol*

Tanjore H, Degryse AL, Crossno PF, Xu XC, McConaha ME, Jones BR, Polosukhin VV, Bryant AJ, Cheng DS, Newcomb DC, McMahon FB, Gleaves LA, Blackwell TS, Lawson WE (2013) beta-catenin in the alveolar epithelium protects from lung fibrosis after intratracheal bleomycin. *Am J Respir Crit Care Med* **187:** 630-639

Tatler AL, Jenkins G (2012) TGF-beta activation and lung fibrosis. *Proceedings of the American Thoracic Society* **9:** 130-136

Taube JH, Malouf GG, Lu E, Sphyris N, Vijay V, Ramachandran PP, Ueno KR, Gaur S, Nicoloso MS, Rossi S, Herschkowitz JI, Rosen JM, Issa JP, Calin GA, Chang JT, Mani SA (2013)

Epigenetic silencing of microRNA-203 is required for EMT and cancer stem cell properties. *Scientific reports* **3:** 2687

Thatcher EJ, Paydar I, Anderson KK, Patton JG (2008) Regulation of zebrafish fin regeneration by microRNAs. *Proc Natl Acad Sci U S A* **105:** 18384-18389

Thomas AQ, Lane K, Phillips J, 3rd, Prince M, Markin C, Speer M, Schwartz DA, Gaddipati R, Marney A, Johnson J, Roberts R, Haines J, Stahlman M, Loyd JE (2002) Heterozygosity for a surfactant protein C gene mutation associated with usual interstitial pneumonitis and cellular nonspecific interstitial pneumonitis in one kindred. *Am J Respir Crit Care Med* **165:** 1322-1328

Thum T, Gross C, Fiedler J, Fischer T, Kissler S, Bussen M, Galuppo P, Just S, Rottbauer W, Frantz S, Castoldi M, Soutschek J, Koteliansky V, Rosenwald A, Basson MA, Licht JD, Pena JT, Rouhanifard SH, Muckenthaler MU, Tuschl T, Martin GR, Bauersachs J, Engelhardt S (2008) MicroRNA-21 contributes to myocardial disease by stimulating MAP kinase signalling in fibroblasts. *Nature* **456:** 980-984

Treiber T, Treiber N, Meister G (2012) Regulation of microRNA biogenesis and function. *Thromb Haemost* **107:** 605-610

Ulsamer A, Wei Y, Kim KK, Tan K, Wheeler S, Xi Y, Thies RS, Chapman HA (2012) Axin pathway activity regulates in vivo pY654-beta-catenin accumulation and pulmonary fibrosis. *J Biol Chem* **287:** 5164-5172

van Rooij E (2011) The art of microRNA research. *Circ Res* **108:** 219-234

Venkatachalam K, Venkatesan B, Valente AJ, Melby PC, Nandish S, Reusch JE, Clark RA, Chandrasekar B (2009) WISP1, a pro-mitogenic, pro-survival factor, mediates tumor necrosis factor-alpha (TNF-alpha)-stimulated cardiac fibroblast proliferation but inhibits TNF-alpha-induced cardiomyocyte death. *J Biol Chem* **284:** 14414-14427

Venkatesan B, Prabhu SD, Venkatachalam K, Mummidi S, Valente AJ, Clark RA, Delafontaine P, Chandrasekar B (2010) WNT1-inducible signaling pathway protein-1 activates diverse cell survival pathways and blocks doxorubicin-induced cardiomyocyte death. *Cell Signal* **22:** 809-820

Ventura A, Young AG, Winslow MM, Lintault L, Meissner A, Erkeland SJ, Newman J, Bronson RT, Crowley D, Stone JR, Jaenisch R, Sharp PA, Jacks T (2008) Targeted deletion reveals essential and overlapping functions of the miR-17 through 92 family of miRNA clusters. *Cell* **132:** 875-886

Vermeulen A, Robertson B, Dalby AB, Marshall WS, Karpilow J, Leake D, Khvorova A, Baskerville S (2007) Double-stranded regions are essential design components of potent inhibitors of RISC function. *RNA* **13:** 723-730

Vettori S, Gay S, Distler O (2012) Role of MicroRNAs in Fibrosis. *Open Rheumatol J* **6:** 130-139

Vuga LJ, Ben-Yehudah A, Kovkarova-Naumovski E, Oriss T, Gibson KF, Feghali-Bostwick C, Kaminski N (2009) WNT5A is a regulator of fibroblast proliferation and resistance to apoptosis. *American journal of respiratory cell and molecular biology* **41:** 583-589

Wang C, Wang X, Liang H, Wang T, Yan X, Cao M, Wang N, Zhang S, Zen K, Zhang C, Chen X (2013) miR-203 inhibits cell proliferation and migration of lung cancer cells by targeting PKCalpha. *PLoS One* **8:** e73985

Wang H, Xu Q, Xiao F, Jiang Y, Wu Z (2008) Involvement of the p38 mitogen-activated protein kinase alpha, beta, and gamma isoforms in myogenic differentiation. *Mol Biol Cell* **19:** 1519-1528

Wang H, Zhang R, Wen S, McCafferty DM, Beck PL, MacNaughton WK (2009a) Nitric oxide increases Wnt-induced secreted protein-1 (WISP-1/CCN4) expression and function in colitis. *Journal of molecular medicine* **87:** 435-445

Wang S, Chong ZZ, Shang YC, Maiese K (2012a) WISP1 (CCN4) autoregulates its expression and nuclear trafficking of beta-catenin during oxidant stress with limited effects upon neuronal autophagy. *Curr Neurovasc Res* **9:** 91-101

Wang S, Chong ZZ, Shang YC, Maiese K (2012b) Wnt1 inducible signaling pathway protein 1 (WISP1) blocks neurodegeneration through phosphoinositide 3 kinase/Akt1 and apoptotic mitochondrial signaling involving Bad, Bax, Bim, and Bcl-xL. *Curr Neurovasc Res* **9:** 20-31

Wang Y, Kuan PJ, Xing C, Cronkhite JT, Torres F, Rosenblatt RL, DiMaio JM, Kinch LN, Grishin NV, Garcia CK (2009b) Genetic defects in surfactant protein A2 are associated with pulmonary fibrosis and lung cancer. *American journal of human genetics* **84:** 52-59

Wen J, Parker BJ, Jacobsen A, Krogh A (2011) MicroRNA transfection and AGO-bound CLIP-seq data sets reveal distinct determinants of miRNA action. *RNA* **17:** 820-834

White ES, Thannickal VJ, Carskadon SL, Dickie EG, Livant DL, Markwart S, Toews GB, Arenberg DA (2003) Integrin alpha4beta1 regulates migration across basement membranes by lung fibroblasts: a role for phosphatase and tensin homologue deleted on chromosome 10. *Am J Respir Crit Care Med* **168:** 436-442

Witte F, Dokas J, Neuendorf F, Mundlos S, Stricker S (2009) Comprehensive expression analysis of all Wnt genes and their major secreted antagonists during mouse limb development and cartilage differentiation. *Gene Expr Patterns* **9:** 215-223

Wolters PJ, Collard HR, Jones KD (2014) Pathogenesis of idiopathic pulmonary fibrosis. *Annual review of pathology* **9:** 157-179

Wynn TA (2011) Integrating mechanisms of pulmonary fibrosis. *J Exp Med* **208:** 1339-1350

Wynn TA, Ramalingam TR (2012) Mechanisms of fibrosis: therapeutic translation for fibrotic disease. *Nature medicine* **18:** 1028-1040

Xiao J, Meng XM, Huang XR, Chung AC, Feng YL, Hui DS, Yu CM, Sung JJ, Lan HY (2012) miR-29 inhibits bleomycin-induced pulmonary fibrosis in mice. *Molecular therapy : the journal of the American Society of Gene Therapy* **20:** 1251-1260

Xie D, Nakachi K, Wang H, Elashoff R, Koeffler HP (2001) Elevated levels of connective tissue growth factor, WISP-1, and CYR61 in primary breast cancers associated with more advanced features. *Cancer Res* **61:** 8917-8923

Xu L, Corcoran RB, Welsh JW, Pennica D, Levine AJ (2000) WISP-1 is a Wnt-1- and beta-catenin-responsive oncogene. *Genes Dev* **14:** 585-595

Yanagita T, Kubota S, Kawaki H, Kawata K, Kondo S, Takano-Yamamoto T, Tanaka S, Takigawa M (2007) Expression and physiological role of CCN4/Wnt-induced secreted protein 1 mRNA splicing variants in chondrocytes. *FEBS J* **274:** 1655-1665

Yang M, Zhao X, Liu Y, Tian Y, Ran X, Jiang Y (2013) A role for WNT1-inducible signaling protein-1 in airway remodeling in a rat asthma model. *International immunopharmacology* **17:** 350-357

Yi R, Poy MN, Stoffel M, Fuchs E (2008) A skin microRNA promotes differentiation by repressing 'stemness'. *Nature* **452:** 225-229

You Z, Saims D, Chen S, Zhang Z, Guttridge DC, Guan KL, MacDougald OA, Brown AM, Evan G, Kitajewski J, Wang CY (2002) Wnt signaling promotes oncogenic transformation by inhibiting c-Myc-induced apoptosis. *J Cell Biol* **157:** 429-440

Yu H, Konigshoff M, Jayachandran A, Handley D, Seeger W, Kaminski N, Eickelberg O (2008) Transgelin is a direct target of TGF-beta/Smad3-dependent epithelial cell migration in lung fibrosis. *FASEB journal : official publication of the Federation of American Societies for Experimental Biology* **22:** 1778-1789

Zemans RL, Briones N, Campbell M, McClendon J, Young SK, Suzuki T, Yang IV, De Langhe S, Reynolds SD, Mason RJ, Kahn M, Henson PM, Colgan SP, Downey GP (2011) Neutrophil transmigration triggers repair of the lung epithelium via beta-catenin signaling. *Proc Natl Acad Sci U S A* **108:** 15990-15995

Zemans RL, McClendon J, Aschner Y, Briones N, Young SK, Lau LF, Kahn M, Downey GP (2013) Role of beta-catenin-regulated CCN matricellular proteins in epithelial repair after inflammatory lung injury. *American journal of physiology Lung cellular and molecular physiology* **304:** L415-427

Zhang J, Zhang H, Liu J, Tu X, Zang Y, Zhu J, Chen J, Dong L, Zhang J (2012) miR-30 inhibits TGF-beta1-induced epithelial-to-mesenchymal transition in hepatocyte by targeting Snail1. *Biochem Biophys Res Commun* **417:** 1100-1105

Zhou B, Liu Y, Kahn M, Ann DK, Han A, Wang H, Nguyen C, Flodby P, Zhong Q, Krishnaveni MS, Liebler JM, Minoo P, Crandall ED, Borok Z (2012) Interactions between beta-catenin and transforming growth factor-beta signaling pathways mediate epithelial-mesenchymal transition and are dependent on the transcriptional co-activator cAMP-response element-binding protein (CREB)-binding protein (CBP). *J Biol Chem* **287:** 7026-7038

Zhu X, Er K, Mao C, Yan Q, Xu H, Zhang Y, Zhu J, Cui F, Zhao W, Shi H (2013) miR-203 suppresses tumor growth and angiogenesis by targeting VEGFA in cervical cancer. *Cellular physiology and biochemistry : international journal of experimental cellular physiology, biochemistry, and pharmacology* **32:** 64-73

Zuo GW, Kohls CD, He BC, Chen L, Zhang W, Shi Q, Zhang BQ, Kang Q, Luo J, Luo X, Wagner ER, Kim SH, Restegar F, Haydon RC, Deng ZL, Luu HH, He TC, Luo Q (2010) The CCN proteins: important signaling mediators in stem cell differentiation and tumorigenesis. *Histol Histopathol* **25:** 795-806

8 APPENDIX

8.1 MiRNA binding sites

Below the long "longest seed" miRNA binding sites are listed.

miR-30 family

7merβ: at position 1811 nt on the hWISP1 3'UTR:

```
GAACCAGCUCUCAUCACACAUUUAAAAGAUGAUUCUGUUUACC WISP1 3'UTR
   ||||   ||               |  ||  |||||||
GAAGGUC---AG--------------CCCCU---ACAAAUGU hsa-miR-30d-5p


GAACCAGCUCUCAUCACACAUUUAAAAGAUGAUUCUGUUUACC WISP1 3'UTR
   ||||   ||              || ||  |||||||
GAAGGUC---AG--------------CUCCU---ACAAAUGU hsa-miR-30a-5p
```

7merβ: at position 2657 nt on the hWISP1 3'UTR:

```
UCUCCACUGAUUGAGUGUUUACU WISP1 3'UTR
  ||||       |  |||||||
GAAGGUCAGCC-CCUACAAAUGU hsa-miR-30d-5p


UCUCCACUGAUUGAG--UGUUUACU NM_001204869
  ||||     |:|||  |||||||
GAAGGUC---AGCUCCUU hsa-miR-30a-5p
```


miR-92a

7merα: at position 1600 nt on the hWISP1 3'UTR:

```
AUAGGAAA--ACAU-UGCAAUA WISP1 3'UTR
|:|||      |||  |||||||
UGUCCGGCCCUGUUCACGUUAU hsa-miR-92a-3p
```

miR-203a

8mer: at position 1125 nt on the hWISP1 3'UTR:

```
CCCGUGUUCAGGACACAUCUAUUGCAGAGACUCAUUUCAC WISP1 3'UTR
   ||| ||         |||          ||||||||
GAUCACCAG---------GAUUU---------GUAAAGUG hsa-miR-203a
```

8.2 Acknowledgement

8.3 Eidesstattliche Versicherung

Hiermit erkläre ich, **Barbara Berschneider**, an Eides statt,

dass ich die vorliegende Dissertation mit dem Thema

„ WISP1 Regulation by microRNAs in pulmonary fibrosis"

selbständig verfasst, mich außer der angegebenen keiner weiteren Hilfsmittel bedient und alle Erkenntnisse, die aus dem Schrifttum ganz oder annähernd übernommen sind, als solche kenntlich gemacht und nach ihrer Herkunft unter Bezeichnung der Fundstelle einzeln nachgewiesen habe.

Ich erkläre des Weiteren, dass die hier vorgelegte Dissertation nicht in gleicher oder in ähnlicher Form bei einer anderen Stelle zur Erlangung eines akademischen Grades eingereicht wurde.

_____   _____
Ort, Datum   Unterschrift